

**NASA CONTRACTOR
REPORT**

NASA CR-753



NASA CR

c.1

LOAN COPY
APRIL 1967
KIRTLAND AFB, TEXAS

0099825

TECH LIBRARY KAFB, NM

**FEASIBILITY, PARAMETRIC DESIGN, AND
COMPARATIVE ANALYSIS OF AN UNGUIDED
SOLID FUEL ROCKET VEHICLE WITH
SOLAR ORBIT, EARTH PROBE, AND
RE-ENTRY MISSION CAPABILITIES**

by T. C. Walker

Prepared by

LTV AEROSPACE CORPORATION

Dallas, Texas

for Langley Research Center

NASA CR-753

TECH LIBRARY KAFB, NM



0099825

FEASIBILITY, PARAMETRIC DESIGN, AND COMPARATIVE
ANALYSIS OF AN UNGUIDED SOLID FUEL ROCKET
VEHICLE WITH SOLAR ORBIT, EARTH PROBE,
AND RE-ENTRY MISSION CAPABILITIES

By T. C. Walker

Distribution of this report is provided in the interest of
information exchange. Responsibility for the contents
resides in the author or organization that prepared it.

Prepared under Contract No. NAS 1-5539 by
LTV AEROSPACE CORPORATION
Dallas, Texas

for Langley Research Center

NATIONAL AERONAUTICS AND SPACE ADMINISTRATION

For sale by the Clearinghouse for Federal Scientific and Technical Information
Springfield, Virginia 22151 - CFSTI price \$3.00

TABLE OF CONTENTS

	<u>Page No.</u>
1.0 SUMMARY	1
2.0 INTRODUCTION	2
3.0 SYMBOLS	3
4.0 FEASIBILITY AND PARAMETRIC DESIGN	5
4.1 Development of the Trans-solar Trajectory Simulation	5
4.1.1 Characteristics of the Nominal Heliocentric Elliptical Trajectories	5
4.1.2 Characteristics of the Geocentric Escape Hyperbolic Trajectories	6
4.1.3 Geocentric to Heliocentric Orbital Transfer	7
4.2 Formulation of Candidate Vehicle Configurations	8
4.2.1 Data Synthesis	8
4.2.2 Staging Analysis	9
4.3 Initial Comparison of Candidate Vehicles	11
4.4 Performance of the Six Candidate Vehicles	12
4.4.1 Performance Capabilities	12
4.4.2 Evaluation of Candidate Vehicles	13
4.4.3 Launch Conditions for Candidate Vehicles	13
4.4.4 Sensitivity of Helocentric Performance	14
4.5 Final Launch Vehicle Selection	15
5.0 428A LAUNCH VEHICLE CHARACTERISTICS	15

	<u>Page No.</u>
TABLE OF CONTENTS	
5.1 428A Launch Vehicle Configuration	16
5.2 Design Data and Analysis	17
5.2.1 Aerodynamic Data	17
5.2.2 Stability Analysis	17
5.2.3 Structural Analysis	18
5.2.4 Weights and Moments of Inertia Data	19
5.2.5 Motor Data	19
5.2.6 Launcher	20
5.3 Trajectory Analysis	21
5.3.1 Trajectory Simulation	21
5.3.2 Flight Profile Restrictions	21
5.3.3 Nominal Trajectory	21
5.3.4 Launch Window Analysis	22
5.4 Error Analysis	23
5.4.1 Error Source Identification	24
5.4.2 Error Propagation	24
5.4.3 Stage Impact Dispersion	25
5.4.4 Mission Accuracy	25
5.5 Guidance and Control	25
5.5.1 Attitude Control System	26
5.5.2 Error Analysis	27
5.6 428A Vehicle Re-entry Studies	27
6.0 VEHICLE COMPARATIVE ANALYSIS	30
6.1 Vehicle Configuration Definition	30

TABLE OF CONTENTS

	<u>Page No.</u>
6.1.1 428A Vehicle	30
6.1.2 Standard Five Stage Scout	30
6.1.3 Improved Five Stage Scout	31
6.2 Payload Volume Comparison	31
6.3 Comparative Performance Analysis	31
6.3.1 Mission Objectives and Requirements	31
6.3.2 Performance Comparison	32
6.3.3 Accuracy Comparisons	34
6.4 Reliability Comparative Analysis	35
6.4.1 Vehicle Reliability Evaluation	36
6.4.2 Reliability Comparative Results	37
7.0 CONCLUSIONS	38
REFERENCES	40
ABSTRACT	41

LIST OF TABLES

<u>Table No.</u>	<u>Title</u>	<u>Page</u>
I	Astrodynamic Constants Utilized in the Study	43
II	List of Motors Considered for Candidate Launch Vehicles	44
III	Candidate Launch Vehicle Configurations	45
IV	Sensitivity of Injection Flight Path Angle to Launch Elevation Angle	46
V	428A Vehicle Weight Statement	47
VI	Sequence of Events	51
VII	428A Vehicle Aerodynamic Heating	52
VIII	428A Vehicle Weights and Inertia Summary	53
IX	Motor Loads Comparison	54
X	Nominal Trajectory Sequence of Events	55
XI	Rocket Motor Variance Data	56
XII	Aerodynamic Variance Data	56
XIII	Launch Conditions, Thrust Misalignment, and Stage Separation Tip-Off Variance Data	57
XIV	Attitude Control System Weight Breakdown	58
XV	Shallow Re-entry Angle Trajectory Guidance Attitude Error Analysis	59
XVI	Intermediate Re-entry Angle Trajectory Guidance Attitude Error Analysis	59
XVII	Comparative Performance Study Objectives and Requirements	60
XVIII	Summary of Trajectory and Launch Vehicle Constraints	61
XIX	Solar Orbit Mission, Comparison of Three Sigma Errors at Injection	62
XX	Earth Probe Mission, Comparison of Three Sigma Errors	63

LIST OF TABLES (Concluded)

<u>Table No.</u>	<u>Title</u>	<u>Page</u>
XXI	Re-entry Mission, Comparison of Three Sigma Errors at Final Stage Burnout	64
XXII	Re-entry Mission Reliability Comparison	65
XXIII	Solar Orbit and Earth Probe Mission Reliability Comparison	65

LIST OF FIGURES

<u>Figure No.</u>	<u>Title</u>	<u>Page</u>
1	Trans-solar Trajectory Definitions	66
2	Determination of the Optimum Departure Direction	67
3	Schematic of the Family of Heliocentric Trajectories under Consideration	68
4	The Variation of Perihelion Radius with Probe Velocity at Sphere of Influence	69
5	Variation of Longitude of \bar{V}_g with Perihelion Radius	70
6	Variation of Period of the Heliocentric Ellipse with Perihelion Radius	71
7	Variation of Perihelion Radius with Energy of the Geocentric Trajectory	72
8	Variation of Perihelion Radius with Injection Velocity	73
9	Variation of Trip Time to Sphere of Influence with Injection Velocity	74
10	Geocentric Portions of Trans-solar Trajectories	75
11	Definition of Sigma Angle and Launch Azimuth	76
12	Relationship Between Range Angle to Sphere of Influence and Flight Path Angle at Burnout	77
13	Typical Launch Vehicle Performance Data	78
14	Launch Conditions for Nominal Heliocentric Trajectory	79
15	Final Stage Weight Estimating Data	80
16	Middle Stages Weight Estimating Data	81
17	Aerodynamic Zero Lift Drag Characteristics	82
18	Algol IIB Booster Performance	83
19	Castor II Booster Performance	84

LIST OF FIGURES (Continued)

<u>Figure No.</u>	<u>Title</u>	<u>Page</u>
20	Optimized Upper Stages for Consumed Weight Versus Ideal Velocity	85
21	Optimized Upper Stages for Inert Weight Versus Ideal Velocity	86
22	Performance Calculations Compared with Computed Trajectories	87
23	Comparison of Candidate Vehicle Heliocentric Performance	88
24	Vehicle Candidate Configurations	89
25	The Effect of Launch Elevation Angle on Conditions at Final Stage Burnout	90
26	The Effect of Launch Azimuth on Burnout Velocity	91
27	Stage Impact Range Data	92
28	Performance Comparison of Candidate Vehicles	93
29	Boost Time Histories of Augmented and Non-Augmented Vehicles	94
30	Launch Conditions for Nominal Heliocentric Trajectory - Vehicle No. 426A, Payload Weight = 10 pounds	95
31	Launch Conditions for Nominal Heliocentric Trajectory - Vehicle No. 428A, Payload Weight = 10 pounds	96
32	Launch Conditions for Nominal Heliocentric Trajectory - Vehicle No. 428A, Payload Weight = 30 pounds	97
33	Vehicle Candidates Performance	98
34	428A Launch Vehicle Configuration External Profile	99
35	428A Launch Vehicle Configuration Inboard Profile	100
36	428A Launch Vehicle Configuration Inboard Profile	101
37	428A Launch Vehicle Configuration Electrical System Schematic Drawing	102

LIST OF FIGURES (Continued)

<u>Figure No.</u>	<u>Title</u>	<u>Page</u>
38	The Variation of Zero Lift Drag Coefficient with Mach Number	103
39	The Variation of First Stage Center of Pressure and Normal Force Coefficient Derivative with Mach Number	104
40	The Variation of First Stage Pitch Damping Coefficient with Mach Number	105
41	The Variation of First Stage Roll Damping with Mach Number	106
42	The Variation of Fin Tip Rolling Effectiveness with Mach Number	107
43	428A Vehicle Structural Design Trajectory	108
44	428A Vehicle Flight Limit Design Loads	109
45	428A Vehicle Hoist Limit Design Loads	110
46	Stage Three Impact Boundary	111
47	Nominal Trajectory Booster Time Histories	112
48	Nominal Trajectory Axial Load and Dynamic Pressure Time Histories	113
49	Time History of Instantaneous Impact Range	114
50	Earth-Sun-Probe Time and Position for a 2/3 Year Period Solar Orbit	115
51	Comparison of Performance Capability	116
52	22 July Launch Window for the Nominal Trajectory - Constant Launch Conditions	117
53	20 March Launch Window - Constant Launch Conditions	118
54	Yearly Launch Window - Constant Daily Launch Conditions	119
55	22 July Launch Window - Variable Launch Conditions	120
56	Stage One Impact Dispersion	121

LIST OF FIGURES (Continued)

<u>Figure No.</u>	<u>Title</u>	<u>Page</u>
57	Stage Two Impact Dispersion	122
58	Stage Three Impact Dispersion	123
59	Joint Density Function of Aphelion and Perihelion Deviations	124
60	Probability of Aphelion and Perihelion Deviations	125
61	Probability of Inclination Deviations	126
62	Attitude Control System Installation, 428A Re-entry Configuration	127
63	Basic Block Diagram of Control System Operation	128
64	Attitude Control System Configuration	129
65	Attitude Control System Pitch and Yaw Deadbands	130
66	Re-entry Performance Capability for One-Up, Three-Down Flight Mode	131
67	Re-entry Range Variation as a Function of Re-entry Angle	132
68	Re-entry Performance Capability for Two-Up, Two-Down Flight Mode	133
69	Re-entry Performance Envelope at Constant Payload Weight	134
70	Re-entry Missions - Altitude - Range and Velocity - Range Flight Profiles for Constant Re-entry Angle	135
71	Re-entry Missions - The Effect of Burnout Altitude on Re-entry Velocity	136
72	Standard and Improved Five Stage Scout Vehicles External Profile	137
73	Payload Volume Comparison - 428A Vehicle Versus Five Stage Scout Vehicle	138
74	Comparison of Solar Orbit Mission Capabilities	139

LIST OF FIGURES (Concluded)

<u>Figure No.</u>	<u>Title</u>	<u>Page</u>
75	Comparison of Earth Probe Mission Capabilities	140
76	Comparison of Injection Velocity for Earth Probe and Solar Orbit Missions	141
77	Comparison of Re-entry Mission Capabilities without Range Restrictions	142
78	Comparison of Re-entry Mission Capabilities at Bermuda for a Constant Payload Weight	143
79	Comparison of Perihelion and Aphelion Deviations	144
80	Comparison of Inclination Deviations	145
81	9 August 1966 Launch Window Comparison	146

FEASIBILITY, PARAMETRIC DESIGN, AND COMPARATIVE
ANALYSIS OF AN UNGUIDED SOLID FUEL ROCKET VEHICLE
WITH SOLAR ORBIT, EARTH PROBE, AND RE-ENTRY
MISSION CAPABILITIES

By T. C. Walker
LTV Astronautics Division

1.0 SUMMARY

An investigation to show the feasibility of orbiting a payload about the sun with an unguided solid fuel rocket vehicle was conducted. An approximate simulation technique was developed for the trans-solar trajectory. Forty-four candidate launch vehicle configurations, composed of existing or development hardware, were formulated for study. After the elimination of all but six candidate configurations, preliminary vehicle performance and launch opportunities were evaluated for each of the prospective vehicles. Based on technical, reliability, and cost considerations, a four stage launch vehicle configuration (428A) was recommended. The motors for this configuration were Algol IIB, X-259, 23KS11000, and BE-3, with two TX-77-13's for first stage thrust augmentation.

The selected 428A vehicle was evaluated from the standpoint of solar trajectory performance and preliminary configurational design. The vehicle was capable of launching from the Mark I launcher at Wallops Station, Virginia, ten and thirty pound payloads into solar orbits with perihelion radii of 0.40 to 0.55 Astronomical Unit, respectively. A nominal trajectory was established within the flight profile restrictions associated with launches from Wallops Station, Virginia. The usable ranges of launch elevation and azimuth angles for this vehicle were determined to be 67.5 to 77.5 degrees and 110 to 140 degrees, respectively. The nominal trajectory was defined as placing a 24 pound payload into a solar orbit with zero inclination angle to the plane of the ecliptic and having a 0.667 year heliocentric orbital period with a 0.528 A. U. perihelion radius. The aerodynamic properties were predicted for the vehicle and a stability analysis was done to evaluate rigid body static longitudinal stability and aerodynamic and structural resonance. Thermodynamic and load characteristics were determined. The Mark I Scout launcher was examined and modifications required to accommodate the 428A vehicle determined.

A launch window analysis determined that for 172 days of the year, the nominal trajectory requirements could be satisfied. The desired trajectory could be closely approximated for the remaining days. For example, on the least desirable day of the year it is possible to obtain an orbit with a heliocentric orbit period of 0.688 year and an inclination to the ecliptic of 3.4 degrees.

An error analysis on the 428A vehicle indicated that stage impact dispersion would present no problems and that solar mission accuracy was sufficient to satisfy the mission requirements. Three-sigma deviations in solar mission accuracy were -0.0155 A.U. in perihelion radius, -0.0017 A.U. in aphelion radius, and -1.32 degrees in inclination to the plane of the ecliptic.

The unguided 428A vehicle was equipped with a simplified attitude control system to provide flight path angle orientation for re-entry missions. A detailed re-entry study was performed on the 428A vehicle to explore its re-entry mission performance capabilities. For a 40 pound payload, re-entry angles as steep as -72.0 degrees at 600 nautical miles and -78.5 degrees at 300 nautical miles can be provided with zero angle of attack at re-entry. The velocities for these angles are 36 150 and 35 300 feet per second, respectively.

The performance of the 428A vehicle was compared with that of two configurations of the five stage Scout vehicle for solar orbit, earth probe, and re-entry missions. There was little difference in the solar orbit payload weight capabilities for the 428A and standard five stage Scout vehicles (26 and 24 pounds, respectively). The improved five stage Scout vehicle showed a 50% increase in payload weight capability (38 pounds). The earth probe capabilities are 89.5 pounds for the improved Scout, 62.0 pounds for 428A, and 60.5 pounds for the standard Scout vehicle for an apogee of approximately 20 earth radii. The re-entry payload weight capabilities for the 428A, standard, and improved five stage Scout vehicles are 47.5, 53.5, and 63.5 pounds, respectively, for a re-entry velocity of 36 000 feet per second at a re-entry angle of -10 degrees without horizontal range restrictions.

Accuracy comparisons for three types of missions and vehicles were made. The difference in solar orbit perihelion radius deviations between the five stage Scout vehicles and the 428A vehicle was 0.004 A.U. at 95% probability. The payload weight capabilities of the five stage Scout vehicles for earth probe missions were about 1.4 times those of the 428A vehicle. For equal payload weight, there was no difference in apogee altitude and time at zero gravity deviations for the three vehicles. The re-entry mission errors in flight path angle and angle of attack were essentially the same for any of the three vehicles, but velocity and altitude errors were larger by 500 feet per second and 80 000 feet, respectively, for the 428A vehicle, based on the fixed flight time at which the effects of error sources were evaluated.

2.0 INTRODUCTION

The LTV Astronautics Division, under the direction of the Langley Research Center, defined feasibility and performed preliminary design on an unguided solid fuel rocket vehicle capable of orbiting a small payload about the sun. The solar orbit, earth probe, and re-entry mission performance of this vehicle were compared to that of two configurations of a five stage Scout vehicle.

Study of this vehicle fulfilled booster requirements associated with solar studies conducted at the Massachusetts Institute of Technology. The mission requirements for these studies are discussed in Reference 1.

The study efforts associated with this vehicle were thorough, but done on a preliminary basis.

This report presents the highlights of the technical investigations and performance comparisons of the 428A launch vehicle configuration. Details of this work may be found in References 2 through 4. This contract has been administered by the Langley Research Center under the technical direction of Mr. C. A. Brown, Jr., of the Applied Materials and Physics Division.

This report is divided into four major sections. Section 4.0 presents a summary discussion of the 428A vehicle's feasibility and parametric design and Section 5.0 discusses characteristics of the 428A vehicle. Section 6.0 presents the comparative analysis with the Scout vehicle. The conclusions of the investigation are presented in Section 7.0.

3.0 SYMBOLS

A.U.	astronautical unit of length (see Table 1)
C_D	aerodynamic drag coefficient
C_{D_0}	drag coefficient at zero angle of attack
C_{N_α}	aerodynamic normal force coefficient per degree of vehicle angle of attack
C_3	total energy parameter, $V^2 - \frac{2K}{R}$, ft ² /sec ²
C.P.	aerodynamic center of pressure
I_{sp}	specific impulse of rocket propellant, sec ⁻¹
i	flight path inclination relative to plane of ecliptic, deg
Δi	inclination deviation, deg
K_\oplus	gravitation constant of earth (see Table 1), ft ³ /sec ²
L.Az.	launch azimuth, deg
L.E.A.	launch elevation angle, deg.
l_{Damp}	aerodynamic roll damping moment, ft-lb
l_{Tip}	aerodynamic roll moment due to fin tip deflection, ft-lb

M	aerodynamic pitching moment, ft-lb
M	Mach number
N_x	longitudinal acceleration, g's
P	spin rate, rad/sec
q	aerodynamic dynamic pressure, lb/ft ²
R	resultant vehicle hoisting force, lb
R	distance (radius) from center of earth, A.U. or n.mi.
ΔR	radius deviation, A.U.
S	aerodynamic reference area, ft ²
S.O.I.	sphere-of-influence where Earth and Sun gravitational forces are equal (see Table 1)
\bar{U}	Earth orbital velocity around the Sun, ft/sec
V	velocity of probe, ft/sec
\bar{V}_s	velocity of probe at S.O.I. = V_{SOI} , ft/sec
V_{SOI}	velocity of probe at S.O.I., ft/sec
W	vehicle weight, lb
α	aerodynamic angle of attack, deg
γ	flight path angle relative to local earth horizontal, deg
γ_{Bo}	flight path angle at time of rocket motor burn-out, deg
δ_{Tip}	vehicle fin-tip deflection, deg
ϵ	vehicle inert weight fraction
μ	vehicle stage mass ratio, initial weight/final weight
σ	inertial range angle between local vertical at launch site and direction of hyperbolic orientation vector, \bar{V}_s (see figure 11), radians
σ_{Act}	Actual range angle from launch site to \bar{V}_s , radians
σ_{Req}	required angle from launch site to V_s , radians
θ	vehicle pitch rate, radians/sec

4.0 FEASIBILITY AND PARAMETRIC DESIGN

A trans-solar trajectory simulation consisting of a geocentric portion and a heliocentric portion was developed along with a technique for matching the geocentric boost trajectories at the sphere of influence with the heliocentric coast trajectories. A family of nominal trajectories was established and candidate launch vehicle configurations were formulated. Initial comparisons eliminated all but six configurations. Performance, launch conditions, and sensitivity to heliocentric performance were evaluated for each vehicle configuration. Based on performance, reliability, and cost, the 428A launch vehicle configuration was recommended. Additional reasons for selection of the 428A vehicle are that it is composed of spin qualified rocket motors and a maximum amount of existing flight proven hardware.

4.1 DEVELOPMENT OF THE TRANS-SOLAR TRAJECTORY SIMULATION

The trans-solar trajectory is a ballistic trajectory that extends from the vicinity of the earth's surface to the vicinity of the sun. In general, a digital simulation of the trans-solar trajectory involves the classical restricted three-body problem of the earth, sun, and space vehicle. It is convenient to subdivide this treatment into two segments for the purpose of preliminary analysis. Each of the two segments is represented by a two-body-problem treatment. The first segment involves the earth and the space vehicle and the second segment involves the space vehicle and the sun. Such a division of a trans-solar trajectory is shown in Figure 1. Within a 500 000 nautical mile radius about the earth, a vehicle may be considered to move on a geocentric escape hyperbolic trajectory influenced only by the earth's gravitational field. The 500 000 nautical mile radius sphere around the earth will be referred to as the earth's Sphere of Influence (S. O. I.). Outside of the earth's S. O. I., a vehicle is considered to move on a heliocentric elliptic trajectory influenced only by the sun's gravitational field. As shown in Figure 1, these two conic section trajectories which are in two different frames of reference can be joined at the earth's S. O. I. by a simple velocity addition for the patch-conic assumption.

4.1.1 Characteristics of the Nominal Heliocentric Elliptical Trajectories

In general, a space vehicle launched from earth with greater than escape velocity will go into a heliocentric orbit with an aphelion radius equal or greater than the earth's orbital radius, a perihelion radius less than or equal to the earth's orbital radius, and will make some inclination angle to the ecliptic plane. Since heliocentric trajectories lying in the plane of the ecliptic (zero inclination angle) require the least geocentric injection energy, the nominal heliocentric trajectories are restricted to lie in the ecliptic plane.

The geometry of an elliptical conic section shows that for a constant geocentric injection energy, a minimum perihelion radius is obtained when the aphelion radius is set equal to the earth's orbital radius of one astronomical unit. This situation is illustrated in Figure 2 using four different orientations of a vehicle's geocentric velocity vector at the earth's S. O. I. In case 1, the velocity vector directly opposes the earth's orbital velocity and a heliocentric velocity less than circular results. The vehicle's exit point at the S. O. I. becomes aphelion and the vehicle follows the minimum-heliocentric-energy trajectory labeled 1 in Figure 2. In case 3, the vehicle's velocity vector directly adds to the earth's orbital velocity and the S. O. I. exit point becomes perihelion. The resulting trajectory is the maximum-heliocentric-energy trajectory labeled 3 in Figure 2. As seen in Figure 2, exiting the S. O. I. in any other direction such as trajectories 2 and 4 will still have greater perihelion than trajectory 1. Escape from the earth's S. O. I. in the retro direction produces minimum energy solar orbits which result in minimum perihelion radius. This technique is used since it gives the greatest above mentioned change in the orbit for a given energy input.

The family of heliocentric orbits considered, schematically represented in Figure 3, have the velocity magnitude and direction and period shown in Figures 4, 5, and 6, respectively.

These heliocentric trajectories encompassed a 0.667 year period orbit which places the probe in opposition to the earth in one year. This orbit is of interest for a specific small payload discussed in Reference 1.

An LTV Astronautics developed patch-conic solar trajectory routine of Reference 5 was utilized in calculating the trans-solar trajectory data. The routine approximates the solution of the classical restricted three-body problem by techniques discussed above. The JPL N-body routine (Reference 6) has shown by comparison that the results derived from the patch-conic simulation are within two percent of the results derived from the N-body routine. The astrodynamic constants used in both the patch-conic solar trajectory routine and the integrating trajectory routine are presented in Table I. A two percent error in velocity and/or perihelion radius is expected since the patch-conic trajectory routine employs a circular earth orbit of one astronomical unit radius whereas the actual earth orbit is slightly elliptical.

4.1.2 Characteristics of the Geocentric Escape Hyperbolic Trajectories

The following guidelines were established:

- (1) Launch Site - Wallops Station, Virginia
- (2) Launch Elevation Angle - 80 degrees maximum
- (3) Launch Azimuth - between 80 to 140 degrees
- (4) Perihelion Radius - 0.4 to 0.9 Astronomical Unit (A.U.)
- (5) Payload Weight - 10 to 30 pounds

The characteristics of the geocentric escape hyperbolic trajectories which connect with the nominal heliocentric ellipses at the sphere of influence are presented in Figures 7, 8, and 9. In Figure 7 the variation of perihelion radius with the energy of the geocentric escape hyperbola is shown. The

energies of Figure 7 have been converted to velocities at three different injection altitudes so that the variation of perihelion radius with injection velocity may be shown in Figure 8. In Figure 9 the variation of the perigee-to-S. O. I. trip time with injection velocity and perihelion radius is shown. It will be noted that the extreme sensitivity of trip time to injection velocity in the region around 0.9 A.U. perihelion radius results because the velocity at the S. O. I. is small. The sensitivity of perihelion can be seen by noting the small incremental velocity separating 0.8 and 0.9 A.U. as compared to 0.4 and 0.5 A.U.

The trajectory simulation from lift-off out to the S. O. I. was accomplished on the modified LTV Near-Earth Mission Analysis Routine (Reference 7) which is a digital computer program that integrates the equations of motion of a vehicle as a six degree-of-freedom rigid body or as a point mass. The modification provides patch-conic routine data at the sphere of influence. The earth and its gravitational potential were represented by an oblate, rotating spheroid whose constants are shown in Table I. The atmosphere simulated in the computations is based on the 1959 ARDC model.

The vehicle was launched from Wallops Station at a specified launch elevation angle and azimuth. A six degree-of-freedom non-spinning simulation was flown for 20 seconds to obtain realistic launch elevation angle simulation. From 20 seconds to final stage burnout the vehicle was represented by a point mass. From lift-off through first stage burnout to a dynamic pressure (q) of three pounds per square foot, the vehicle followed a zero-lift or gravity turn trajectory. At $q = 3.0$ pounds per square foot the second stage was ignited and the vehicle maintained a constant inertial attitude through final stage burnout. From final stage burnout to the sphere of influence, the equations of the conic were solved in closed form to provide the desired trajectory parameters at the S. O. I.

4.1.3 Geocentric to Heliocentric Orbital Transfer

In this discussion, the terminology "orbital transfer" refers to the matching of geocentric boost trajectories at the sphere of influence with the heliocentric coast trajectories. In Figure 10 the planes of three escape hyperbolas are shown which have different inclinations to the earth's equator and pass over Wallops Island at different times of day and with different azimuths. These hyperbolas are part of a family which contains the vector \bar{V}_s that is the required direction of the probe's velocity vector at the earth's sphere of influence. \bar{V}_s makes an angle of 90 degrees with the earth-sun line and lies in the plane of the ecliptic. If the probe has a velocity vector in the direction of \bar{V}_s at the sphere of influence, a minimum energy heliocentric trajectory essentially in the ecliptic will result. Thus, launches from Wallops Station may occur at various times of day, depicted by the three hyperbolas, and a nominal heliocentric trajectory will result.

In Figure 11, the angle sigma required (σ_{req}) is defined as the angle between the local vertical at the launch site and the vector \bar{V}_s . The variation in this range angle with time of day is indicated by the two hyperbolas shown in this figure. The variation of σ_{req} and burnout flight path

angle, $\gamma_{B.O.}$, with time of day is shown in a planar projection in Figure 12. If all three of these boost trajectories of Figure 12 were flown with the same boost vehicle, the launch angle must be varied to provide the desired burnout flight path angle, $\gamma_{B.O.}$, and burnout velocity which then will produce the correct range angle, σ_{act} . Thus, in Figure 12, for a launch at a given time of day to result in a nominal heliocentric trajectory, launch angle must be adjusted to make σ_{act} equal σ_{req} . Figure 13 illustrates the variation of σ_{act} with launch angle for a typical candidate launch vehicle. In addition, Figure 13 presents the variation of injection flight path angle and velocity at the sphere of influence with launch angle as functions of payload weight and launch azimuths.

Figure 14 illustrates how the actual equating of σ_{act} to σ_{req} is accomplished, and thus illustrates the matching of boost and coast trajectories such that nominal heliocentric trajectories are obtained. The lines marked March 21, June 22, September 23, and December 22 show the variation of σ_{req} with launch azimuth at the time of the vernal equinox, summer solstice, autumnal equinox, and winter solstice, respectively. The dashed lines give the required time of day of launch at Wallops Station in Eastern Standard Time. The horizontal lines of launch angle and injection flight path angle (flight path angle at burnout of the last stage) represent the value of σ_{act} corresponding to these parameters and are determined from plots of launch vehicle trajectory data similar to Figure 13. The lines of σ_{req} marked March 21 and September 23 respectively represent the minimum and maximum values of σ_{req} attainable at any given launch azimuth from Wallops Station. The range safety launch azimuth limits specified for Wallops Station are 80 degrees and 140 degrees. Finally, the upper and lower horizontal boundaries represent vehicle maximum dynamic pressure and maximum launch angle limits respectively. Thus, for the vehicle and payload depicted in Figure 14, the launch may occur within the crosshatched boundaries and a nominal minimum energy heliocentric trajectory will result. It will be shown later that launches may also occur outside of these limits with only slight degradation of performance (i.e., perihelion radius and inclination of the heliocentric trajectory to the ecliptic).

4.2 FORMULATION OF CANDIDATE VEHICLE CONFIGURATION

The performance design objective for the launch vehicle candidate is that a 10 pound payload attain a perihelion radius of 0.4 Astronomical Units (A.U.) or a 30 pound payload attain a perihelion radius of 0.7 A.U. using existing or in-development rocket motors. Further, these vehicle candidates should, where possible, utilize existing hardware and be launched from Wallops Station, Virginia.

4.2.1 Data Synthesis

A comprehensive survey of the propulsion industry was made to obtain existing rocket motor ballistic data. The criteria for selection was the vacuum specific impulse or the propellant weight fraction should exceed 250 seconds and 0.80, respectively. A list of rocket motors considered is presented in Table II.

In the preliminary design of launch vehicles, a general practice is to assign representative values of inert weight fraction to the various stages and assume that this fraction remains constant while the overall stage size and weight are varied. This method can result in unrealistic values for actual inert weights because the assumptions are not valid over a wide variation of stage sizes. To avoid this problem, a survey of actual hardware weights for the LTV RAM, SLV-1B (Version 21), SLV-1B (Version 22), Scout, and LV-1B vehicles was made. The total motor weights were subtracted from the actual hardware in order to obtain a set of consistent parametric weights data. In the case of the Scout vehicle, guidance and control system weights were also deleted. It has been determined from past experience that stage inert weight variation correlates well with stage propellant consumed weight. Therefore, the stage inert weight without motors is presented as a function of stage consumed weight for final and middle stages in Figures 15 and 16, respectively. These weight data were used to determine the inert weights for all the candidate launch vehicle configurations.

Representative drag data were selected from existing LTV vehicles and are presented in Figure 17. In general, the booster drag losses for vehicles of this general type are from 10 to 15 percent of the total first stage ideal velocity (or 1000 to 1500 feet per second for a first stage with 10 000 feet per second ideal velocity capability). While these general drag data do not precisely define the drag for the full spectrum of vehicles considered, they are accurate within 10 percent which represents only a one percent change in first stage velocity.

4.2.2 Staging Analysis

The technique of flight involves no guidance system. The first stage of the launch vehicle is aerodynamically stabilized with fins while the upper stages are spin stabilized. For this reason, second stage ignition is delayed until the dynamic pressure falls to 3.0 pounds per square foot. This method of flight results in a substantial weight savings because of no required guidance or second stage fins.

In the strictest sense, a vehicle staging analysis involves the determination of the minimum weight vehicle that satisfies a specific set of mission requirements. The existing motor/hardware requirement of this investigation dictated an approach which would not necessarily result in a minimum weight vehicle.

Because of the high mission velocity requirements, the first-stage motor candidates were determined by selecting the largest solid rocket motors presently fired from the Wallops Station launch site. These were the Algol IIB and Castor II (TX-354-2). Performance capabilities of these two motors as a function of stage one burnout weight are presented in Figures 18 and 19. This performance has incorporated first stage drag, gravity, and thrust-pressure losses to where the dynamic pressure has decreased to 3.0 pounds per square foot and allows for a closed form conic solution to upper stage performance.

The upper stage design analysis consisted of the development of a family of near-optimum vehicles and the development of a family of realistic motor combinations to complete the parametric spectrum.

Propulsion and weights data were used to establish a range of ideal velocity capability for the upper-stages of a four stage launch vehicles. The size relationship of the upper three stages as a function of ideal velocity is shown in Figure 20. The corresponding inert weight of each stage is shown in Figure 21. These figures were determined by holding the relationship $I_{SP} (1 - \epsilon \mu)$ constant for the upper stages, where

I_{SP} = Stage specific impulse

ϵ = Inert Weight fraction of stage

μ = Mass ratio of stage

This formulation provides a near-minimum weight multi-stage vehicle.

Eleven 4-stage configurations were designed utilizing the data of Figure 20 for the approximate stage consumed weight. They range in upper-stage ideal velocity from 30 000 to 36 000 feet per second. After obtaining approximate stage sizes, Figure 15 and 16 and Table II were utilized to obtain vehicle configurations that would match as nearly as possible the optimization requirements of Figure 20. The actual upper-stage motor combinations utilized were designated Vehicles 401 and 411 and are listed in Table III. The key to the vehicle numbering system is as follows:

- (1) The first digit indicates the total number of stages and the second and third digits number the vehicle.
- (2) No letter after the vehicle number indicates that the Algol IIB is used for the first stage.
- (3) Letter "A" after vehicle number indicates an Algol IIB first stage augmented with two TX-77-2 rocket motors.
- (4) Letter "C" after vehicle number indicates a Castor first stage.

On the basis of the staging analysis for Vehicles 401 through 411, additional four and five-stage configurations were designed to complete the parametric spectrum. The additional configurations were designated 412 through 430 and 501 through 505 as shown in Table III. These upper stage configurations, when combined with the two first stages, resulted in a total of 44 candidate vehicle configurations.

The performance of the 44 candidate vehicle configurations was computed utilizing the stage one boost data of Figures 18 and 19 and the ideal velocity and gravity loss equations to obtain the velocity and flight path angle at final stage burnout. The accuracy of this method is compared in Figure 22 to integrated trajectory calculations with final updated weights. The comparison shows less than a one percent velocity error. The general spread of all vehicle configurations considered is illustrated in Figure 33 as payload

weight as functions of final stage burnout velocity and perihelion radius. A performance comparison of candidate vehicle injection velocity for a 20 pound payload is presented in Table III.

4.3 INITIAL COMPARISON OF CANDIDATE VEHICLES

The performance design objective discussed in Section 3.2 can be satisfied by many of the four stage vehicle configurations as can be seen in Figure 23. Therefore, the more complex five stage configurations were eliminated from further consideration.

A detailed investigation revealed that the degree of rocket motor qualification varied when compared against the requirements for an unguided spinning vehicle with a 3 to 5 revolution-per-second range of spin rate. A review of all candidate vehicle configurations showed that vehicle number 428 utilized existing motors which were qualified for spinning and met the 30 pound payload performance design objective. This vehicle was selected as a standard for performance comparison and all vehicles which did not equal or exceed the performance of the 428 vehicle were eliminated from further consideration.

Vehicle number 410 had the greatest performance potential of the optimized configurations and was retained as a candidate configuration even though its upper stage motors were not fully qualified for spinning applications. This selection eliminated all other optimized vehicle configurations and any other non-optimum configuration having performance greater than vehicle number 428, but utilizing any of the motors from vehicle number 410.

The remaining five vehicles with performance capability between vehicles number 428 and 410 are 422, 423, 426, 427, and 429 as shown in Table III. The undeveloped FW-10 motor used on vehicles number 422 and 423 was included mainly to show the potential gain as a replacement for the X-259 motor, therefore, these vehicles were eliminated. Vehicle number 426 has higher performance than either 427 or 429 and was therefore retained as a candidate configuration.

In order to compare first stage booster differences, vehicle number 426C was retained as a candidate configuration. This vehicle has the highest performance capability of the 400C vehicles (i.e., vehicles using the Castor first stage), is composed of available hardware, shows a 10 pound payload weight capability between 0.5 and 0.6 A.U. perihelion radius, and weighs 15 000 pounds less than the other configurations.

Vehicles number 426A and 428A were added to the list of candidate configurations to show the effect of stage one thrust augmentation to reduce sensitivity to wind and first stage thrust variations.

The six candidate vehicle configurations are illustrated in Figure 24 along with pertinent configurational characteristics. The propulsion, weight and aerodynamic characteristics of each configuration were refined in order

that detailed trajectory analyses could be performed. Two significant motor changes were incorporated. They involved substituting the Castor I (XM33-E-7) for the Castor II (TX-354-2) and substituting the XM-85 for the Cygnus 17. The XM33-E-7 (Castor I) change was necessary because recent modifications to the Castor II resulted in less total impulse than expected and decreased initial thrust level. The impulse decrease reduced the velocity advantage of the Castor II to only 600 feet per second over the XM33-E-7. The decreased initial thrust of the Castor II reduced the usable launch elevation angle of this motor to less than 2 degrees. The Cygnus 17 to XM-85 change was made because the Cygnus 17 is not a developed motor.

4.4 PERFORMANCE OF THE SIX CANDIDATE VEHICLES

The performance capabilities of each of the six candidate vehicles were evaluated. Based on this evaluation, all but two configurations were eliminated. First stage thrust augmentation was retained as it reduced launch angle sensitivity by a factor of two. Yearly launch conditions were determined for each configuration and the effect of payload weight on these conditions evaluated.

4.4.1 Performance Capabilities

The performance capability of vehicle number 428, which is representative of the six configurations considered, is presented in Figure 25 as final stage burnout conditions as a function of launch elevation angle for a 10 pound payload weight and a 110 degree launch azimuth. Velocity is fairly insensitive to a change in launch elevation angle while flight path angle varies considerably. Within the range of launch elevation angles considered, the change in energy (C_3) results in a change of perihelion radius of only 0.006 A.U. The minimum launch elevation angle is dictated by a maximum dynamic pressure criterion of 5000 pounds per square foot.

For a constant payload weight, final stage burnout velocity (Figure 26) is fairly insensitive to changes in launch azimuths between 80 and 140 degrees. From Figure 27 minimum and maximum impact ranges of the three stages are as follows:

Stage	Minimum Range (Nautical Miles)	Maximum Range (Nautical Range)
1	298	380
2	920	1620
3	6000	11 400

4.4.2 Evaluation of Candidate Vehicles

The performance of the six candidate vehicles is summarized in Figure 28 for payload weight as a function of final stage burnout velocity and perihelion radius. The performance of Vehicles 426 and 428 did not change appreciably from the preliminary computations. The addition of the TX-77-2 thrust augmentation rockets on Vehicles 426 and 428 decreased the injection velocity by approximately 300 feet per second because the expended augmentation rockets were not jettisoned until stage one burnout.

On Vehicle 410, the change from the Cygnus 17 to the XM-85 decreased the performance appreciably. As can be seen in Figure 28, the performance of Vehicle 410 is below that of Vehicle 426 at payload weights between 10 and 20 pounds. Because of this decreased performance, Vehicle 410 was eliminated as a candidate vehicle.

The performance of Vehicle 426C is more than 4000 feet per second below that of Vehicle 426A. Since the vehicle was analyzed only to compare the first stages, this performance penalty justified the elimination of the 426C or the Castor booster as a candidate configuration.

The sensitivity of injection (final stage burnout) flight path angle to launch elevation angle with-and without stage-one thrust augmentation is presented in Table IV. Note that the launch angle sensitivity is reduced by a factor of two by using thrust augmentation on both Vehicles 426 and 428. From the data of Table IV it can be inferred that thrust augmentation reduces the effects of winds by increasing the lift-off thrust-to-weight ratio. As shown in Figure 29, the maximum dynamic pressure will also be reduced for equal injection flight path angles because the altitude time history is always higher for thrust augmented vehicles.

Because of the practical advantage in thrust augmentation, it was decided to use this approach and accept the slight velocity penalty. Therefore, Vehicles 426 and 428 were eliminated leaving only Vehicles 426A and 428A.

4.4.3 Launch Conditions for Candidate Vehicles

The launch conditions for launching a 10 pound payload into a nominal heliocentric trajectory are presented in Figures 30 and 31 for Vehicles 426A and 428A, respectively. As the launch conditions for both vehicles are similar, only Vehicle 428A will be discussed. In Figure 31, Vehicle 428A exhibits a launch opportunity period covering an entire calendar year. On the date of the vernal equinox (March 21), launches into the nominal heliocentric trajectory, may occur at launch azimuths ranging from 80 degrees (at 12.3 PM, E. S. T. with a launch angle of 74.8 degrees) to 96 degrees (at 2.0 PM, E. S. T., with a maximum allowable launch angle of 80 degrees). On the dates of the summer and winter solstices (June 22 and December 22, respectively), launches into the nominal heliocentric trajectory may occur

throughout the entire permissible range of launch azimuths. On these dates, launches from Wallops Station into the nominal heliocentric trajectory are possible until approximately 3.3 PM, E. S. T. At this time of day the maximum permissible launch azimuth of 140 degrees is required. The launch angle required is 79.3 degrees and the resulting burnout flight path angle is approximately 57 degrees. On the date of the autumnal equinox (September 23), the range of required launch azimuths is 87 to 140 degrees. The range of required launch angles is 64.4 degrees, which is the maximum dynamic pressure limit, to 72.2 degrees. The range of times of day of launch varies from 8.5 AM to 2.15 PM E. S. T. Perihelion radii for the resulting nominal trajectories vary only from 0.41 to 0.43 A.U. inside the boundaries shown.

The effect of payload weight change on launch conditions is evident by comparing Figures 31 and 32. The significant difference is that the 30 pound payload weight shown in Figure 32 reaches perihelion radii of between 0.57 to 0.60 A.U. while the 10 pound payload weight shown in Figure 31 goes down to 0.41 to 0.43 A.U.

The cross hatched lines shown in these figures do not represent absolute limits on the launch conditions that may be utilized with a given vehicle. Operation inside the limits only assures that the minimum energy heliocentric trajectories will be attained. The sensitivities of perihelion distance and inclination of the heliocentric trajectory to the ecliptic as a function of the launch conditions are extremely low and operation outside of the limits shown in Figures 30 through 32 may be permitted without a significant reduction in overall performance.

4.4.4 Sensitivity of Heliocentric Performance

For 1.0 A.U. aphelion radius orbits, performance is characterized by perihelion radius and inclination angle of the heliocentric trajectory plane to the ecliptic. These two parameters are affected directly by final stage burnout flight path angle, velocity, altitude, and azimuth. A sensitivity analysis was conducted for a trajectory with a nominal perihelion radius of 0.5 A.U. and injection flight path angle of 20 degrees to evaluate the anticipated accuracy for an unguided solar probe. The deviations in perihelion radius resulting from variations in flight parameters are as follows:

<u>Parameter Variation</u>	<u>Perihelion Radius Deviations</u>
2.0 deg Launch Elevation	0.006 A.U.
1000 ft/sec Injection Velocity	0.047 A.U.
5.0 deg Launch Azimuth	≈ 0

These combined errors result in an overall perihelion radius deviation of less than 5 percent.

4.5 FINAL LAUNCH VEHICLE SELECTION

The criteria to be used in selecting the final rocket motor configuration for the solar orbit mission are:

- (1) Maximum velocity attainable with a 10 pound payload
- (2) Rocket motor reliability
- (3) Cost

The performance of the two remaining vehicle configurations is presented in Figure 33. The 426A vehicle performance exceeds that of the 428A configuration, however, further development of the 426A vehicle's 15 inch Aerojet motor would be required. A motor development program did not appear justified as the 428A configuration exceeds the 30 pound payload weight design objective and lacks less than 0.02 A.U. achieving the 10 pound payload weight design objective. The 428A vehicle utilizes more existing hardware than the 426A configuration and this hardware has been proven on the SLV-1B vehicle. Therefore, it is concluded that Vehicle 428A could best accomplish the mission energy requirements with existing motors and hardware.

The reliability history and existing funded programs for the motors used on the 428A vehicle preclude a need for additional development. The third and fourth stage motors of Vehicle 426A are not fully qualified. The third stage FW-4 motor has a minor insulation problem. The fourth stage 15 inch Aerojet motor has not been qualified to the lower spin rates. Rocket motor selection and use of existing hardware are the two major sources of total program cost. In general, there is a small recurring cost advantage with Vehicle 426A, however, there is a rather large non-recurring cost advantage with Vehicle 428A. Based on a three vehicle program, the total cost difference would be in favor of the 428A vehicle.

The 428A launch vehicle configuration is recommended as the final selection based on technical, reliability, and cost considerations. This configuration satisfies performance design objectives using existing motors and minimum modification to existing hardware. In addition, the mission is insensitive to errors usually associated with unguided probes and daily launch opportunities exist from Wallops Station, Virginia.

5.0 428A LAUNCH VEHICLE CHARACTERISTICS

Preliminary design analysis were conducted to evaluate the 428A launch vehicle's aerodynamic, stability, structural and mass characteristics. A review of the motors used on this vehicle was made. Feasibility of launching the 428A vehicle from the Scout Mark I launcher with minor modifications was

established. A launch window analysis was done to investigate daily and yearly launch opportunities with both fixed and variable launch conditions. An error analysis was conducted to determine stage impact dispersion and mission accuracy. The 428A vehicle was equipped with simplified attitude control system and its re-entry performance evaluated. Different schemes for performing re-entry missions were studied both with and without horizontal range restrictions.

5.1 428A LAUNCH VEHICLE CONFIGURATION

The external profile of the selected 428A configuration is shown in Figure 34. The vehicle is composed of the following major components:

- (1) Heatshield for payload and upper stage motors
- (2) BE-3 A3 fourth stage motor
- (3) Section "J" interstage structure between fourth and third stage motors
- (4) 23KS11000 third stage motor
- (5) Section "G" interstage structure between third and second stage motors
- (6) X-259-A4 second stage motor
- (7) Section "G" interstage section between second and first stage motors
- (8) Algol IIB first stage motor
- (9) Two TX-77 first stage auxilliary thrust motors
- (10) Two 0.24KS9900 spin-up motors and support ring
- (11) Base "A" structure and four aerodynamic fins

The heatshield is almost identical to that currently used on the SLV-1B launch vehicle with a 24.0 inch aft end extension. The rocket motors are described in Section 5.2.5. A weights statement for this vehicle is presented in Table V. Four aerodynamic fins are attached to Base "A" of the vehicle in a cruciform configuration. Each fin has a 45 degree delta platform consisting of an exposed area of 7.15 square feet. The fin section is an eight degree wedge. The tips of each of the fins are pre-set in deflection in order to establish a final vehicle spin rate of three revolutions per second at first stage burn-out.

Additional internal details of the structural components of the vehicle are shown in Figures 35 and 36. Electrical system schematic drawings are presented in Figure 37 along with location, function, and electrical component

part numbers.

The data presented in Table VI describes in detail a typical sequence of events for the 428A Vehicle.

5.2 DESIGN DATA AND ANALYSIS

5.2.1 Aerodynamic Data

The aerodynamic properties of the 428A vehicle were predicted based on transonic and supersonic wind tunnel test data for the configurationally similar SLV-1B and Scout vehicles. Minor differences such as flare angles, adjusted fin size, and body diameter and length were adjusted, using reference data accumulated from previous LTV booster design efforts and wind tunnel tests. The drag effect of the two TX-77 motors was evaluated from data presented in Reference 8. Computed variation of zero lift drag coefficient as a function of Mach number is presented in Figure 38 for both the first and second thrusting stages of the vehicle. First stage variations of center of pressure and normal force coefficient derivative with Mach number are presented in Figure 39. First stage pitch and roll damping are presented in Figures 40 and 41, respectively. Fin tip rolling effectiveness is presented in Figure 42.

5.2.2 Stability Analysis

During the stage-one ascent burn phase, the unguided 428A vehicle is stabilized with aerodynamic fins which provide a minimum of rigid body static margin of approximately 18 inches. Upper stages of the vehicle are gyroscopically stabilized external to the sensible atmosphere (zero dynamic pressure) by spinning the vehicle about its longitudinal axis. Vehicle spinning is initiated immediately after lift-off with the firing of two 0.2 MKS9900 solid propellant rocket motors mounted tangentially on opposite sides of the Algol motor. The four first stage fin tips are canted 12.7 degrees to produce a spin rate at first stage burnout of approximately 3.0 revolutions per second. This spin rate will result in a constant inertial attitude of the upper stages of the vehicle until final stage burnout. While vehicle spinning is done primarily to stabilize the upper stages, it will tend to nullify first stage errors resulting from thrust misalignment and fin misalignment. This stabilization technique has been successfully demonstrated on the LTV Astronautics RAM, SLV-1B, and LV-1B probe vehicles.

Calculated spin rate time histories have shown that aerodynamic resonance will occur shortly after lift-off as the spin rate overtakes and exceeds the pitch natural frequency of the 428A vehicle. However, this will occur during only a small fraction of a cycle and will not result in any significant resonance response. The spin rate and the first natural structural bending frequency are separated at least 50 percent and adequate assurance against structural resonance is provided.

An analysis of upper stage tip-off errors resulting from stage separation revealed that by using a V-band clamp, rather than a blowout diaphragm the three-sigma separation tip-off angles would be 1.5 degrees for the second stage and 2.0 degrees for the third and fourth stages.

5.2.3 Structural Analysis

The most critical aerodynamic heating and maximum aerodynamic loads result from the launch trajectory corresponding to the lowest usable launch elevation angle. Based on consideration of injection path angle and dynamic pressure limitations subsequent to jettison of the first stage, a minimum usable launch angle of 65 degrees was selected for the design trajectory. Altitude, Mach number and dynamic pressure for the structural design trajectory are presented on Figure 43.

A preliminary aerodynamic heating analysis was performed to determine transient temperature histories at eight locations on the launch vehicle external surface structure. These time-temperature histories are shown in Reference 3. A summary of the maximum external and internal temperatures computed for each location is shown in Table VII. In all cases the maximum computed temperatures exceeded the allowable temperatures for the structural materials except for the X-259 motor which is currently delivered with cork protection. Subsequent analyses were performed to determine feasibility of applying external thermal protection, namely cork, or increasing the back wall heat sink to reduce structural temperatures to an acceptable level. It was determined that addition of the cork external layer or increasing heat sink were feasible approaches to provide the necessary thermal protection. A detailed analysis to optimize the thermal protection thicknesses was not made.

The structural design loading conditions considered included the combined effects of maximum aerodynamic loads imposed on the vehicle during boost, the acceleration loads due to rocket thrust, and loads due to a Sissenwine synthetic wind for one percent risk and a one percent probability step function. The design factor used for the product of dynamic pressure and aerodynamic angle of attack, $q\alpha$, was 10 000 degree-pounds per square foot. Design loads were also computed for hoisting of the vehicle on the launcher based on a ground handling factor of 1.5. Flight design loads are presented in Figure 44 and launcher hoist loads in Figure 45. Weights distribution, stiffness, and free-free bending modes were calculated and are contained in Reference 3.

Limit flight loads were multiplied by a factor of 1.25 to obtain ultimate flight loads. Limit ground handling loads were multiplied by 1.5 for ultimate ground handling loads. Using the ultimate design loads, a stress analysis was performed on each of the major structural components of the vehicle. A detailed description of each of the structural components and stress analyses can be found in Reference 3.

5.2.4 Weights and Moments of Inertia Data

Table VIII presents a summary weight statement for the 428A vehicle. In addition, center of gravity location along with pitch and roll moments of inertia are presented as functions of vehicle stage weight.

5.2.5 Motor Data

The following is a brief discussion of the usage history of each of the motors selected for the 428A vehicle. Nominal and plus and minus three standard deviation propulsion data for these motors are contained in Reference 3.

ALGOL IIB - A total of 35 Algol series motors have been fired. Of this group, 23 were the Algol IIA and 12 were Algol IIB configurations. The single failure of the Algol IIA was due to nozzle insert and insert bonding deficiency. Appropriate redesign was accomplished and the modified motor was redesignated Algol IIB. No failures have been experienced with Algol IIB. The Algol motor was successfully fired while spinning during a demonstration flight conducted on 17 March 1960.

TX-77-2 - This motor has been in use for many years on various NASA probe vehicles. It has demonstrated an outstanding record of nine static firings and 138 flight firings without failure. For the 428A vehicle application, the cant angle of nozzle will be increased from 7 degrees to 8.5 degrees by a minor modification of the nozzle attachment flange.

X-259-A-3 - This motor has been flown on 25 Scout vehicles with a record of no failures. The X-259 is also used on the Fire Velocity Package and the SLV-1B probe vehicles which are spin stabilized.

23KS11000 - This motor has been subjected to seven successful static firing tests including one spin test. The 23KS11000 is an improved version of the 3OKS8000 which has been successfully fired 26 times. The 3OKS8000 motor was used on the RAM B and SLV-1B spin stabilized launch vehicles.

BE-3 A3 - This motor has been utilized for a variety of launch vehicle and spacecraft applications. It was qualified by seven static firings and thirty development rounds. To date, the BE-3 motor has been successfully fired 46 times including flights with spin rates up to five revolutions per second.

0.24KS9900 - This motor is to be used as a spin motor for the 428A vehicle and has been used on the RAM B, LV-1B, and SLV-1B launch vehicles. An exceptional record has been demonstrated with 175 firings without failure.

The X-259, Algol, and 23KS11000 motors have been structurally qualified by previous usage for the 428A vehicle flight and hoisting ultimate design loads. A comparison of design loads on these motors to previous flight and test loads on the motors is shown in Table IX.

5.2.6 Launcher

The design of the Mark I (Scout) launcher which exists at Wallops Station has been analyzed to determine the feasibility of launching the 428A vehicle from this complex. It is concluded that minor modifications, which can be made in the field, will provide compatibility between the 428A vehicle and the Mark I launcher.

The first stage of the 428A vehicle differs from the Scout in the use of the two TX-77 auxiliary booster motors and the larger aerodynamic fins. The Mark I aft launch support structure will be extended eight inches to clear the larger fins, and the upper horizontal members will be lowered to clear the TX-77 nozzles. In addition, the upper support arms (split hooks) will be extended eight inches to maintain the proper vehicle alignment.

The desired launch elevation and azimuth of the 428A vehicle will vary as a function of the payload weight and time of launch. The Mark I launcher does not include provisions for rapid variations in launch angle since this angle is constant for each Scout launch. The pitch adjustment capability can be easily provided by simple reinstallation of a hydraulic mechanism which was initially included on the Mark I launcher. This equipment will provide a pitch adjustment between 70 and 90 degrees. A new lifting jack and locking mechanism would be required for the beam if launch angles less than 70 degrees were desired.

Remote positioning of the launcher azimuth, within a twenty degree segment, can be accomplished by including switches in the blockhouse console unit for control of the racine hydraulic solenoid valves which actuate the azimuth drive motor. An azimuth readout system could be simply devised by mounting a television camera on the back of the launcher in a position to read azimuth marks on the outer launcher rail. Experience has shown that the area suggested for the television camera does not receive blast damage. The camera would be installed just prior to the scheduled launch and removed afterwards, similar to the existing arrangement on the Mark II fueling unit. The existing television screen which is mounted on the Mark I blockhouse console unit four would be used for launch azimuth readout.

5.3 TRAJECTORY ANALYSIS

During this portion of the study, emphasis was shifted to detailed investigation of the vehicle's capabilities for one specific set of payload requirements.

5.3.1 Trajectory Simulation

The non-spinning trajectory simulation discussed in Section 4.1.2 was used in this performance analysis. From a performance standpoint, use of a spin-stabilized or a non-spinning gravity turn profile causes no reduction in vehicle performance. The previous performance work was based on a second stage ignition dynamic pressure of 3.0 pounds per square foot. In this analysis the second stage ignition dynamic pressure is 1.0 pound per square foot.

5.3.2 Flight Profile Restrictions

The restrictions placed on the vehicle's flight profile were derived from stage impact considerations. It is desirable for all vehicle components to nominally impact in water and should any upper stage fail to ignite or have to be destructed subsequent to stage-one burnout, all debris should impact within the Wallops Station and Atlantic Missile Range.

Investigations have shown that launch azimuths greater than 140 degrees could result in impact of stage two on or near the island of Antigua. Figure 46 presents a map of stage-three impact locations for the vehicle launched at various launch elevation and azimuth angles. For launch azimuths less than 110 degrees, there is a possibility of stage-three impact on South Africa. Launch elevation angles greater than 77.5 degrees could result in stage three impact on South America. For launch elevation angles less than 67.5 degrees, the injection flight path angle becomes extremely sensitive to changes in launch elevation angle. Therefore, these values constitute the usable ranges of launch elevation and azimuth angles for 428A vehicle.

5.3.3 Nominal Trajectory

The nominal trajectory for the 428A launch vehicle was selected using three basic criteria; 1) location of stage three impact, 2) requirement for a 0.667 year period solar orbit, and 3) availability of mission launch dates.

In consideration of the three criteria, a launch azimuth of 120 degrees from the Scout Mark I launch facility at Wallops Station, a launch elevation angle of 73.8 degrees, and a payload weight of 24 pounds were selected. The characteristics of the resulting nominal trajectory are presented in Table X and Figures 47 through 49.

Table X presents the sequence of events and Figure 47 shows the boost time histories. Figure 48 presents the axial load and dynamic pressure for the 428A vehicle's nominal trajectory. The maximum axial force is 105 g's and occurs at final stage burnout. The maximum dynamic pressure is 2770 pounds per square foot and occurs at 28.5 seconds after lift-off. Variation of instantaneous impact range from the launch point as a function of time is presented in Figure 49.

The selected combination of launch conditions and payload weight produces a nominal heliocentric trajectory having a 0.667 year period, zero degrees inclination to the ecliptic, and minimum heliocentric energy, i.e., maximum utilization of launch vehicle's energy. The earth-sun-probe time and position relationships for this trajectory are illustrated in Figure 50.

Figure 51 presents a comparison of the 428A vehicle's current performance capability to the capability shown in the earlier preliminary analysis. There is approximately 150 feet per second reduction in injection velocity for a 10 pound payload weight. These differences result from the following changes:

Weight increase and updated rocket motor data	-246 feet per second
Second stage ignition at a dynamic pressure of 1.0 instead of 3.0 pounds per square foot	-48 feet per second
Addition of 2.0 second coast period to upper stages	-85 feet per second
Change in drag coefficient	<u>+227</u> feet per second
Net change	= -152 feet per second

5.3.4 Launch Window Analysis

The launch window characteristics such as launch conditions to be used on any given hour of any given day of the year and heliocentric performance associated with these conditions are heavily dependent upon the type of heliocentric trajectory required for a given experiment and the launch operations philosophy adopted.

The launch window data were computed for the powered portion of the trajectories using a non-spinning six-degree-of-freedom digital simulation to injection conditions. These injection conditions were used in conjunction with the LTV developed patch-conic solar trajectory routine which calculated all the elements of the resulting heliocentric trajectories.

The conditions used to compute the launch window data are as follows:

- (1) Payload is 24.0 pounds
- (2) Inclination of the heliocentric trajectory to the ecliptic plane is nominally zero degrees.

- (3) The period of the heliocentric trajectory is nominally 0.667 of a year.
- (4) Aphelion distance is nominally 1.0 A.U. which permits maximum utilization of the energy developed by the launch vehicle.
- (5) Launch azimuth is restricted to the 110 to 140 degrees range because of upper stage impact considerations.
- (6) Launch elevation angle is restricted to lie in the range of 67.5 to 77.5 degrees.

Daily launch windows for the 428A launch vehicle are presented in Figures 52 and 53 for constant launch conditions. Figure 52 is a launch window for 22 July 1966, an example of one of the best times of year to launch. The best time of year to launch the 428A vehicle from Wallops Station, Virginia, covers a 172 day period from 25 June 1966 to 14 December 1966. Figure 53 presents the window for the worst time of year to launch, 20 March 1966 (the approximate vernal equinox). Even then the orbital period can be brought down to 0.688 years with an inclination angle of only 3.4 degrees.

The duration of a daily window is determined once the limits are established for the amount of tolerance to be allowed on such parameters as perihelion radius, inclination angle, or period. Figure 54 presents a yearly launch window for the period of time between the vernal equinoxes of 1966 and 1967. This figure illustrates, for any given day, the choice of launch azimuth and elevation angles required to produce minimum perihelion radii along with the corresponding inclination angles and orbital periods.

In Figure 54 the 172 day time period between 25 June and 14 December during which the inclination angle can be maintained at zero degrees and period at 0.667 of a year is clearly shown. An alternate mode of operation would be to remove the 0.667 of a year period restriction and let perihelion radius decrease to a minimum in the vicinity of the autumnal equinox. However, such an operation would require a change in the launch azimuth and launch elevation angle schedules. Another alternative would be to reduce the payload weight to the minimum allowable. This would permit a reduction in perihelion radius throughout the year or an increase in inclination angle. Figure 55 presents a daily launch window with variable launch conditions. The launch elevation and azimuth angles were varied in such a manner as to keep the variations in perihelion radius, inclination angle, and period to a minimum.

The nominal launch date was chosen to be 22 July 1966 and the launch windows such as Figure 52 and 55 will result for the nominal boost trajectory.

5.4 ERROR ANALYSIS

An error analysis was conducted to assess the accuracy with which the 428A vehicle could perform the solar mission and to establish the impact dispersion of the expended stages. The nominal mission defined by the following requirements was selected for the analysis:

Payload Weight = 24 pounds

Solar Orbit Period = 0.667 year

Inclination to the Ecliptic = 0 degrees

Perihelion Radius = 0.528 A.U.

The launch conditions producing this nominal trajectory are:

Launch Site = Wallops Station, Virginia

Launch Elevation Angle = 73.8 degrees

Launch Azimuth = 120 degrees

The selection of the nominal trajectory permits the presentation of deviations about a planned mission and represents a typical set of results.

5.4.1 Error Source Identification

The identification of error sources was made and the associated magnitudes determined utilizing experience from previous error analyses since these data were not readily available for most error sources associated with the 428A vehicle. The three-sigma deviations in rocket motor, aerodynamic, and stage separation tip-off variance data are presented in Tables XI through XIII.

5.4.2 Error Propagation

Boost trajectories were computed on a six-degree-of-freedom computer program (Reference 7) incorporating three-sigma values of each individual error source. The results of these trajectories show the manner in which each individual error is propagated through the trajectory to produce deviations in stage impact points and injection (final stage burnout) conditions. The deviations were assumed linearly related to the error source magnitudes and the root-sum-square of the deviations due to individual three-sigma errors were interpreted as overall three-sigma deviations in stage impact dispersions and injection conditions. Previous Scout launch vehicle experience has shown this to provide a good first order approximation to the overall dispersion.

Accuracy of perihelion radius, aphelion radius, and inclination of the heliocentric trajectory to the ecliptic were developed using a theoretical sampling technique of Reference 9. Boost trajectories were generated for each of 19 statistically independent errors to evaluate the deviations injection conditions. These deviations were propagated to the heliocentric side of the earth's sphere of influence using a patch-conic coast trajectory routine to evaluate deviations in radius, velocity, flight path angle, and azimuth relative to the sun and ecliptic plane at the initial point of the heliocentric trajectory. Finally, the deviations at the sphere of influence were sampled by

a Monte-Carlo error analysis program which determined the statistical distribution of deviations in heliocentric orbit characteristics.

5.4.3 Stage Impact Dispersions

The dispersion patterns about the nominal impact point for stages 1, 2, and 3 are presented in Figures 56 through 58, respectively. The dispersion pattern for stage three differs from those for stages 1 and 2 because stage three is near orbital velocity at burnout and errors affecting both velocity and flight path angle result in predominantly in-plane range dispersion.

5.4.4 Mission Accuracy

Figure 59 presents the joint density function of aphelion and perihelion radius deviations which is the basic result of the mission accuracy dispersion analysis. The origin of this figure represents the values of aphelion and perihelion radii associated with the nominal booster trajectory and the resulting nominal heliocentric trajectory. Each square on the grid represents a 0.001 A.U. deviation in aphelion and perihelion radii. The numbers in the squares represent the total number of times out of 10 000 tries that aphelion and perihelion radii will fall within the limits defined by any one square. Considering each separately, the probability that aphelion or perihelion radius will fall within certain limits is shown in Figure 60. These data were obtained from Figure 59 by summing all the occurrences within a given range of either aphelion or perihelion radius and dividing by 10 000. A deviation of ± 0.0155 A.U. perihelion radius and a ± 0.0017 A.U. aphelion radius is associated with a probability of 99.7 percent.

Figure 61 presents the probability of deviation in the inclination of the heliocentric trajectory to the ecliptic plane. The three-sigma deviation in inclination angle is 1.32 degrees.

5.5 GUIDANCE AND CONTROL

In order to conduct re-entry mission performance studies on the 428A vehicle as specified in this phase of study, the unguided vehicle required an attitude control system to provide flight angle control.

Development of an attitude control system for the 428A vehicle was not feasible because of the associated large non-recurring cost involved. Therefore, a survey of the control system industry was made to evaluate and select an existing attitude control system for the spinning 428A vehicle. The Whittaker Corporation of Charsworth, California, proposed the most desirable control system to provide re-entry flight path control for the 428A vehicle and as proposed, the system meets the vehicle control requirements.

5.5.1 Attitude Control System

The selected attitude control system is similar to the one which was used on the Sandia Corporation's Nike-Tomahawk vehicle in the Solar Eclipse Program. The system is a self contained, nitrogen gas, attitude control system and requires only one vehicle support system. The control system is dependent upon a ground command signal to activate a preset programmer. This technique was chosen in order to eliminate the flight time clock from the programmer. The system only controls the vehicle as it spins during coasting phases external to the atmosphere (zero dynamic pressure). However, telemetry attitude data are monitored from lift-off up to third stage ignition. This system can be adapted to the 428A vehicle with minor modifications (i. e., system gain changes, deadbands, control nozzle thrust levels, and nitrogen tank size).

This attitude control system has the capability of producing control during the first two coast phases of a re-entry mission. The first coast phase occurs between first stage separation and second stage ignition in which pitch control rates of 0.522 degrees per second can be produced. The second coast phase occurs between second stage burnout and second stage separation in which pitch control rates of 1.710 degrees per second can be produced. The second coast phase control rates are higher than the first because of the absence of the second stage motor propellant. These pitch control rates are sufficient to accommodate the re-entry control requirements.

The control system components are presented in Table XIV with Whittaker part numbers and weights. Installation of the control system components in the vehicle's transition sections "G" and upper "C" is illustrated in Figure 62.

A block diagram of the control system's functional operation is presented in Figure 63. Referring to Figure 63, the miniature attitude reference system (MARS) sensor employs a pair of free gyros mounted on a platform roll stabilized with a servo motor and a gear train link. Gimbal movements of these gyros furnish roll, pitch, and yaw attitude information which are processed electronically to derive rate information. Analog error signals for all three body axes are obtained by summing the product of the rate signals and system gains with the displacement signals. The analog roll error signal is used to drive the servo motor which stabilizes the platform. The analog pitch and yaw error signals are used to control the attitude of the vehicle. Two wipers are fixed to the roll-stabilized platform and are each connected to a single control jet. The two diametrically opposed control jets are mounted normal to the vehicle spin axis. The analog mixed error signals in pitch and yaw, used to fire the control jets, are fed to a four bar commutator which rotates with the vehicle. When one of the bars of the rotating commutator which has an error signal makes contact with one of the non-rotating wipers, the selected control jet is fired provided the error signal exceeds the system deadband. The wiper, commutator, and control jet arrangements are illustrated in Figure 64. The control system deadbands in pitch and yaw are illustrated in Figure 65 on phase planes of rate as a function of displacement. The deadbands have been estimated to be 0.2 degree in both pitch and yaw. The amount of pitch orientation

desired is preset into the system in the form of an electrical bias.

The pneumatic reaction control system consists of a 1300 cubic inch toroidal tank, a squib actuated valve, a single stage regulator, two control jet nozzles, and associated plumbing.

The control system has guidance reference adjustment capability to accommodate launcher final wind aiming requirements and provides twenty-four hour launch capability.

This system serves a dual role. For re-entry missions, the attitude control system is utilized for flight path control and telemetry attitude data. For solar orbit missions, the reaction control system is removed and the attitude sensor and associated electronics are used for telemetry attitude data. A detailed discussion of the control system and its selection is presented in Appendix C of Reference 4.

5.5.2 Error Analysis

Additional modifications to the standard MARS sensor were considered in order to improve the accuracy of control. These modifications are special production techniques including individual gyro bearing testing and selection, photopotentiometer pickoffs, increased precision of pivot and bore alignment, and new high precision fixturing for gimbal inspection.

An error analysis was performed on the improved MARS sensor and is documented in Reference 10. The total guidance attitude errors in the pitch and yawaxes for the shallow and intermediate re-entry angle trajectories are presented in Tables XV and XVI. The roll error has been broken down and included in the pitch and yaw errors.

5.6 428A VEHICLE RE-ENTRY STUDIES

A study was conducted which determined that it is feasible to use the 428A launch vehicle to perform re-entry missions. The only significant modification to the basic 428A vehicle is the addition of a simplified guidance and control system to pitch the spinning vehicle during first and second stage coast phases. The re-entry mission trajectories considered were fundamentally of two types; ballistic trajectories with no horizontal range restriction and shaped trajectories which were constrained in range.

The maximum allowable launch elevation angle was taken to be 82 degrees due to range safety considerations associated with launching an unguided vehicle from Wallops Station. Separation of the first stage was not permitted until the dynamic pressure fell below 0.001 pounds per foot to ensure that destabilizing aerodynamic forces would not be encountered. A further constraint on the re-entry trajectories required final stage burnout to occur at or above 400 000 feet.

One scheme for performing re-entry missions with the 428A vehicle utilizes one ascent stage and three descent stages. The descent stages are fired sequentially with little or no coast time between stages. Figure 66 shows re-entry performance for one-up, three-down flights. Zero angle of attack occurs at the assumed re-entry altitude of 250 000 feet (final stage burnout is at 400 000 feet). This figure indicates the relationships between re-entry velocity, payload, and re-entry angle without range restrictions. The payload impact ranges vary between 370 nautical miles and 650 nautical miles for this flight mode, as can be seen on the one-stage up-three down portion of Figure 67.

Firing the second stage soon after first stage burnout (two-up, two-down flight mode) results in much longer range trajectories. Payload impact ranges for this mode are typically in excess of 1100 nautical miles. Figure 68 presents re-entry velocity as a function of payload weight for various re-entry angles. The corresponding variation of payload impact range is indicated on the right-hand portion of Figure 67.

A 40 pound payload re-entry performance envelope is presented in Figure 69. The loci of one-up, three-down trajectories are indicated as dashed boundaries. Lines of constant re-entry angle running between these boundaries represent variable coast durations before second stage ignition. Figure 69 represents ballistic or gravity turn performance; i. e., the vehicle was essentially aligned with the flight path angle at ignition of the second and third stages. A cut-off line is indicated for that performance which exceeds a launch elevation angle of 82 degrees. A constant 550 nautical miles range line at 400 000 feet altitude is also shown in Figure 69; this line represents the Wallops to Bermuda range for various flight path angles. Figure 70, which gives altitude and velocity versus range, is presented to explain the presence of the minimum re-entry velocity as a function of range for constant re-entry angle lines of Figure 69. More gravity loss is encountered during ascent coast for the trajectories of type "2", resulting in lower re-entry velocities. This figure also indicates the losses associated with trajectory shaping.

The term "shaped trajectory" is used to describe trajectories which result from igniting the second and/or third stages at an angle of attack and variable coast durations to achieve a different value of payload impact range from that of a gravity turn trajectory, operating either in the one-up, three down or two-up, two-down modes. Shaping may be performed with the second stage, third stage, or both, since the guidance system can orient the vehicle prior to the ignition of each of these stages. Investigation of different shaping methods has led to the conclusion that due to system constraints such as maximum launch elevation angle of the first stage and minimum burnout altitude of the final stage, it is not always possible to achieve a zero angle-of-attack re-entry at specified values of flight path angle and range. Trajectory shaping is required to achieve re-entry angles above 20 degrees when restricting the range between Wallops and Bermuda. Trajectories with two ascent boost stages produce payload impact ranges which are too long, and those with a single ascent boost stage are too short.

The following is an illustration of performance penalties associated with re-entering near Bermuda and at optimum ranges:

<u>Parameter</u>	<u>Two-up, two-down Gravity Turn</u>	<u>Shaped</u>	<u>One-up, three-down Gravity Turn</u>
Re-entry velocity (feet per second)	36 800	34 700	35 500
Re-entry angle (degrees)	24	24	24
Payload impact range (nautical miles)	1 430	700	520
Angle of Attack (degrees)	0	0	0

Restricting the range from the gravity turn or optimum values to 700 nautical miles caused a 2100 feet per second decrease in re-entry velocity when the optimum range is reduced and an 800 feet per second decrease in re-entry velocity when the optimum range is increased.

An additional second stage shaping scheme was used to produce steeper trajectories than those obtainable with an 82 degree launch elevation angle, two-up, two-down flight mode. This was accomplished by pitching the vehicle up to create a positive angle of attack at second stage ignition. Very steep re-entry trajectories are obtainable this way; re-entry angles as steep as -72.0 degrees at 600 nautical miles and -78.5 degrees at 300 nautical miles can be provided with zero angle of attack at re-entry. The velocities for these angles are 36 150 and 35 300 feet per second, respectively, for a 40 pound payload. A variation of this shaping technique, employed to reduce the flight path angle, that allows none-zero angles of attack at re-entry was also investigated. A typical example of a mission near Bermuda Island having a re-entry angle of -46.5 degrees is contrasted below with the optimum range, two-up, two-down case for the same re-entry angle at a payload weight of 40 pounds.

<u>Parameter</u>	<u>Two-up, two-down Gravity Turn</u>	<u>Shaped</u>
Re-entry velocity (feet per second)	36 500	32 100
Re-entry angle (degrees)	-46.5	-46.5
Payload impact range (nautical miles)	1 375	600
Angle of Attack (degrees)	0	12.7

The loss in re-entry velocity for this example was 4400 feet per second and the shaped trajectory had almost 13 degrees angle of attack present at the re-entry altitude of 250 000 feet.

A study was conducted to determine the effects of final stage burnout altitude on re-entry velocity and flight path angle. Increasing the burnout altitude from 400 000 feet to 500 000 feet caused only small changes in the re-entry performance. Figure 71 shows re-entry angle versus re-entry velocity at two payload levels: 40 and 120 pounds. Velocity differences are on the order of 200 feet per second, which indicates that the performance penalties associated with using the 500 000 feet burnout altitude are not significant.

6.0 VEHICLE COMPARATIVE ANALYSIS

The 428A vehicle was compared with two configurations of a five stage Scout vehicle on the basis of flight performance and reliability for not only solar orbit missions, but earth probe and re-entry missions as well. The payload volumes of the vehicle's heatshields were compared. A discussion and definition of each type of mission considered were given. Mission objectives and requirements and vehicle constraints were reviewed. The performance comparisons for three types of missions were made on a common basis where ever possible. Solar orbit launch opportunities were compared for each vehicle. Accuracy comparisons were made for the solar orbit, earth probe, and re-entry missions. Reliability comparisons for the 428A and five stage Scout vehicles were made for the three types of missions.

6.1 VEHICLE CONFIGURATION DEFINITION

6.1.1 428A Vehicle

The unguided 428A vehicle configuration has been defined in Section 4.1 of this report. An attitude control system was added to this vehicle in this phase of study to provide flight path angle control as a result of the re-entry mission comparison requirement. For re-entry missions the complete attitude control system including electronics and gaseous nitrogen propellant and jets are included in the vehicle. For solar orbital missions the electronics section only is retained to sense of vehicle attitude up to time of final stage ignition. This control system was discussed in Section 5.5.

6.1.2 Standard Five Stage Scout Vehicle

This vehicle is composed of the operational Scout, used up to 1965, with the addition of a fifth stage consisting of the BE-3A3 rocket motor and associated structure. The geometry and volume capacity of the standard Scout (34 inch diameter, nose station -25) heatshield are discussed in Section 6.2. The Scout control system is discussed in Reference 4.

The vehicle is composed of the following rocket motors:

- (1) BE-3A3 fifth stage motor
- (2) X-258 fourth stage motor
- (3) X-259-A4 third stage motor
- (4) Castor I second stage motor
- (5) Algol IIB first stage motor

These motors are discussed in Reference 4 along with a detailed weights statement for this vehicle. The external profile and general arrangement for this vehicle are presented in Figure 72.

6.1.3 Improved Five Stage Scout Vehicle

This vehicle is identical to the standard five stage Scout with the exception of the second and fourth stage motors. The improved five stage Scout vehicle has a Castor II second stage motor and a FW-4S fourth stage motor. The four stage version is the vehicle used in the Scout program since 1965.

A discussion of vehicle weights and motors can be found in Reference 4. The external profile and general arrangement for this vehicle are presented in Figure 72 also.

6.2 PAYLOAD VOLUME COMPARISON

The heatshield used on the 428A vehicle is almost identical to the one used on the SLV-1B launch vehicle with a 24.0 inch aft end extension. The usable volume is approximately 8.6 cubic feet and is illustrated in Figure 73.

The heatshield for the standard and improved five stage Scout vehicles is the standard (34 inch diameter, nose station -25) heatshield presently used on the NASA four stage Scout vehicle. The usable volume is approximately 9.8 cubic feet and is illustrated in Figure 73. As shown in the figure, the 428A vehicle's heatshield can accommodate a payload with more length than the Scout heatshield, even though it has less volume.

6.3 COMPARATIVE PERFORMANCE ANALYSIS

6.3.1 Mission Objectives and Requirements

The technical requirements and objectives of the comparative performance study are summarized in Table XVII. These requirements were utilized to develop the parametric and flight performance capabilities on the three specified launch vehicles for the various missions. For each mission, a general description in terms of the required flight sequence and profiles is discussed. In addition, any trajectory or launch vehicle constraints that must be observed

in order to obtain a realistic performance simulation are also summarized. The detailed performance analyses of this study effort are presented in Appendix E of Reference 4.

The solar orbit mission launches were from Wallops Station, Virginia, into a trans-solar trajectory having an injection (final stage burnout) velocity greater than earth escape velocity (positive value of C_3 , the total energy). The resulting heliocentric orbit has an aphelion radius greater than or equal to the earth's orbital radius, a perihelion radius less than or equal to the earth's orbital radius, and some inclination angle to the ecliptic. For this study effort, the trajectories were shaped to have nominally zero inclination to the ecliptic plane and an aphelion radius equal to the earth's orbital radius about the sun (1.0 astronomical unit). Thus, for a given geocentric injection energy, a minimum perihelion radius is obtained and the resulting heliocentric trajectory also has minimum heliocentric energy. Payload capabilities of each vehicle having values of perihelion radius between 0.3 astronomical unit to 1.0 astronomical unit were investigated.

The earth probe mission is similar in flight profile to the solar orbit mission during powered flight. The main difference is that the earth probe mission injects with less than escape velocity (negative values of C_3). However, the injection velocity was kept above circular orbital velocity in order to obtain high apogee altitudes. Payload capabilities of the three vehicle configurations having apogee altitudes from 5000 nautical miles to 200 000 nautical miles were determined.

The re-entry mission flight profiles consisted of an upward power phase followed by a coast period and a downward power phase. Re-entry conditions were varied by changing impulse distribution for each of the power phases. For example, the 428A vehicle re-entry conditions were varied by boosting with one stage up and three stages down or by boosting with two stages up and two stages down. The same trajectory shaping technique was also utilized in the analyses of the Scout configurations. Re-entry velocities from 30 000 to 40 000 feet per second and re-entry angles from -10 degrees to maximum were computed for each of the three vehicles with payload weights ranging from 10 pounds to 150 pounds.

Any valid performance analysis must include trajectory and launch vehicle constraints. The parametric performance data were first developed over a wide range of variables, then, the constraining parameters and their effects on performance were evaluated to establish appropriate limits. Table XVIII summarizes the constraints for each mission and launch vehicle utilized in this study. With the proper demarcation, the usable performance envelope for each vehicle was established making possible a performance comparison.

6.3.2 Performance Comparison

The performance comparison analysis is categorized into solar orbit, earth probe, and re-entry missions. Whenever possible, all vehicles are compared with the same reference injection conditions (e.g., velocity versus payload

weight at the same re-entry angle and burnout altitude). Finally, the weights and propulsion data utilized for each vehicle are briefly discussed.

Solar orbit capabilities - The solar orbit capabilities of the 428A and Scout vehicles are compared in Figure 74 at a 20 degree injection (final stage burnout) flight path angle. For a 0.525 astronomical unit perihelion radius mission (approximately 0.667 year orbital period), the payload capability of the three launch vehicles is as follows:

Improved Scout	38 pounds
428A	26 pounds
Standard Scout	24 pounds

Basically, there is little difference between the standard Scout and the 428A vehicles and the improved Scout shows a 50% greater payload capability over both the standard Scout and the 428A vehicles.

Earth probe capabilities - Low injection angles are desirable in order to obtain maximum apogee altitude for a given velocity when the injection velocity is large (between circular and escape velocity). Therefore, in Figure 75, an injection flight path angle of 20 degrees was again chosen to compare the three vehicles' earth probe capabilities. The payload capability of each vehicle for a 80 000 nautical miles apogee (approximately 20 earth radii) is as follows:

Improved Scout	89.5 pounds
428A	62.0 pounds
Standard Scout	60.5 pounds

Again, the improved Scout has a 50% greater payload capability than the 428A and the standard Scout and there is little difference in capability between the latter two vehicles.

Figure 76 compares the injection velocity of the three vehicles as a function of payload weight at a constant injection flight path angle of 20 degrees. This figure illustrates the demarcation between solar orbit and earth probe missions. As would be expected, the velocity difference at a fixed payload weight between the three vehicles exhibits the same trend as the payload capability. At 50 pounds payload weight, the injection velocities are:

Improved Scout	37 950 feet per second
428A	36 550 feet per second
Standard Scout	36 350 feet per second

Re-entry capabilities - The re-entry performance comparison is presented in Figure 77 for a low re-entry angle of -10 degrees and a high re-entry angle of

-35 degrees. Without constraints on the range at re-entry, each vehicle's capability was maximized for the specified re-entry angle and payload weight while the range at re-entry was allowed to vary between 300 nautical miles to 11 000 nautical miles. For a re-entry velocity of 36 000 feet per second at a re-entry angle of -10 degrees, the payload capabilities are as follows:

Improved Scout	63.5 pounds
Standard Scout	53.5 pounds
428A	47.5 pounds (2 up, 2 down flight mode)

In Figure 78, the re-entry performance is compared at 40 pounds payload weight for the Wallops to Bermuda Mission - Range equals 550 nautical miles at 400 000 feet altitude. For a re-entry angle of -10 degrees and 40 pound payload, the velocity capabilities are as follows:

Improved Scout	37 180 feet per second
Standard Scout	36 980 feet per second
428A	36 440 feet per second

6.3.3 Accuracy Comparisons

In order to assess the accuracy with which each vehicle configuration can achieve a specified mission, an accuracy comparison was performed utilizing new and previously developed data. A detailed description of each error analysis can be found in Appendix E of Reference 4. This accuracy comparison is categorized into the solar orbit, earth probe, and re-entry missions.

Solar orbit mission - Since the standard and improved Scout differ only in the motors used on the second and fourth stages and these motors have essentially the same standard deviations, it was assumed that errors experienced by these two vehicles flying the same mission would be the same.

The solar orbit mission accuracy comparison is divided into two parts, (a) an orbital deviation comparison and (b) a launch window sensitivity comparison.

(a) Comparison of solar orbital elements - Table XIX presents the three-sigma deviations at injection of the 428A and Scout vehicles. As can be seen, the Scout errors are less than the 428A errors. These injection errors, when propagated through the appropriate equations, provide the deviations of the solar orbital elements. The deviations in aphelion and perihelion radii in astronomical units as a function of probability are compared in Figure 79 for the 428A and Scout vehicles. The absolute perihelion radius deviation for the Scout configurations is about one-half that of the 428A, although the perihelion radius deviation for the 428A is only 0.01 astronomical unit for a 95% probability. Figure 80 compares the inclination deviation of the Scout and 428A and shows that the Scout values are approximately one-quarter those of the 428A.

However, at 95% probability, the 428A inclination deviation is less than one degree.

(b) Launch window comparison - Figure 81 depicts a typical daily launch window comparison between the improved Scout and the 428A vehicles for fixed values of launch azimuth and launch elevation angles. It will be noted that the duration of the daily window can be determined after establishing limits on inclination angle, period, and/or perihelion radius. It can also be seen in Figure 81 that if a plus or minus one hour limit were allowed from the best time of launch, the deviations in period, inclination angle, and perihelion radius would be approximately the same. The Scout and the 428A vehicles have equal launch opportunities or sensitivities for a given day of the year. It should be noted that the Scout vehicle has a fixed guidance program which can not be changed on a daily basis. The nominal day and hour of launch for the Scout vehicle will be established at the time the pitch program is incorporated into the guidance system. The 428A vehicle has the flexibility to compensate for earth geometric position changes during launch delays by simply changing the launch beam elevation and azimuth angle settings minutes before lift-off. Thus, launch delays will not be an added error source for the 428A vehicle.

Earth probe mission - The accuracy comparison for the earth probe mission is summarized in Table XX. This comparison is based on equal payload weight between the improved Scout and the 428A vehicle.

The 428A vehicle deviations in apogee altitude and time at zero "g" are about equal to the Scout deviations. The 428A payload impact dispersions are much larger than the impact dispersions of the Scout which indicates the 428A errors in apogee altitude and time at zero "g" would be greater than Scout if the errors were compared at equal apogee altitudes.

Re-entry mission - For the re-entry mission accuracy comparison, nominal trajectories with approximately equal flight path angles having velocities between 32 000 and 35 000 feet per second were selected. In addition, the nominal trajectories for both the Scout and the 428A vehicles were shaped to provide 550 ± 20 nautical miles range at re-entry (range from Wallops Station to Bermuda). Table XXI compares the velocity, altitude, and angular errors at final stage burnout. This table shows that the errors in flight path angle and angle of attack are essentially the same for the 428A and Scout, but that the velocity and altitude errors are considerably larger for the 428A vehicle.

6.4 RELIABILITY COMPARATIVE ANALYSIS

This section summarizes the reliability evaluation for each vehicle configuration for the missions selected. Appendix D of Reference 4 presents the details of this comparative reliability analysis. This study has used pertinent portions of NPC 250-1 with the objective of being consistent with philosophy employed on the NASA Scout program as of 1 July 1965.

6.4.1 Vehicle Reliability Evaluation

Inherent reliability, or probability of mission success, may be defined as that reliability established by the basic design and it can only be improved (or degraded, as the case may be) by design changes. It is, therefore, a measure of the potential present in a particular design and, so long as the basic assumptions are consistent, may be used as a tool in comparing the relative merits of several designs. In keeping with this philosophy, trajectories for each type of mission for the five stage Scout and the 428A vehicles were selected with similar mission profile parameters for comparison purposes. Two versions of the five stage Scout vehicle were used in the performance comparisons conducted during this investigation, namely the standard and the improved five stage Scout vehicles. No distinction is made between these two vehicles in the reliability analysis since the only difference is in the second and fourth stage motors used and these are assumed to have the same reliability.

Two re-entry missions were selected for comparison purposes for both the five stage Scout and the 428A vehicles. The missions were for re-entry angles of -15 degrees (shallow trajectory) and -45 degrees (steep trajectory). These are arbitrarily selected as examples for which comparable data for both vehicle types were available. Table XXII presents the probability of mission success (reliability) for each trajectory for each type of vehicle.

The difference in reliabilities between re-entry missions is due to the different mission times required for the -15 degrees and -45 degrees re-entry angle trajectories. The steep trajectory for the -45 degrees re-entry angle requires a longer mission time than the shallow trajectory for the -15 degrees re-entry angle mission. The longer operating time results in a lower reliability for the -45 degrees re-entry angle mission.

The 428A vehicle is inherently more reliable than the five stage Scout vehicle, for the re-entry missions studied, because the 428A vehicle is less complex and has a significantly shorter mission operating time for both re-entry angle trajectories. The major difference in complexity is that the five stage Scout vehicle requires a complex guidance and control system while the 428A vehicle requires a relatively simple attitude control system. The mission time required for the 428A vehicle is approximately one-half that for the five stage Scout vehicle.

Although a significant difference in mission operating time and vehicle complexity is present, the difference in predicted reliability between vehicles for the missions is relatively small. This lack of sensitivity to time and complexity occurs because approximately one-half of the unreliability for both types of vehicles for any mission is attributable to the motors. Since the motor reliability is unchanged for each mission under study, the net effect on the overall vehicle reliability of changes in vehicle complexity and/or mission times is reduced.

In so far as the launch vehicle is concerned, from a probability of mission success standpoint, the solar orbit and earth probe missions are so nearly the

same no distinction need be made between them. The boost vehicles are identical for both missions and the variations required in boost and coast durations for each stage do not change appreciably. For comparison purposes in this study, a mission was chosen for each type of vehicle with comparable apogee altitude and payload performance time at zero gravity; namely 38 500 nautical miles and 24.0 hours, respectively, for the five stage Scout vehicle, and 39 600 nautical miles and 24.1 hours, respectively, for the 428A vehicle. Table XXIII presents the probability of mission success (reliability) for each type of vehicle for the solar orbit and earth probe missions.

A comparison of Tables XXII and XXIII discloses that both vehicles exhibit a higher reliability for the solar orbit and earth probe mission than for the two re-entry missions.

The difference in the reliability values determined for the five stage Scout vehicle for the two types of missions is due entirely to the difference in operating time requirements. Although the time requirement for the solar orbit and earth probe mission is significantly less than that required for the re-entry mission, the net effect on the overall vehicle reliability is reduced as a result of motor unreliability as previously discussed. This accounts for the relatively small difference in inherent reliability between the two types of missions.

For the 428A vehicle, both the operating time and the vehicle complexity are less for the solar orbit and earth probe mission than for the re-entry mission. Removal of the attitude control system hardware, used for the re-entry missions, reduces the complexity of this vehicle for the solar orbit and earth probe mission. This reduction in vehicle complexity, coupled with the reduction in operating time, accounts for the solar orbit and earth probe mission reliability being higher than that for the re-entry missions for the 428A vehicle.

Though the 428A vehicle has a shorter mission operating time than the five stage Scout vehicle for the solar orbit and earth probe mission, the difference is insignificant. The higher inherent reliability of the 428A vehicle, as compared to that of the five stage Scout vehicle, is due almost entirely to the reduced complexity of the 428A vehicle.

6.4.2 Reliability Comparative Results

In comparing the relative reliability of the five stage Scout and 428A vehicles in Table XXII and XXIII, it is apparent that both types of vehicles are capable of performing the various missions with a high probability of success. However, the 428A vehicle is shown to be inherently more reliable than the five stage Scout vehicle.

7.0 CONCLUSIONS

1. The feasibility of orbiting a payload about the sun with the unguided 428A solid fuel vehicle composed of existing motors and interstage hardware was proven. The 428A vehicle was selected because it is composed of spin qualified motors and a maximum amount of existing flight proven hardware.
2. The variation in final stage burnout velocity is fairly insensitive to changes in launch elevation and azimuth angles, while the flight path angle varies considerably.
3. Mission objectives for the nominal trajectory could be satisfied for 172 days of the year. For a launch on the least desirably day of the year, it is still possible to obtain an orbit with a heliocentric period of 0.688 years (as compared to the desired 0.667 years) with an inclination to the ecliptic of 3.4 degrees (as compared to zero degrees).
4. Launch azimuths of 110 and 140 degrees and launch elevation angles of 67.5 and 77.5 degrees used to establish the solar orbit are compatible with range safety requirements.
5. An error analysis has determined three-sigma dispersion of the 428A vehicle to be -0.0155 astronomical units for the perihelion radius, -0.0017 astronomical units for the aphelion radius, and -1.32 degrees inclination to the ecliptic plane.
6. A preliminary reliability analysis has shown that a reliability design goal of 0.95 is both feasible and practical.
7. The maximum negative re-entry flight path angles attainable without horizontal range restrictions are -78.5 degrees and -45 degrees for the 428A vehicle and five stage Scout vehicles, respectively.
8. The effect of the Bermuda re-entry mission horizontal range restriction on the 428A vehicle is to reduce the re-entry velocity from 2% to 6% of that obtainable at optimum ranges.
9. The re-entry payload weight capabilities for the 428A, standard, and improved five stage Scout vehicles are 47.5, 53.5, and 63.5 pounds, respectively, for a re-entry velocity of 36 000 feet per second at a re-entry angle of -10 degrees without horizontal range restrictions.
10. There is little difference in the solar orbit payload weight capability of the 428A and standard five stage Scout vehicles. The improved five stage Scout vehicle shows a 50% increase in payload weight capability. The payload weight capabilities for a 0.667 year period solar orbit are 24, 26, and 38 pounds for the standard five stage Scout, 428A, and improved five stage Scout vehicles, respectively.

11. The earth probe capabilities are 89.5 pounds for the improved Scout, 62.0 pounds for 428A, and 60.5 pounds for the Standard Scout vehicle for an apogee of approximately 20 earth radii.
12. The re-entry mission errors in flight path angle and angle of attack are essentially the same for any of the three vehicles, but velocity and altitude errors are larger by 500 feet per second and 80 000 feet, respectively, for the 428A vehicle, based on the fixed flight time at which the effects of error sources were evaluated.
13. The difference in solar orbit perihelion radius deviations between the five stage Scout vehicles and the 428A vehicle is 0.004 astronomical units.
14. For the earth probe mission, the payload capabilities of the five stage Scout vehicles are about 1.4 times those of the 428A vehicles. The apogee altitude and time at zero gravity deviations are about equal for all three vehicles with equal payload weight.
15. All three vehicles have equal launch opportunities on a yearly basis and equal sensitivities for a given day of the year. The 428A vehicle has the flexibility to compensate for earth geometric position changes during launch delays by changing the position of the launch beam minutes before lift-off. The Scout has a fixed guidance program which can not be changed on a daily basis. This will be an added error source for Scout if a launch delay becomes a reality. This type error was not included in the study.

LTV Aerospace Corporation,
LTV Astronautics Division,
Dallas, Texas, September 1966

REFERENCES

1. Harington, J.V.: First Order Analysis of Sunblazer Orbits
Massachusetts Institute of Technology, Center for Space Research,
Cambridge, Massachusetts, July 20, 1964.
2. Brice, J. W., and Huang, R. S.: Feasibility and Parametric Study
of an Unguided Solid Fuel Rocket Vehicle with Solar Orbital Capabilities,
Phase I, Report 00.537, LTV Astronautics Division, December 9, 1964
(CONFIDENTIAL).
3. Russ, K. M.: Feasibility and Parametric Design Study of an Unguided
Solid Fuel Rocket Vehicle with Solar Orbital Capabilities, Final
Report, Report 00.598, LTV Astronautics Division, March 15, 1965.
4. Russ, K. M.: Sunblazer Program Definition and Comparative Study,
Volume I, Technical Report, Report 00.729, LTV Astronautics Division,
December 30, 1965.
5. Spaceck, J. A.: Solar Patched-Conic Trajectory Routine, LV-VG-06
LTV Astronautics Division, (To Be Published).
6. Dobson, W. F. and Everett, H. U.: Computer Routine for Simulation of
Ballistic Interplanetary Trajectories, Report 00.382, LTV Astronautics
Division, March 10, 1964.
7. Dobson, W.F. and Everett, H. U.: The Near-Earth Mission Analysis
Trajectory Routine, LV-VC-27, Report 00.251, LTV Astronautics Division,
October 4, 1963.
8. Brown, Jr., C. A. and Carraway, A. B.: Static Aerodynamic Characteristics
of a Two-Stage and a Three-Stage Rocket Vehicle at Mach Numbers from
1.47 to 4.63, NASA TN D-1232, April 1962.
9. Kilpatrick, P.B., Miller, W. T., and Yonowitch, S.: Mission Accuracy
Analysis for the Scout Launch Vehicle, Report 23.41, LTV Astronautics
Division, November 30, 1962.
10. Clark, R.: Error Analysis - Cold Gas ACS for Sunblazer Using Improved
MARS, Report DR 1242-B-511, Whittaker Corporation, November 18, 1965.

ABSTRACT

A study was made of an unguided solid fuel rocket vehicle to orbit a payload about the sun. Descriptions of the solar trajectory simulation technique, vehicle configuration selection, flight performance, launch opportunities, stage impact dispersion, and mission accuracy are presented. The vehicle was provided with a simplified attitude control system for re-entry mission flight path angle control and comparisons were made with two configurations of a five stage Scout vehicle for solar orbit, earth probe and re-entry mission performance capabilities.

Table I
Astrodynamic Constants Utilized in the Study


Symbol	Name	Units	Value
R_s	Sphere of Influence radius of the Earth relative to the Sun	n. mi.	500 077.848
$R_{\oplus/\odot}$	Earth-Sun distance = Length of the Astronomical Unit (A.U.)	n. mi.	80 776 997.8
T_{\oplus}	Sidereal Period of Earth's orbit (Mean sidereal period for 1966)	days	365.256360
V_{\oplus}	Earth's mean orbital velocity	ft/sec	97 719.690
K_{\odot}	Gravitation Constant of the Sun	ft ³ /sec ²	4.68680171 X 10 ²¹
K_{\oplus}	Gravitation Constant of the Earth	ft ³ /sec ²	1.407654 X 10 ¹⁶
R_{\oplus}	Equatorial Radius of the Earth	feet	20 925 738
ω_{\oplus}	Rotational rate of the Earth (Mean rate for 1966)	rad/sec	7.29211505 X 10 ⁻⁵
π			3.14159265
J.D. _{γ}	Julian Date of 1966 vernal equinox	days	2 439 205.56636268
λ_L	Longitude of Wallops Station	deg-min-sec	75°28' 11.92'' W
μ_L	Latitude of Wallops Station	deg-sec-min	37° 50' 52.4747'' N
e_{\oplus}^2	Eccentricity squared		0.0067035358
J	Second Harmonic coefficient	—	0.00162345
H	Third Harmonic coefficient	—	-5.75 X 10 ⁻⁶
K	Fourth Harmonic coefficient	—	7.875 X 10 ⁻⁶
g_0	Mass conversion constant	ft/sec ²	32.17405
	Longitude, Mark II Launcher	deg	75.4905887 W
	Latitude, Mark II Launcher	deg	37.8479096 N
	Kilograms/lb		0.45359237
	Feet/n. mi.		6076.11549
	Meters/foot		0.3048

TABLE II
LIST OF MOTORS CONSIDERED FOR
CANDIDATE LAUNCH VEHICLES

1. TE-375	19. TE-364-3
2. TE-345	20. X-254-A1
3. CYGNUS 15 (AGC)	21. X-259-A3
4. XM-85	22. XM-81
5. NOTS 100B	23. FW-10
6. CYGNUS 17	24. TX-175
7. BE-3A3	25. UTC TM-4
8. X-248-A5	26. M57-A1
9. MG-18	27. TX-174-11
10. X-258 C1	28. XM-80
11. FW-4S	29. TX-238-5
12. XM-86	30. TX-238-6
13. TX-306	31. XM33-E7
14. FW-3S	32. CASTOR II, TX-354-2
15. 30KS 8000	33. CASTOR II, TX-354-1
16. 23 KS 11000	34. ALGOL ID
17. TE-364-1	35. ALGOL IIA
18. TYPHON	36. ALGOL IIB

Table III

Candidate Launch Vehicle Configurations ^{a, b}

Vehicle Number	Stage 2	Stage 3	Stage 4	Stage 5	Ideal Injection Velocity ft/sec
401	TX-238-5	23KS11 000	BE3-A3		40 205
402	TX-354-1	TE-364-1	BE3-A3		41 344
403	UTC-TM4	X258-C1	XM-85		38 868
404	XM-80	FW3-U0	BE3-A3		42 007
405	M57-A-1	FW-4S	NOTS 100B		39 091
406	FW-10	X258-C1	XM-85		39 573
407	X259-A3	MG-18	XM-85		38 896
408	M57-A-1	XM-86	XM-85		40 612
409	TX-174-35	TX-306-0	CYGNUS 17		39 609
410	XM-80	FW3-U0	CYGNUS 17		42 775
411	M57-A-1	XM-86	CYGNUS 17		42 011
412	FW-10	FW4-S	BE3-A3		41 587
413	XM-80	FW-10	FW-4S		39 545
414	FW-10	23KS11 000	BE3-A3		41 209
415	TX-238-6	TYPHONE	23KS11 000		36 956
416	TX-238-6	TE-364-3	FW-4S		38 442
417	XM-80	TE-364-3	BE3-A3		42 227
418	XM-80	23KS11 000	BE3-A3		41 840
419	FW-10	FW3-U0	CYGNUS 15		42 253
420	TX-238-6	TE-364-3	BE3-A3		41 756
421	TX-238-6	TYPHONE	BE3-A3		38 093
422	FW-10	TE-364-1	BE3-A3		41 368
423	FW-10	FW-4S	CYGNUS 15		42 341
424	FW-10	FW3-U0	BE3-A3		41 749
425	X259-A3	FW3-U0	BE3-A3		41 032
426	X259-A3	FW-4S	CYGNUS 15		41 035
427	X259-A3	TE-364-1	BE3-A3		40 755
428	X259-A3	23KS11 000	BE3-A3		40 538
429	X259-A3	23KS11 000	CYGNUS 15		40 663
430	X259-A3	FW3-U0	CYGNUS 15		41 444
501	XM-80	FW-10	FW3-U0	BE3-A3	45 062
502	TX-238-6	TYPHONE	23KS11 000	BE3-A3	42 325
503	TX-238-6	X-259-A3	FW3-U0	BE3-A3	44 458
504	XM-80	FW-10	FW-4S	CYGNUS 15	46 009
505	TX-238-6	TYPHONE	30KS8000	CYGNUS 15	42 003

^a Algol IIB First Stage

^b Injection Velocity for 20 lb Payload Weight and 10° Burnout Flight Path Angle

TABLE IV
SENSITIVITY OF INJECTION FLIGHT PATH
ANGLE TO LAUNCH ELEVATION ANGLE

Vehicle Number	$\left[\frac{\text{Change In Injection Flight Path Angle}}{\text{Change In Launch Angle}} \right]$
410	8.0
426	6.9
428	7.0
426C	8.0
428A	3.0
426A	2.9

TABLE V

428A VEHICLE WEIGHTS STATEMENT

ITEMS	Total Weight, Pounds
FOURTH STAGE WEIGHTS	
1. Inert 4th Step	(23.8)
a. Payload	0.0
b. Payload Adapter	2.0
c. Inert Motor	20.8
d. Contingency	<u>1.0</u>
4th Stage Burnout	23.8
2. Consumed Weight	<u>193.2</u>
4th Stage Ignition	217.0
THIRD STAGE WEIGHTS	
3. Inert 3rd Step	(171.1)
a. Upper Structure	25.0
b. Ignition	16.7
(1) Relay	4.5
(2) Pressure Switch	1.8
(3) Plumbing	0.8
(4) Squib Switch	0.0
(5) Wiring	2.1
(6) Headcap Transducer	0.5
(7) Ignition Batteries	7.0
c. Telemetry	8.0
(1) Transmitter	1.3
(2) Amplifier	0.1
(3) SCO ^a (9)	1.1
(4) SCO ^a Rack	0.5
(5) Commutator	0.7
(6) J Box	1.0
(7) Antenna & Coax	1.5
(8) Battery	1.0
(9) Contingency	0.8
d. Telemetry Mounting Penalty	2.0
e. Inert Motor	89.0
f. Intertransition Wiring	5.6
g. Balance Weights (Est.)	2.0
h. Lower Structure	19.0

^a Subcarrier Oscillator

TABLE V (Continued)

428A VEHICLE WEIGHTS STATEMENT

THIRD STAGE WEIGHTS (Continued)		Total Weight, Pounds
i.	Ignition Batteries	0.0
j.	Beacon System	0.0
	(1) Battery	
	(2) Antenna & Coax	
	(3) Beacon	
	(4) Relay & Wiring	
	(5) Duplexer	
k.	Contingency	<u>3.8</u>
	3rd Stage Burnout	388.1
4.	Consumed Weight	<u>921.0</u>
	3rd Stage Ignition	1309.1
SECOND STAGE WEIGHTS		
5.	Inert 2nd Step	(484.0)
a.	Upper Structure	79.0
b.	Ignition	10.9
	(1) Wiring	5.7
	(2) Pressure Switch	1.8
	(3) Tubing	0.4
	(4) Relay	2.5
	(5) Headcap Transducer	0.5
c.	Inert Motor	212.0
d.	Tunnels	9.8
e.	Intertransition Wiring	4.5
f.	Destruct Charge	0.0
g.	Lower Structure	104.8
h.	Wiring	9.8
i.	Destruct, Command Fire & C-Band Beacon	30.0
	(1) Antenna	5.6
	(2) Destruct Receivers	5.6
	(3) Batteries	3.6
	(4) J Box	2.0
	(5) Relay Box	3.2
	(6) Safe Arm Unit	0.0
	(7) Destruct Charge	0.0
	(8) Beacon	2.3
	(9) Antenna	1.0

TABLE V (Continued)

428A VEHICLE WEIGHTS STATEMENT

SECOND STAGE WEIGHTS (Continued)		Total Weight, Pounds
(10) Relay	0.5	
(11) Contingency	6.2	
j. Telemetry		21.2
(1) Three Axis Ref. Sys.	8.0	
(2) Contingency (To be used as a general weight contingency since total vehicle telemetry system weighs 81b and is located in the third step)	13.2	
k. Mounting Penalty (For C-Band Beacon and Three Axis Refer- ence System)		2.0
l. Contingency		<u>0.0</u>
2nd Stage Burnout		1793.1
6. Consumed Weight		<u>2587.0</u>
2nd Stage Ignition		4380.1
FIRST STAGE WEIGHTS		
7. Inert Step 1		(4872.0)
a. Nose Cone		267.0
b. Upper Structure		112.0
c. Destruct		10.7
(1) Batteries	0.0	
(2) Safe Arm	4.4	
(3) Destruct Charge	4.8	
(4) Pressure Switch	0.9	
(5) Tubing	0.2	
(6) Lanyard Switch	0.4	
d. Ignition		4.8
(1) Timers	0.0	
(2) Tubing	0.2	
(3) Pressure Switch	0.9	
(4) Relay	3.2	
(5) Headcap Transducer	0.5	
e. Wiring		9.0
f. Launch Ring		93.4

TABLE V (Concluded)

428A VEHICLE WEIGHTS STATEMENT

FIRST STAGE WEIGHTS (Continued)		Total Weight, Pounds
g.	Torque Shell	0.0
h.	Upper Booster Attach Penalty (Includes Spin Ring)	150.0
i.	Inert Spin Motors ^b	64.0
j.	Inert Motor	2365.0
k.	Inert Boosters	892.0
l.	Lower Booster Attach Penalty	100.0
m.	Lower Structure	231.0
n.	Fins & Tips	373.0
o.	Jet Vanes	0.0
p.	Boattail	0.0
q.	Contingency	<u>200.1</u>
	1st Stage Burnout	9252.1
8.	Consumed Weight	23 769.0
a.	Sustainer	21 355.0
b.	Boosters	2414.0
c.	Thermolag	0.0
	1st Stage Ignition	33021.1

^b Does not include spin motor grain of 26 pounds which is consumed at lift-off

Table VI. - Sequence of Events^{a, b, c}

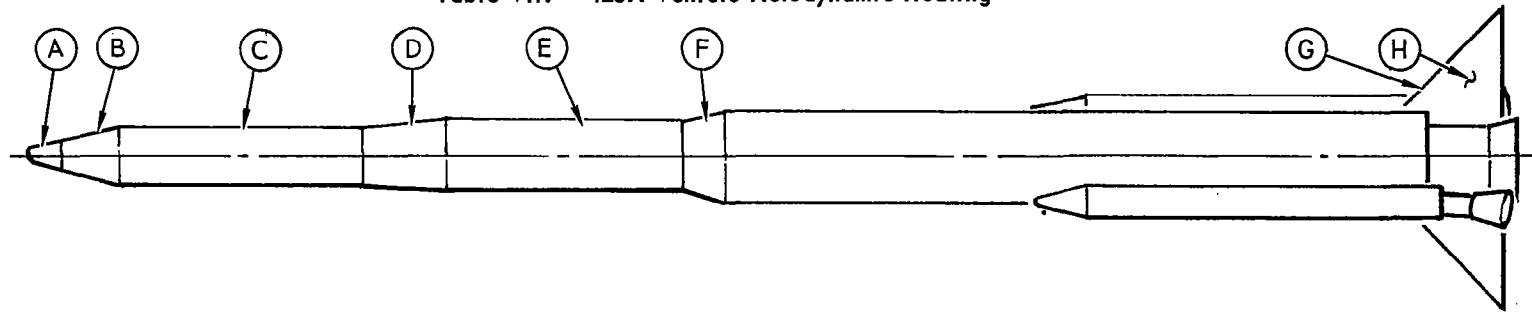
Time, sec	Event	Resultant Action
0.0	Blockhouse command for Algol and TX-77 Motor Ignition	First motion lanyard switch closed Vehicle on internal power
0.15	Spin Motor Lanyard pulled	Spin Motor ignition
0.40	Spin Motor Burnout	None
8.0	TX-77 Motor Burnout	None
72.5	Algol motor pressure decay to 25 psi--sensed by headcap pressure switch	Power available to command fire relay
78.6	Blockhouse command for second stage ignition - sensed by Command Fire and Destruct receiver.	Command Fire Relay closed (2nd Stage). Heat Shield and inert First Stage jettisoned by activation of explosive nuts which release V-Band clamps. Power applied to 2 sec delay squib which will result in 2nd Stage ignition.
80.6	X-259 Motor Ignition	None
113.4	X-259 Motor Pressure decay to 25 psi--sensed by Headcap Pressure Switch	Inert 2nd Stage jettisoned by activation of explosive nuts releasing V-Band Clamp. Power applied to 2 sec delay squib resulting in 3rd Stage Motor ignition
115.4	23 KS 11 000 Motor Ignition	None
143.4	23 KS 11 000 motor pressure decay to 25 psi - sensed by headcap pressure switch	Power applied to V-Band clamp explosive nuts which will result in jettison of inert 3rd Stage motor. Power applied to BE-3 igniter which incorporates a two second time delay.
145.4	BE-3 Motor Ignition	None
154.0	BE-3 Motor Burnout	None - 428A vehicle mission completed

^a Command destruct prior to command ignition of Stage two will result in conical shaped charge ignition and consequent destruction of the Algol, plus disarm of the ignition system for the upper stages of the vehicle.

^b Command no-fire during second stage burn will result in disarm of stages three and four ignition circuits.

^c If second stage command ignition is received prior to Algol burnout, the command will not be executed until two seconds after Algol burnout due to first stage motor pressure switch.

Table VII. - 428A Vehicle Aerodynamic Heating



Item	Component	Structure Analyzed		Maximum Outside Temperature, °F	Maximum Inside Temperature, °F	Additional Thermal Protection Requirements
		Material	Thickness, Inches			
A	2.125" Radius Nose Cap	Stainless Steel	0.10	2300	2300	Steel thickness must be increased to reduce temperature
B	Heat Shield Fwd. Cone	Laminated Fiberglass Faces	0.05	1700	650	Addition of 0.1" to 0.2" cork required to maintain 300°F maximum temperature
		Honeycomb Fiberglass Core	0.50			
C	Heat Shield Body	Laminated Fiberglass Faces	0.05	1100	370	Addition of 0.1" to 0.2" cork required to maintain 300°F maximum temperature
		Honeycomb Fiberglass Core	0.50			
D	Transition "G" 4° Flare	Laminated Fiberglass	0.10	940	830	Thin layer of cork required to reduce fiberglass temperature
E	ABL X-259 Motor	Spiralloy Fiberglass Case	0.145	450 Cork-Case Interface	280	Acceptable as is
		Cork Insulation	0.05			
F	Transition "C" 12° Flare	Laminated Fiberglass	0.12	1110	960	Thin layer of cork required to reduce fiberglass temperature
G	Fin L.E. 0.25" Radius 45° Sweep	4130 Steel	0.071	2600	2600	Steel thickness must be increased to reduce temperature
H	Fin Surface 4° Wedge 24" from L.E.	Laminated Fiberglass	0.12	1130	990	Thin layer of cork required to reduce fiberglass temperature

Table VIII
428A Vehicle Weights and Inertia Summary

Condition	Step Weight, Pounds	Stage Weight, Pounds	Horizontal C.G. Location, Inches	Roll Moments of Inertia, Slug-Feet ²	Pitch or Yaw Moments of Inertia, Slug-Feet ²
Payload		0			
Inert 4th Step	23.8				
Burnout 4th Stage		23.8	37.0	0.15	0.62
Consummable 4th Step	193.2				
Ignition 4th Stage		217.0	35.8	1.76	2.00
Inert 3rd Step	171.1				
Burnout 3rd Stage		388.1	60.2	4.98	98.20
Consummable 3rd Step	921.0				
Ignition 3rd Stage		1309.1	81.9	16.80	196.00
Inert 2nd Step	484.0				
Burnout 2nd Stage		1793.1	115.7	35.70	1554.00
Consummable 2nd Step	2587.0				
Ignition 2nd Stage		4380.1	152.9	93.80	2727.00
Inert 1st Step ^a	4872.0				
Burnout 1st Stage		9252.1	315.6	643.00	75 028.00
Consummable ^b 1st Step	23 795.0				
Ignition 1st Stage		33 047.1	403.8	2128.00	139 233.00

^aIncludes payload and upper stage heat shield which is ejected at 1st step separation

^bIncludes spin motor consummable weight which is expended during first 0.4 second of flight

TABLE IX

MOTOR LOADS COMPARISON

Motor	428A Ultimate Design Loads (Preliminary)	Previous Load History
X-259	Flight Conditions Mom = 312 000 in-lb Axial Load = 36 200 lb	Static Test Loads Mom = 780 000 in-lb Axial Load = 25 800 lb
	Hoisting Condition Mom = 645 000 in-lb	
Algol	Flight Conditions Mom = 432 500 in-lb Axial Load = 57 500 lb	Scout Ultimate Flight Design Loads Mom = 760 000 in-lb Axial Load = 89 000 lb
	Hoisting Condition Mom = 2 310 000 in-lb	Scout Hoisting Condition Mom = 2 500 000 in-lb
23KS1100	Flight Condition Mom = 105 500 in-lb Axial Load = 17 400 lb	Static Test Loads Mom = 186 920 in-lb Axial Load = 27 302 lb

Table X
Nominal Trajectory Sequence of Events^a

Event Number	Event	Time, sec	Inertial Velocity, ft/sec	Altitude, ft	Range, n. mi.	Inertial Flight Path Angle, deg
1	Lift-off	0.0	1206	0	0	—
2	TX-77 Burnout	8.0	1823	4100	0.3	29.28
3	Stage 1 Burnout	72.5	8344	223 400	33.1	38.21
4	H/S Separation & Stage 2 Ignition	80.6	8188	264 200	40.3	36.95
5	Stage 2 Burnout	113.4	15 391	488 300	83.0	37.35
6	Stage 3 Ignition	115.4	15 354	507 000	86.6	37.23
7	Stage 3 Burnout	143.4	25 344	844 700	150.6	39.22
8	Stage 4 Ignition	145.4	25 306	876 650	156.5	39.22
9	Stage 4 Burnout	154.6	39 288	1 057 600	188.7	41.25
10	Stage 1 Vacuum Impact	470.4	—	0	378.3	—
11	Stage 2 Vacuum Impact	1030.8	—	0	1544.3	—
12	Stage 3 Vacuum Impact	3896.8	—	0	5731.8	—

^a Launch Conditions: Launch Elevation Angle = 73.8°, Launch Azimuth = 120°
Wallops Station Launch Site, Payload Weight = 24.0 lb

TABLE XI
ROCKET MOTOR VARIANCE DATA

Motor Variable	Three-Sigma Deviations, Percent			
	Algol IIB	X-259-A3	23KS11000	BE 3-A3
Propellant Weight	0.1405	0.2513	0.9229	0.7764
Total Loaded Motor Weight	0.1012	0.1429	1.3861	0.7009
Vacuum Specific Impulse	0.5786	1.2722	0.4822	1.0136
Motor Burn Time	6.9322	10.8108	5.4614	11.0437
Total Vacuum Impulse	0.6784	1.3751	1.3598	1.5009

TABLE XII
AERODYNAMIC VARIANCE DATA

Parameter	Three-Sigma Deviations
Zero Lift Drag Coefficient	±10%
Center of Pressure	±20 Inches
Atmosphere	±5%
Measured Wind Velocity ^a	
In-Plane	±5 ft/sec
Out-Plane	±5 ft/sec

^a Assumed wind aiming technique to be used at launch.

TABLE XIII
LAUNCH CONDITIONS, THRUST MISALIGNMENT,
AND STAGE TIP-OFF VARIANCE DATA

Stage	Item	Three-Sigma Deviations
1	Launch Elevation	± 0.10 deg
1	Launch Azimuth	± 0.15 deg
1	Thrust Misalignment	
	In-Plane	± 0.25 deg
	Out-Plane	± 0.25 deg
2	Tip-Off	
	In-Plane	± 1.5 deg
	Out-Plane	± 1.5 deg
3	Tip-Off	
	In-Plane	± 2.0 deg
	Out-Plane	± 2.0 deg
4	Tip-Off	
	In-Plane	± 2.0 deg
	Out-Plane	± 2.0 deg

TABLE XIV
ATTITUDE CONTROL SYSTEM WEIGHT BREAKDOWN ^a

Component	Whittaker Part Number	Weight, Pounds
MARS (Miniature Attitude Reference System)	526085	7.0
Electronics Package	526405	2.5
Programmer	527615	3.5
Power Supply	525795	1.0
Battery	-----	6.0
Toroidal Nitrogen Receiver Assembly	129419	31.4
Pressure Regulator	128065-1	1.5
Two 10 lb Thrust Reaction Valves	128045-1	2.0
Nitrogen Supply	-----	18.0
Wiring Harness & Pneumatic Plumbing	-----	7.0
	Total	79.9

^a Mounting fixture weight is not included

TABLE XV

SHALLOW RE-ENTRY ANGLE TRAJECTORY GUIDANCE
ATTITUDE ERROR ANALYSIS^a

Time From Lift-Off, sec	Event	Pitch Attitude Error, deg	Yaw Attitude Error, deg
221.0	2nd Stage Ign.	0.866	0.798

^aErrors are 3 sigma values

TABLE XVI

INTERMEDIATE RE-ENTRY ANGLE TRAJECTORY GUIDANCE
ATTITUDE ERROR ANALYSIS^a

Time From Lift-Off, sec	Event	Pitch Attitude Error, deg	Yaw Attitude Error, deg
306.0	2nd Stage Ign.	0.899	1.184
552.2	3rd Stage Ign.	1.134	1.806

^aErrors are 3 sigma values

Table XVII. - Comparative Performance Study Objectives and Requirements

<u>Launch Vehicle Configurations</u>	<u>Accuracy Analysis and Comparison</u>
1. 428A: Algol + TX-77 AUGM., X-259, 23KS11 000, BE-3	1. Solar Mission Deviations: a. Perihelion Radius b. Inclination to Ecliptic
2. Standard Scout: Algol IIB, Castor I, X-259, X-258, BE-3	2. Earth Probe Mission Deviations: a. Apogee Altitude b. Azimuth
3. Improved Scout: Algol IIB, Castor II, X-259, FW-4, BE-3	3. Reentry Deviations: a. Flight Path Angle b. Velocity
<u>Payload</u>	<u>Range Complex</u>
1. Weight: 10 to 150 lb (Mission and Vehicle Dependent)	1. Launch Site: Wallops Station, Virginia a. Longitude = 75.4728° West b. Latitude = 37.8492° North c. Elevation = 0 ft
2. Ballistic Coefficient: Assume Vacuum Impact	2. Tracking Station: Bermuda (Reentry only) a. Longitude = 64.6541° West b. Latitude = 32.3473° North c. Elevation = 65 ft
3. Ascent Heat Protection: Required	
<u>Mission Types</u>	
1. Solar Orbit (Inbound)	
2. Earth Probe	
3. Reentry	
<u>Mission Comparison Analysis</u>	
1. Solar Orbit Capabilities a. Perihelion Radius b. Launch Opportunity	
2. Earth Probe Capabilities a. Apogee Altitude b. Time at Zero "G"	
3. Reentry Capabilities a. Burnout Altitude at 400 000 ft . Velocity: Maximum . Flight Path Angle: -10° to maximum b. Effects of Burnout Altitude at 500 000 ft	
	<u>Launch Constraints</u>
	1. Azimuth: 140° maximum
	2. Elevation: a. 82° maximum 428A configurations b. 88° maximum Scout configurations
	3. Stage Impacts: No impacts on land using vacuum trajectories

Table XVIII. - Summary of Trajectory and Launch Vehicle Constraints

Parameter		428A Launch Vehicle		Standard and Improved Five Stage Scout	
		Earth Probe & Solar Orbit Missions	Reentry Missions	Earth Probe & Solar Orbit Missions	Reentry Missions
Launch Elevation Angle	Maximum	77.5° (Stage 3 Impact)	82° (Range Safety)	87.6° (Stage 4 Impact)	88° (Range Safety)
	Minimum	67.5° (Stage 1 Max q)	67.5° (Stage 1 Max q)	85.5° (Stage 4 Impact)	84.8° (Stage 1 Max q)
Launch Azimuth	Maximum	140° (Range Safety)	140° (Range Safety)	134° (Stage 3 Impact)	140° (Range Safety)
	Minimum	110° (Stage 3 Impact)	Payload Impact Range Dependent	110° (Stage 4 Impact)	Payload Impact Range Dependent
Minimum Coast Times	Stage 1	2 sec	Mission Dependent	0 sec	0 sec
	Stage 2	2 sec	Mission Dependent	5 sec	5 sec
	Stage 3	2 sec	2 sec	21 sec	21 sec
	Stage 4	None	None	7.5 sec	7.5 sec
Maximum Coast Times	Stage 1	Not Applicable	Not Applicable	q Dependent	q Dependent
	Stage 2			Not Applicable	620 sec
	Stage 3				1060 sec
	Stage 4				-
Maximum Stage Ignition q	Stage 2	1 lb/sq ft	0.001 lb/sq ft	40 lb/sq ft	35 lb/sq ft
	Stage 3	0 lb/sq ft	0 lb/sq ft	1 lb/sq ft	1 lb/sq ft
	Stage 4	0 lb/sq ft	0 lb/sq ft	0 lb/sq ft	0 lb/sq ft
	Stage 5	0 lb/sq ft	0 lb/sq ft	0 lb/sq ft	0 lb/sq ft

TABLE XIX

SOLAR ORBIT MISSION, COMPARISON OF THREE
SIGMA ERRORS AT INJECTION

	Parameter	428 A Launch Vehicle	Standard & Improved Scout
Nominal Conditions	Injection Velocity (ft/sec)	39 300	38 700
	Injection Angle (deg)	41.3	36.3
	Payload Weight (lb)	24	22 (Standard) 34 (Improved)
Three Sigma Errors (a)	Velocity Error (ft/sec)	±328	±182
	Altitude Error (ft)	±115 650	±32 200
	Flight Path Angle Error (deg)	±6.95	±0.94
	Heading Error (deg)	±5.18	±1.80

^a A selected nominal trajectory established the time sequence of events for the above mission. Each error source was individually used to perturb the nominal trajectory. The three sigma errors tabulated above reflect the root sum square of the effects of individual errors at a fixed time.

TABLE XX

EARTH PROBE MISSION, COMPARISON
OF THREE SIGMA ERRORS

	Parameter		428A Vehicle	Improved Scout
Nominal Conditions	Apogee Altitude (n.mi.)		12 700	16 450
	Time at Zero "G" (hrs)		5.50	7.12
	Payload Impact Range (n.mi.)		6427	4878
	Payload Weight (lb)		100	100
Three Sigma Errors ^b	Apogee Altitude Error ^a (n.mi.)		±1121	±1167
	Time at Zero "G" Error (hrs)		±0.55	±0.60
	Payload Impact Error (n.mi.)	Up & Down Range	±1517	±116
		Cross Range	±390	±65

^a 428A altitude errors are referenced to nominal time to apogee; Scout altitude errors are referenced to zero flight path angle.

^b A selected nominal trajectory established the time sequence of events for this mission. Each source of error was individually used to perturb the nominal trajectory. The results reflect the root sum square of the effects of these errors at a fixed time.

TABLE XXI

RE-ENTRY MISSION, COMPARISON OF THREE SIGMA ERRORS
AT FINAL STAGE BURNOUT

	Parameter	428 A Vehicle	Standard & Improved Scout
Nominal Conditions (a)	Re-Entry Angle (deg)	-22.1	-25.0
	Burnout Altitude (ft)	400 000	400 000
	Payload Weights (lbs)	40	96 (standard) 100 (improved)
	Re-Entry Velocities (ft/sec)	34 800	31 600 (standard) 32 000 (improved)
Three Sigma Errors (b)	Velocity Error (ft/sec)	±728	±232
	Altitude Error (ft)	±164 200	±82 300
	Flight Path Angle Error (deg)	±2.05	±1.52
	Angle of Attack Error (deg)	±1.65	±1.42

^a All trajectories were shaped to provide 550 ± 20 nautical mile range at re-entry.

^b A selected nominal trajectory established the time sequence of events for this mission. Each source of error was individually used to perturb the nominal trajectory. The results reflect the root sum square of the effects of these errors at a fixed time.

TABLE XXII

RE-ENTRY MISSION RELIABILITY COMPARISON

Launch Vehicle	Reliability	
	-15° Re-entry Angle	-45° Re-entry Angle
Five Stage Scout	.912348	.909502
428A	.930073	.928287

TABLE XXIII

SOLAR ORBIT AND EARTH PROBE MISSION RELIABILITY
COMPARISON

Launch Vehicle	Reliability
	Solar Orbit and Earth Probe
Five Stage Scout	.919859
428A	.934460

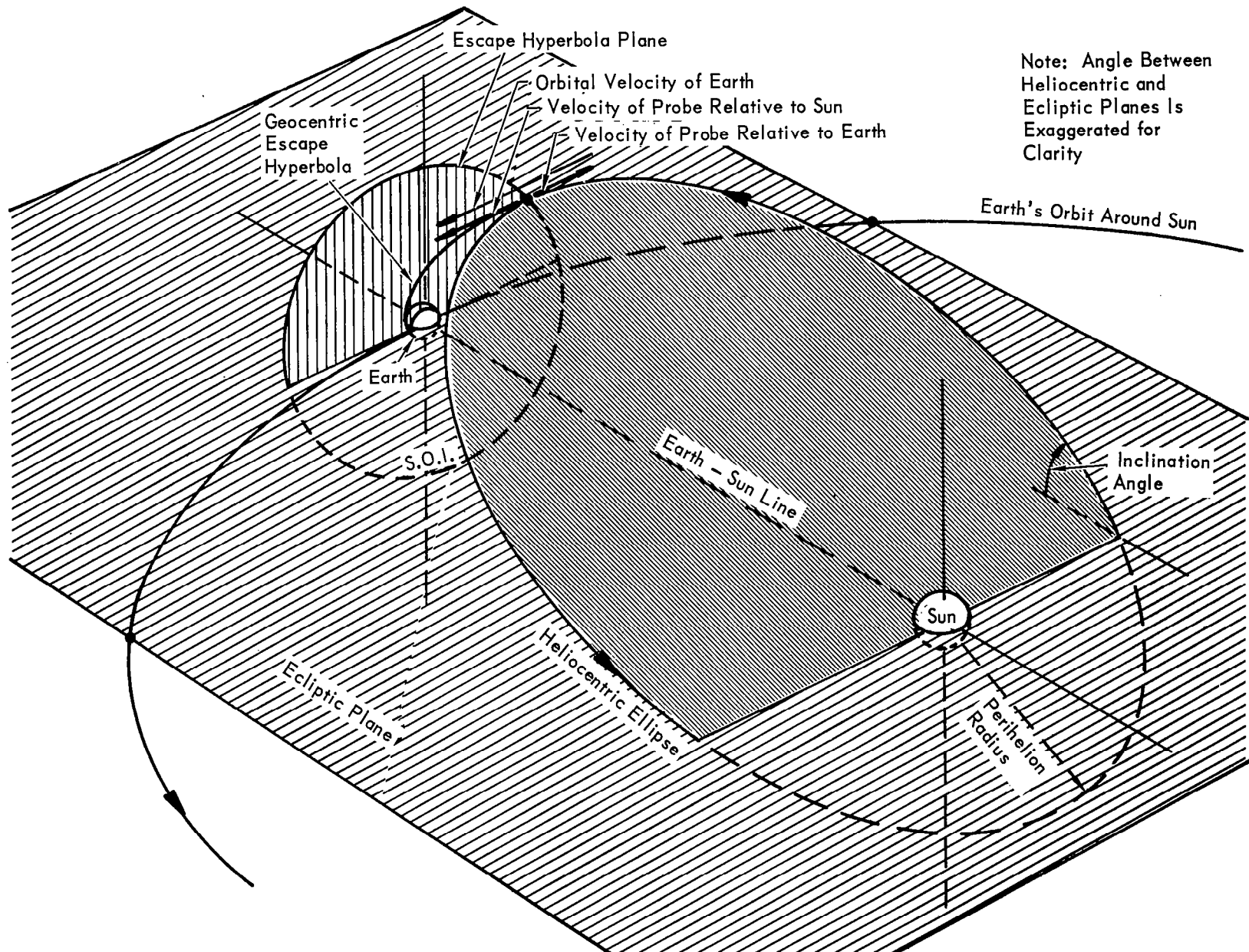


Figure 1.- Trans-Solar Trajectory Definitions

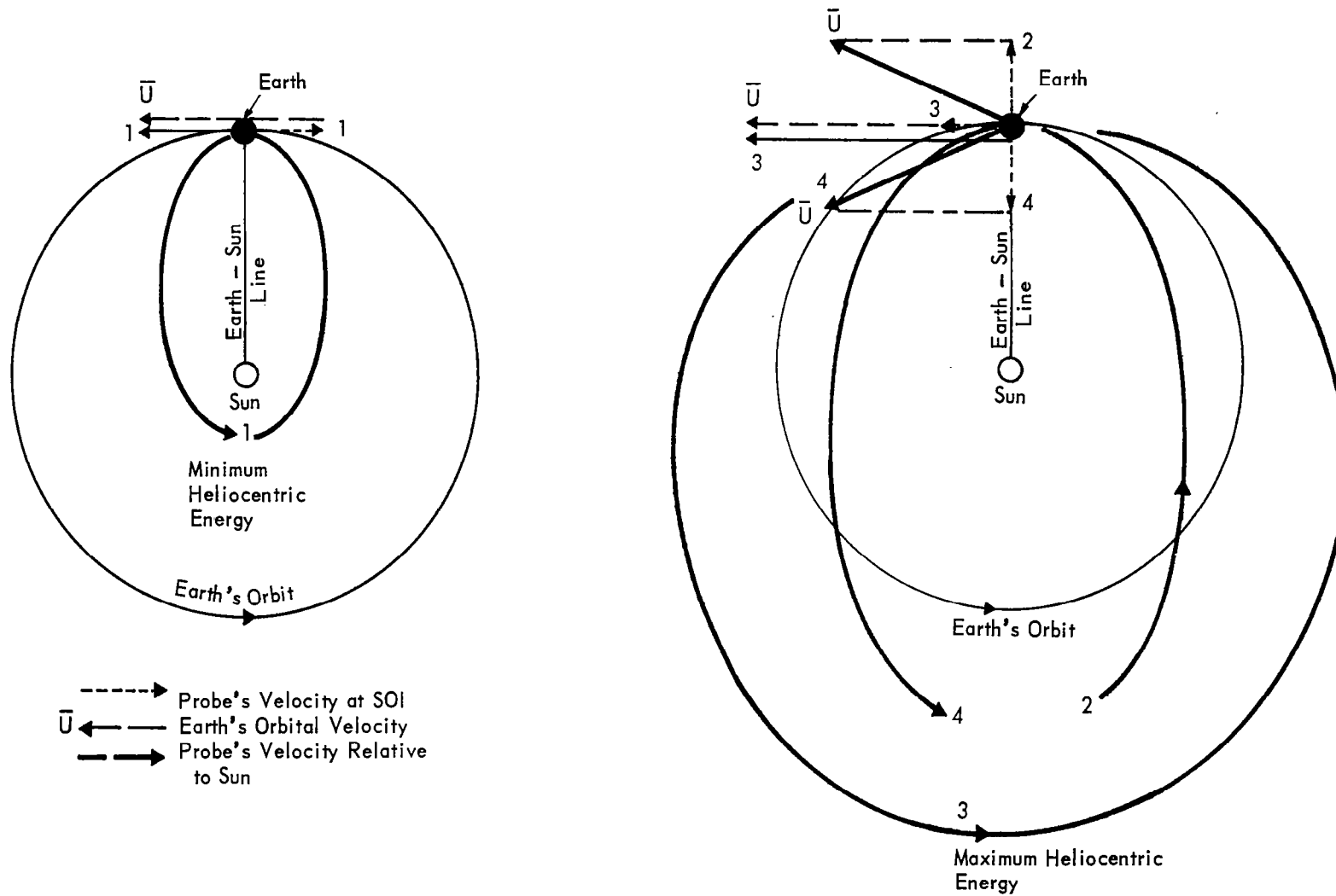


Figure 2. - Determination of the Optimum Earth Departure Direction

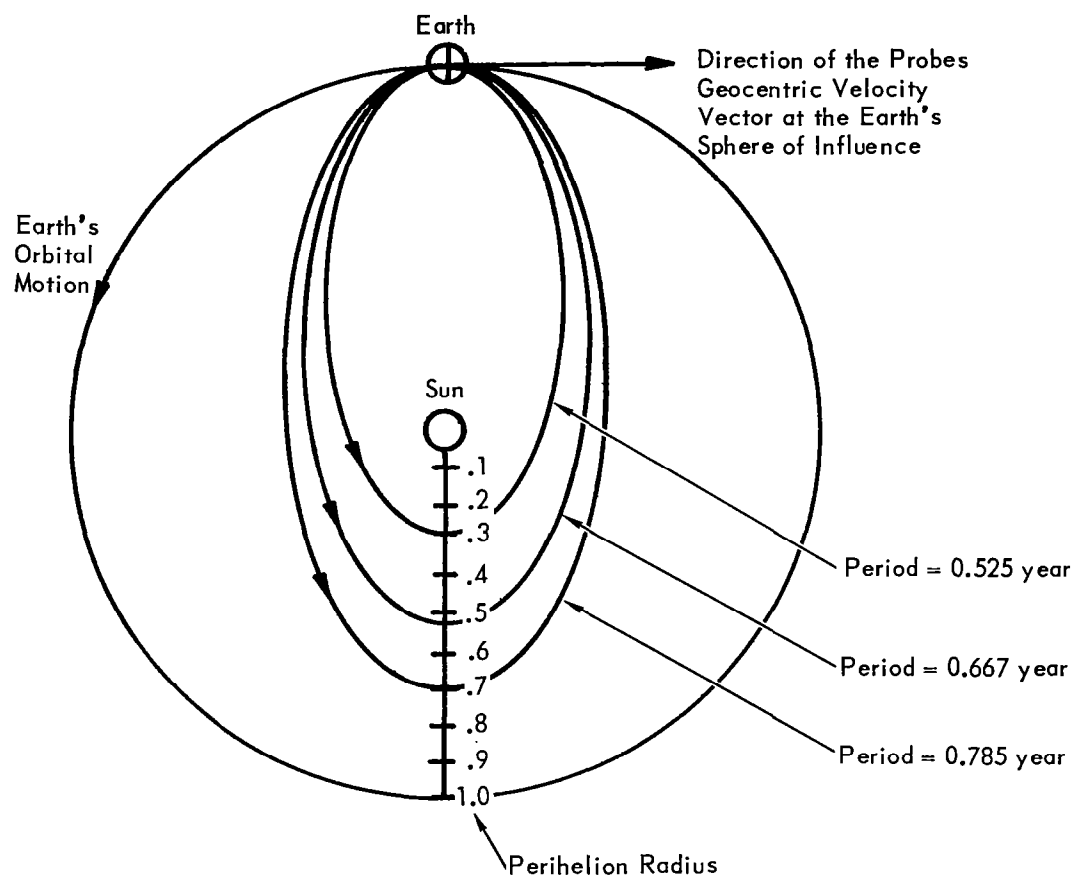


Figure 3. – Schematic of the Family of Heliocentric Trajectories Under Consideration

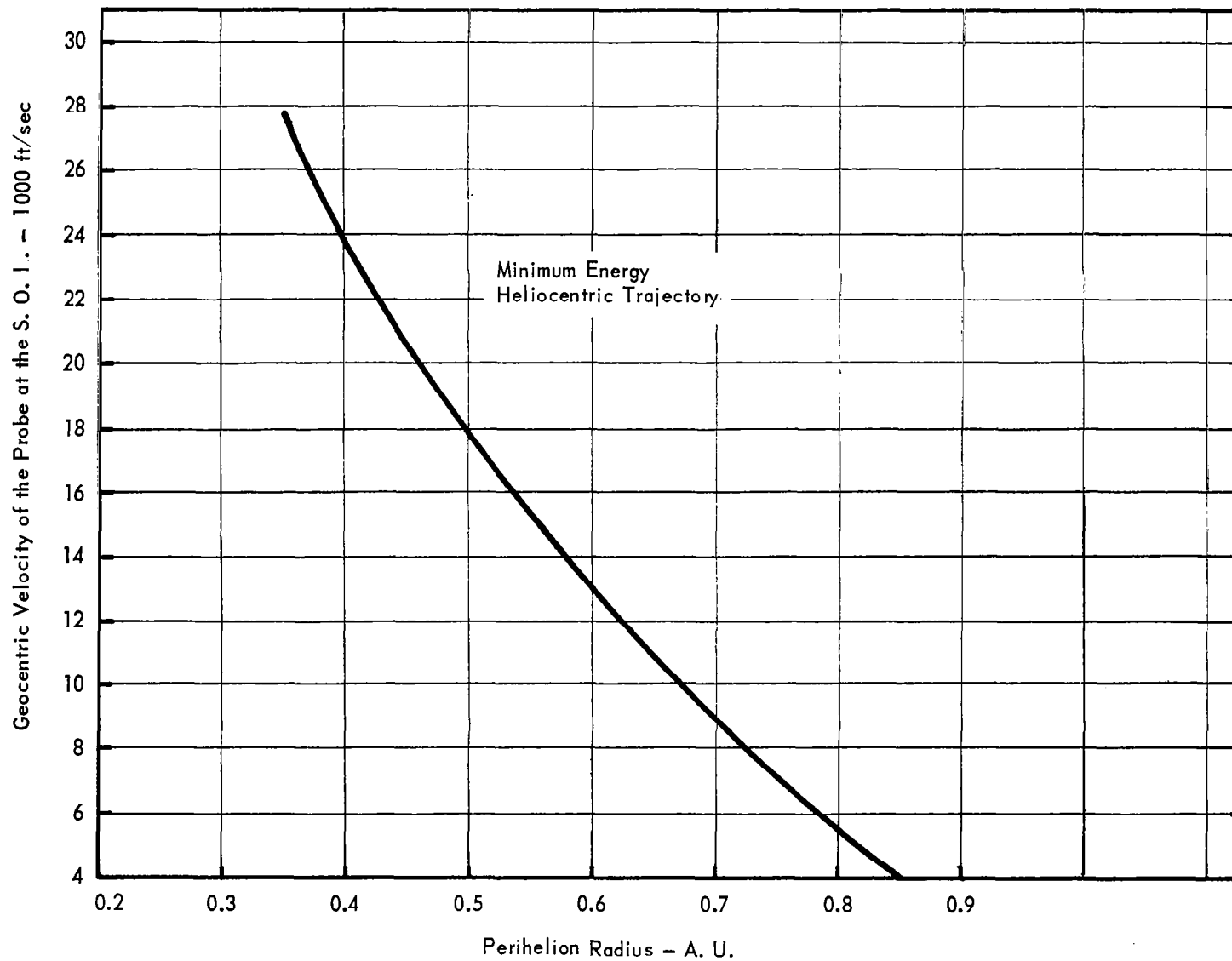


Figure 4.- Variation of Perihelion Radius with Probe Velocity at Sphere of Influence

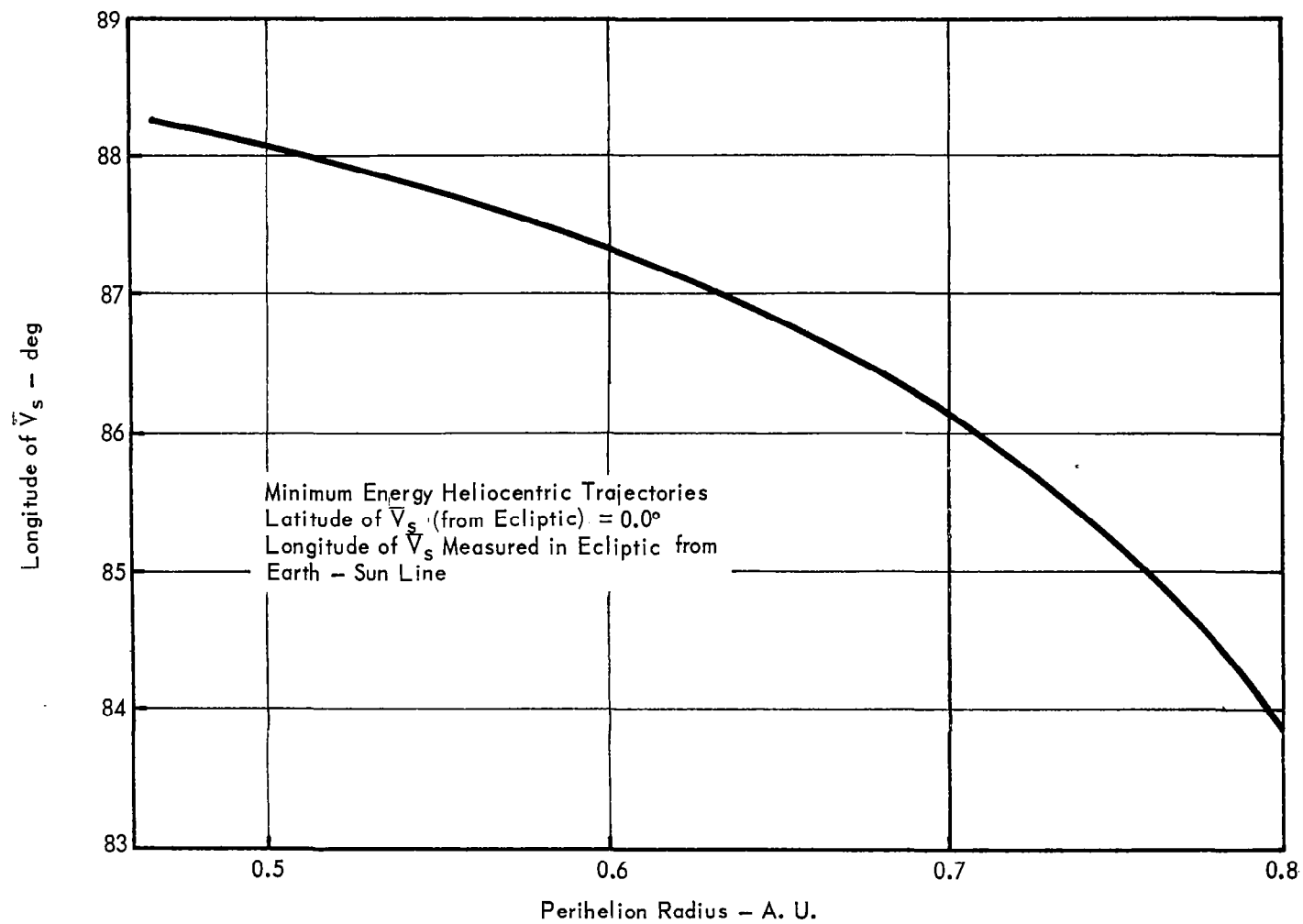


Figure 5.— Variation of Longitude of \bar{V}_s with Perihelion Radius

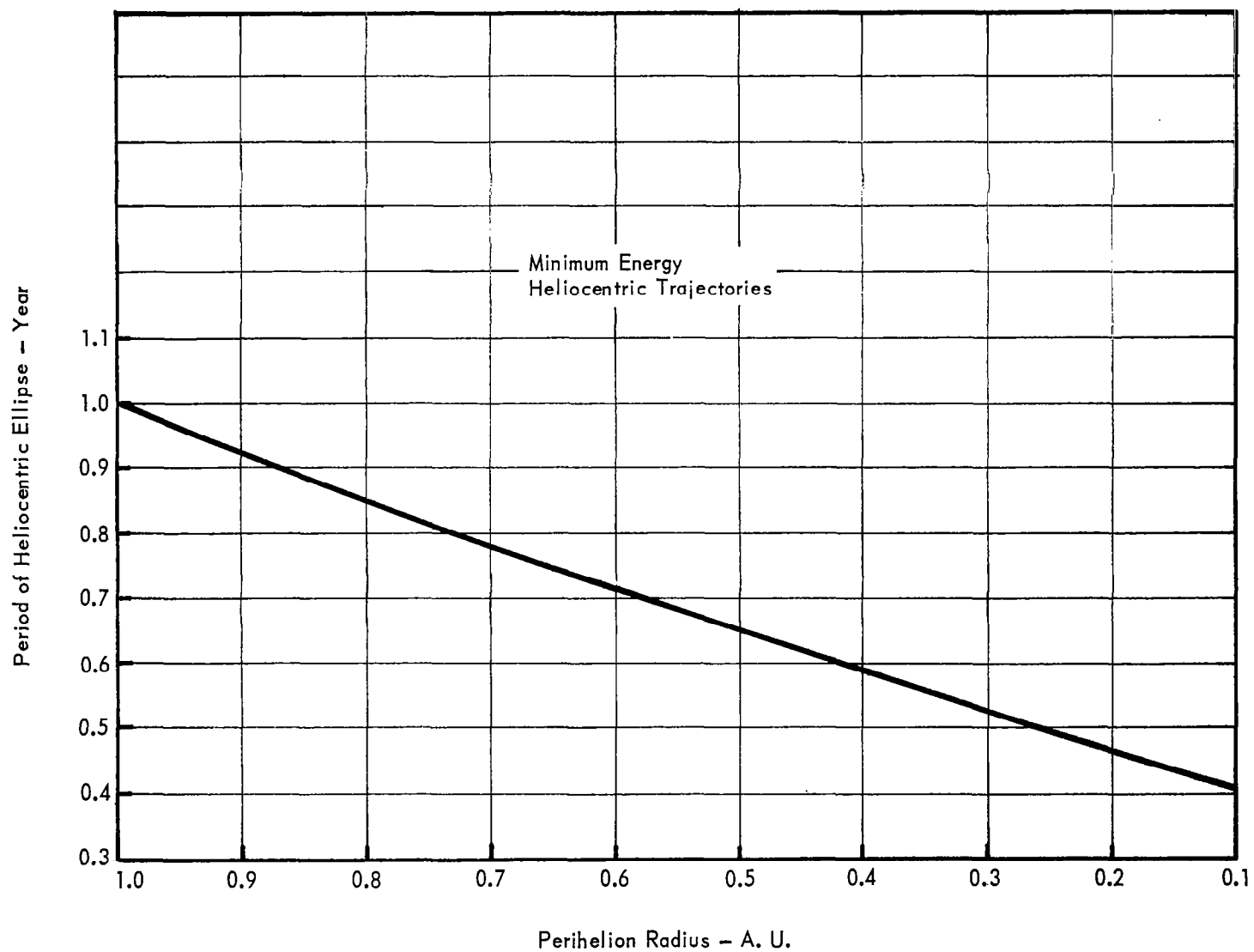


Figure 6. - Variation of Period of the Heliocentric Ellipse
with Perihelion Radius

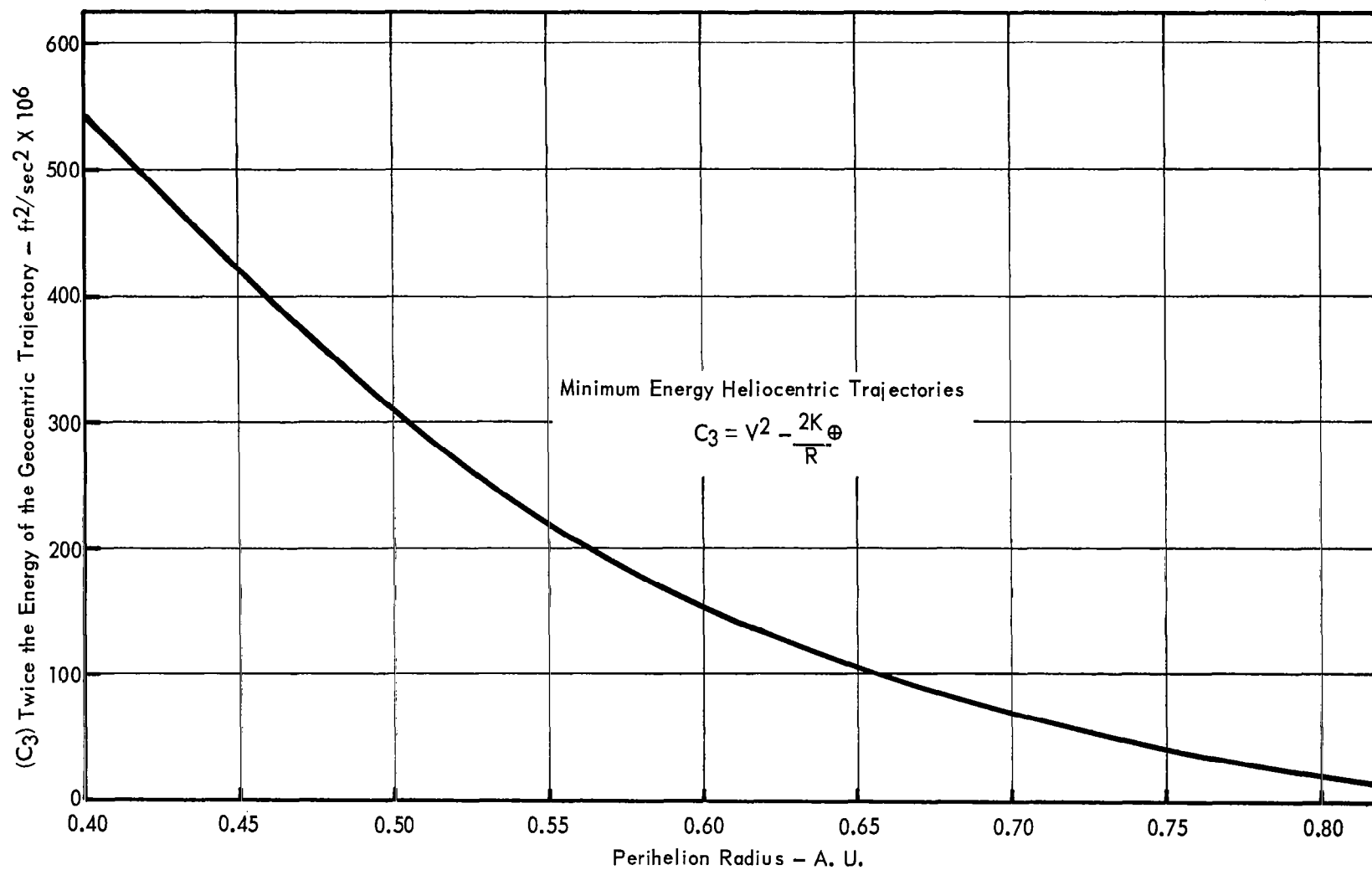


Figure 7.-Variation of Perihelion Radius with Energy of the Geocentric Trajectory

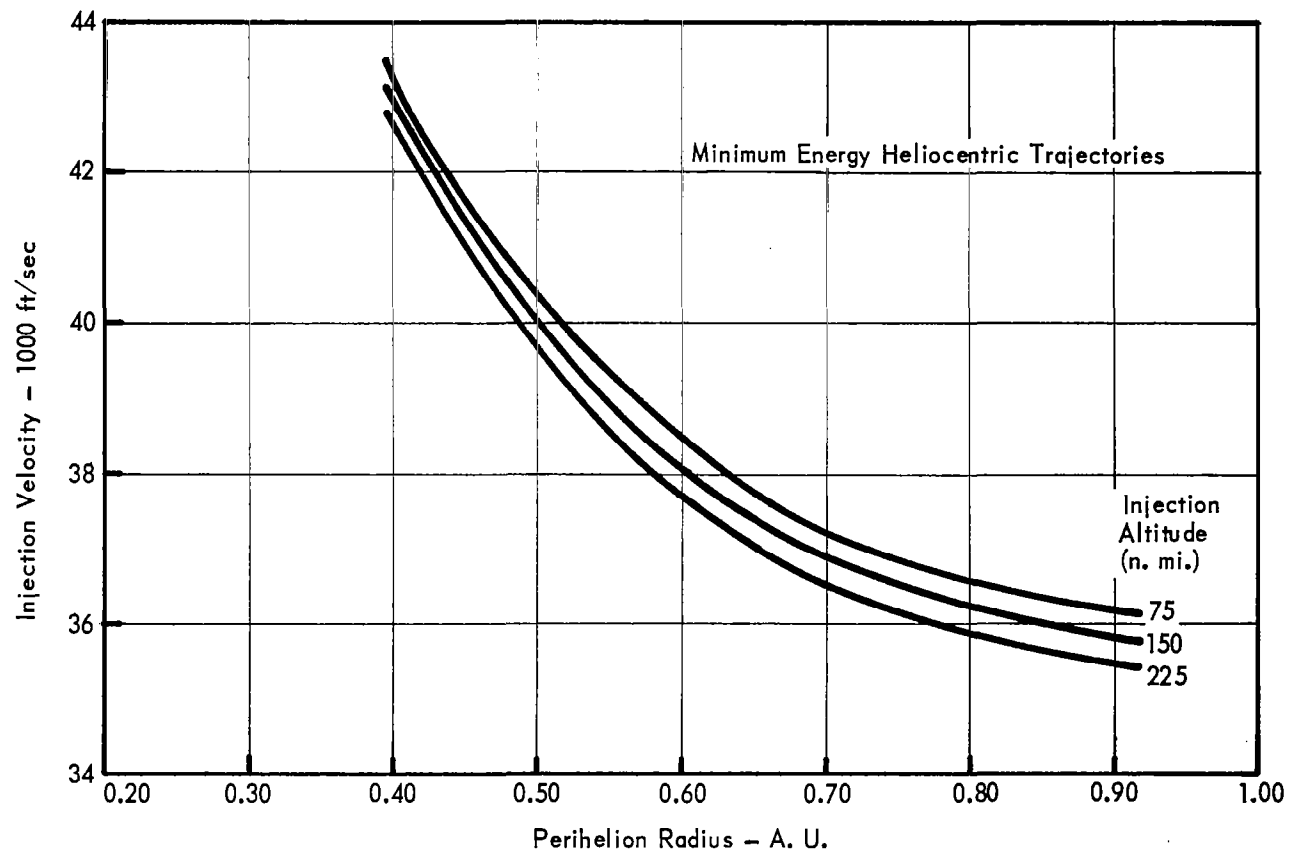


Figure 8._ Variation of Perihelion Radius with Injection Velocity

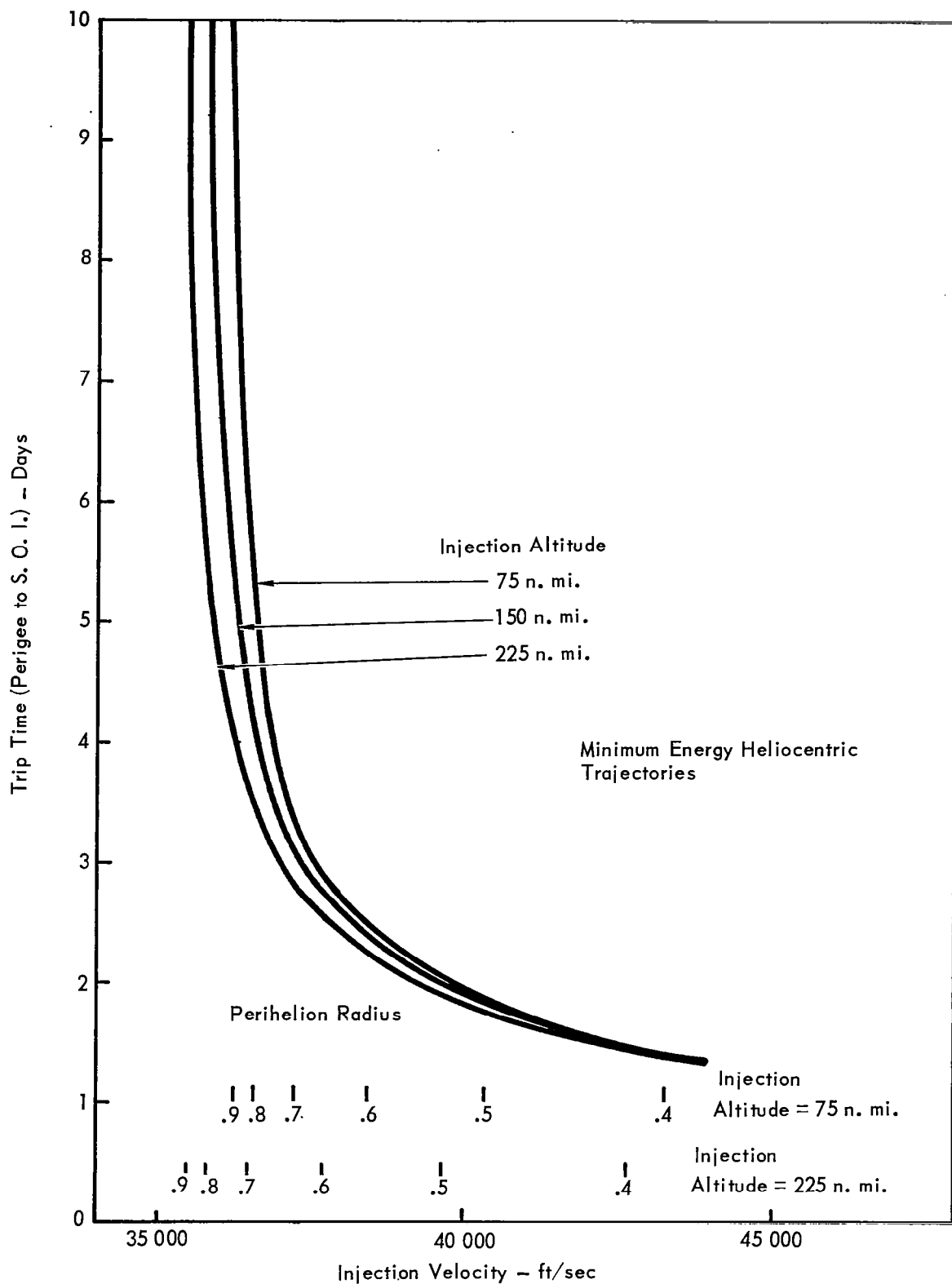


Figure 9.-Variation of Trip Time to Sphere of Influence with Injection Velocity

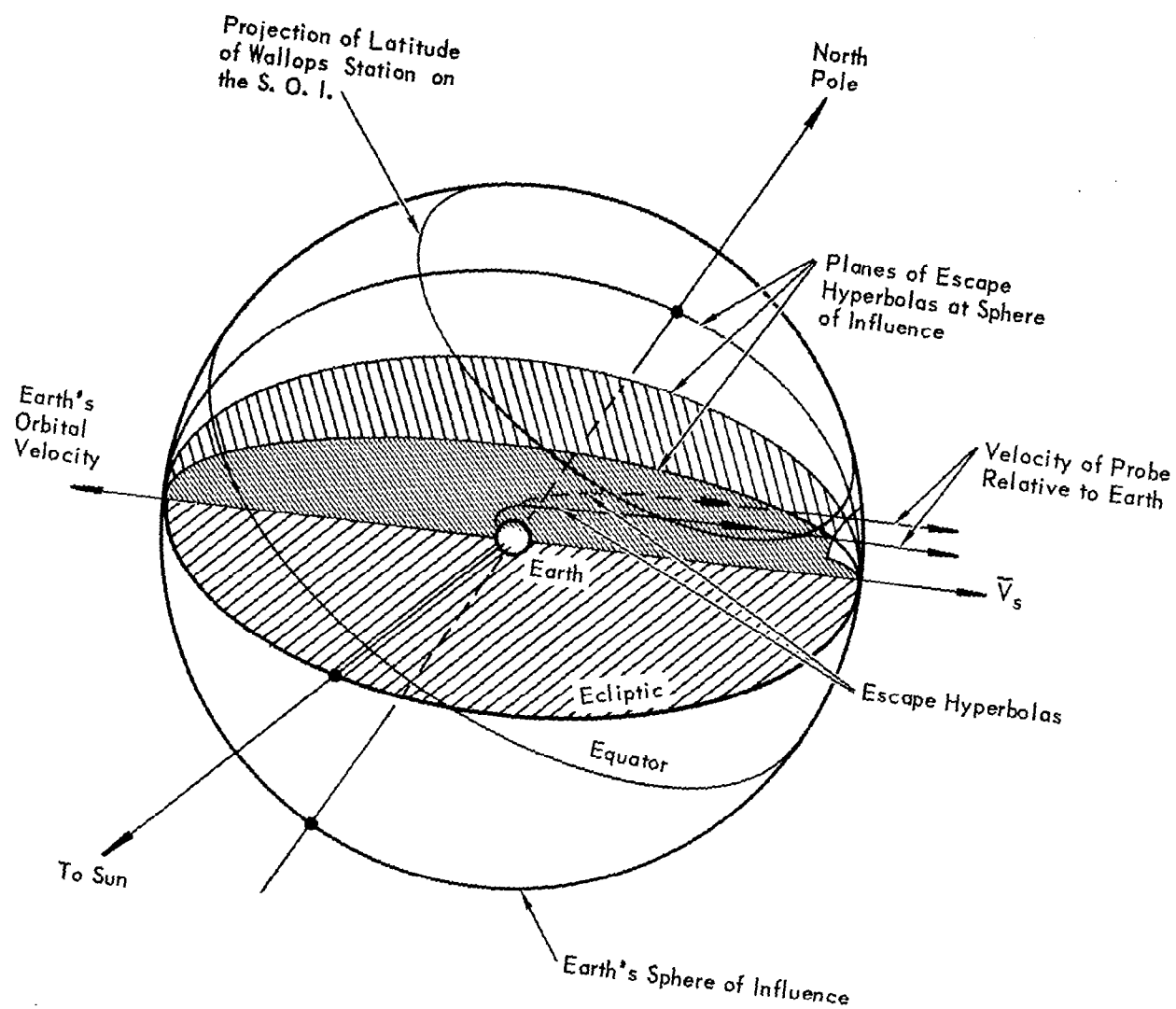


Figure 10. - Geocentric Portions of Trans-Solar Trajectories

σ - Inertial Range Angle Between Local Vertical at Launch Site and Direction of Hyperbolic Orientation Vector (V_s)

L. AZ - Launch Azimuth

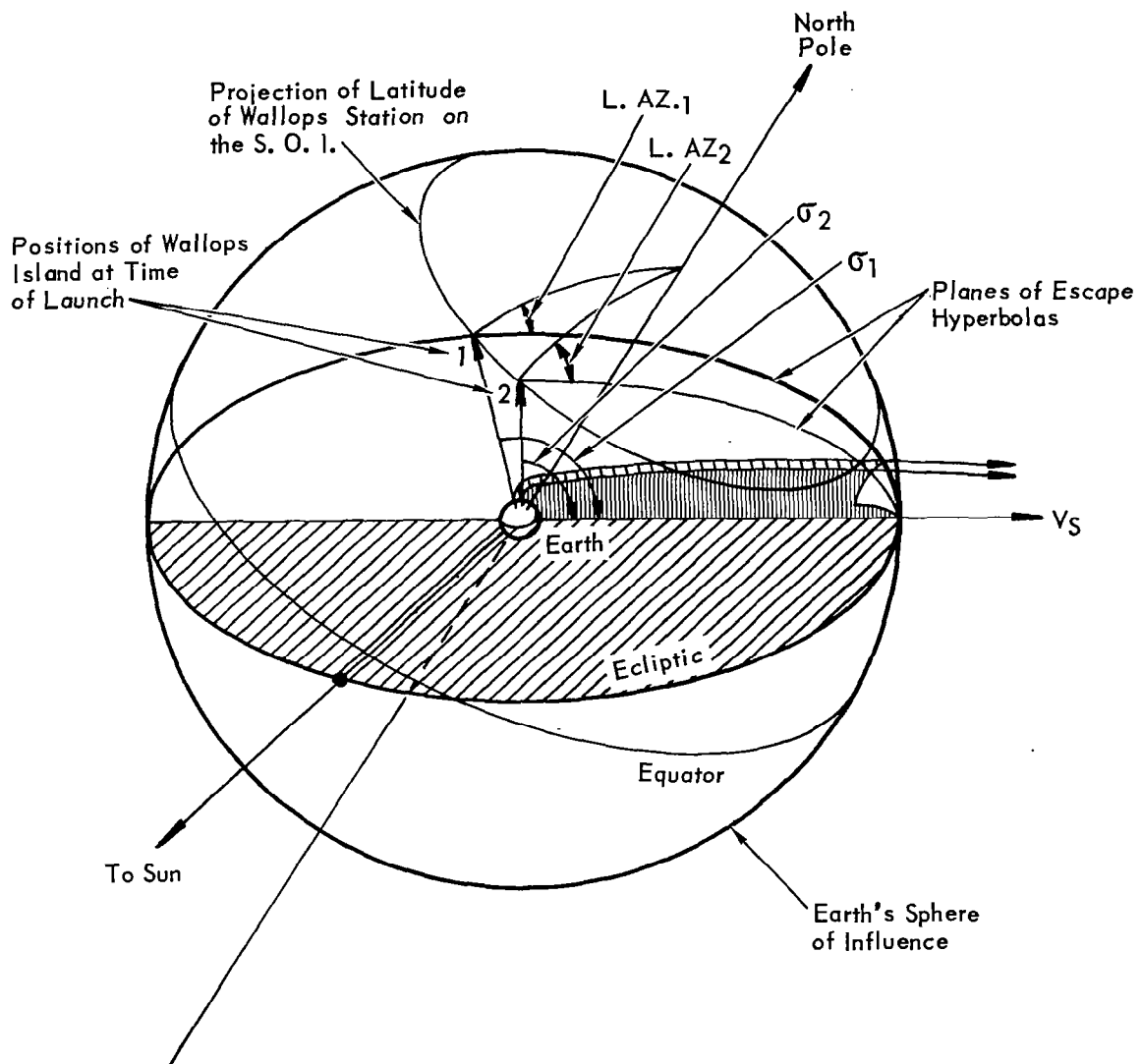
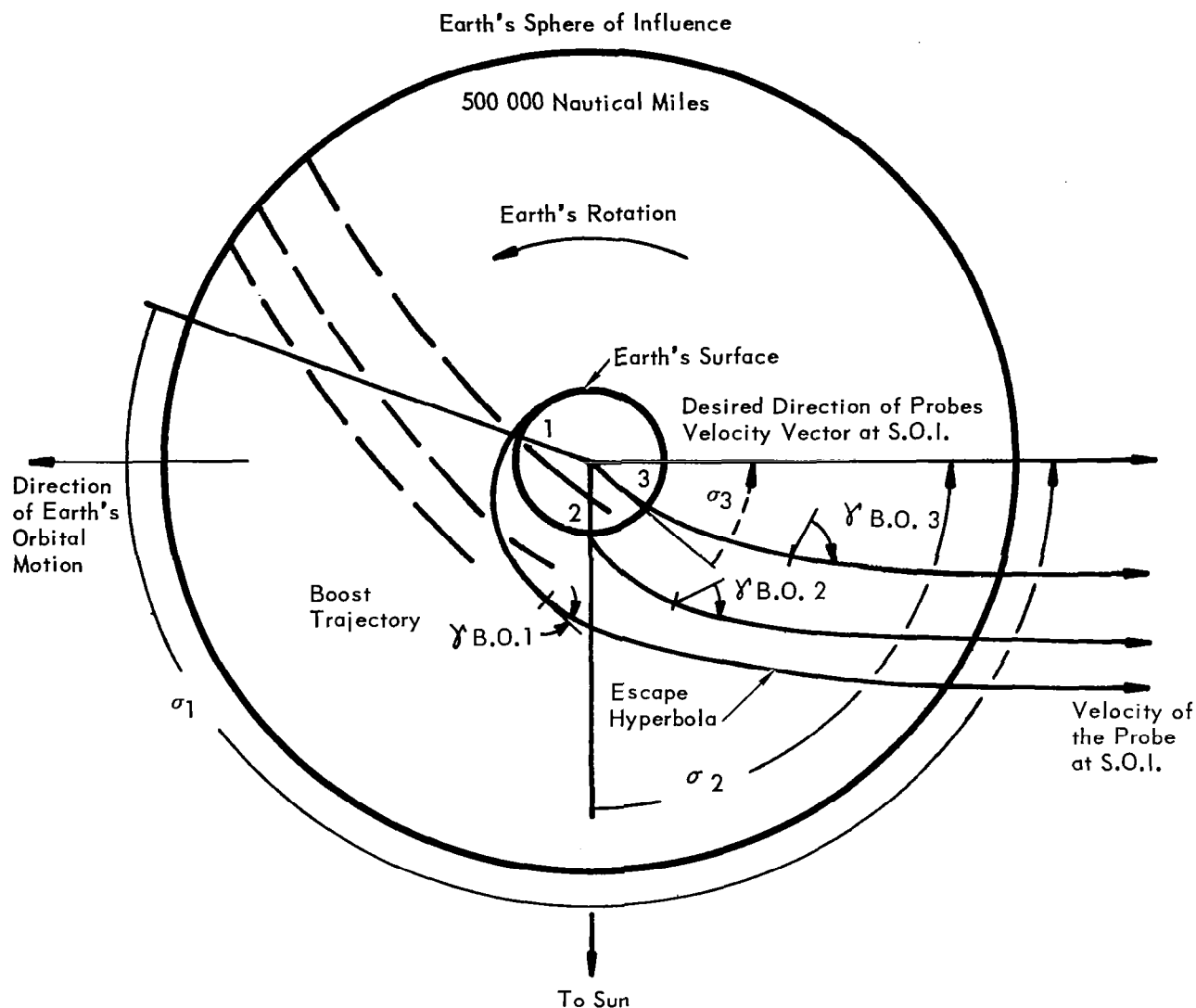


Figure 11. - Definition of Sigma Angle and Launch Azimuth



Launch Site Position	Launch Angle	Burn-out Altitude	Burnout Flight Path Angle $\gamma_{B.O.}$	Range Angle σ	Time of Day of Launch
1	Low	Low	0°	Large	A.M.
2	Medium	Medium	Medium	Medium	Noon
3	High	High	High	Small	P.M.

Figure 12. – Relationship Between Range Angle to Sphere of Influence and Flight Path Angle at Burnout

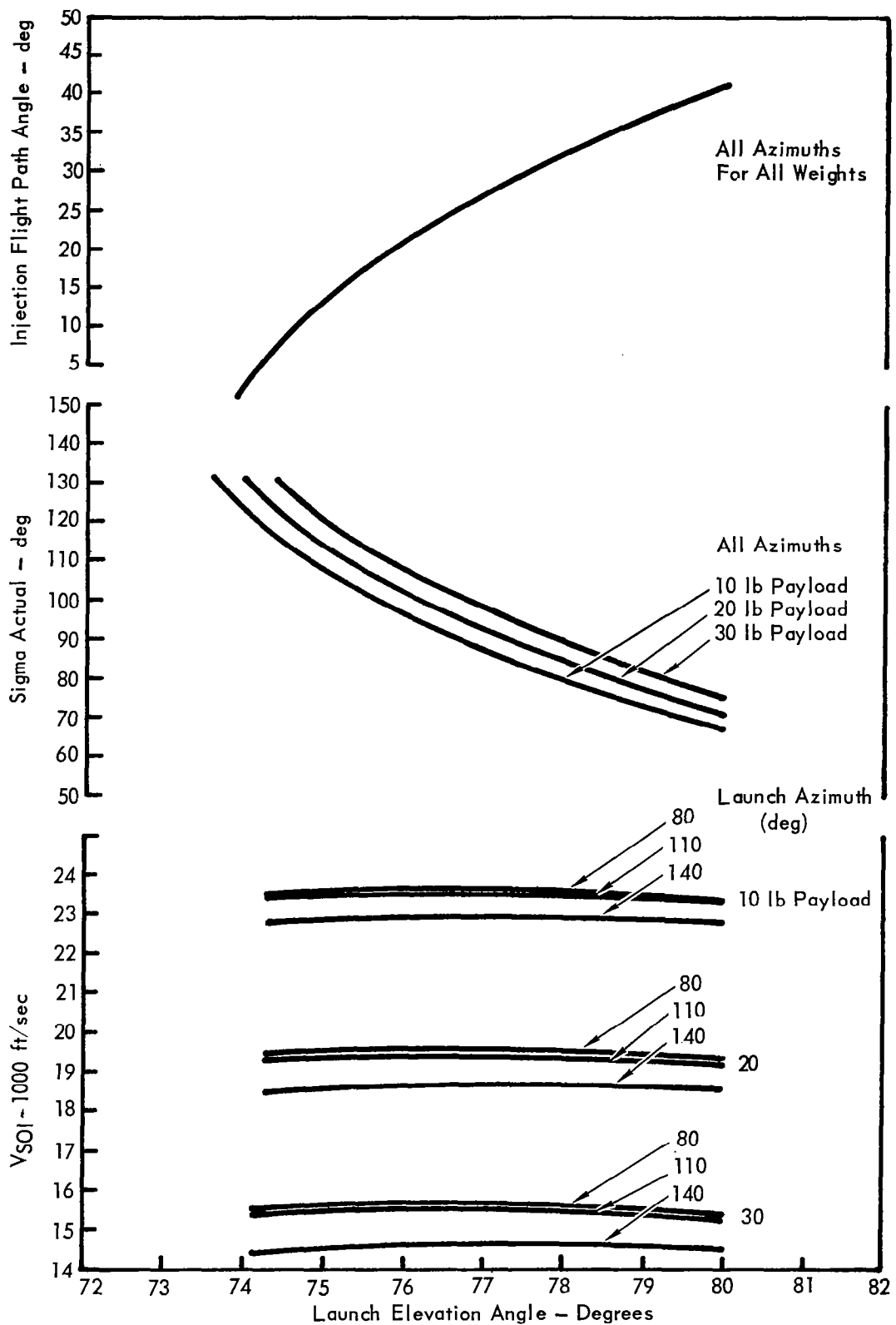


Figure 13.-Typical Launch Vehicle Performance Data

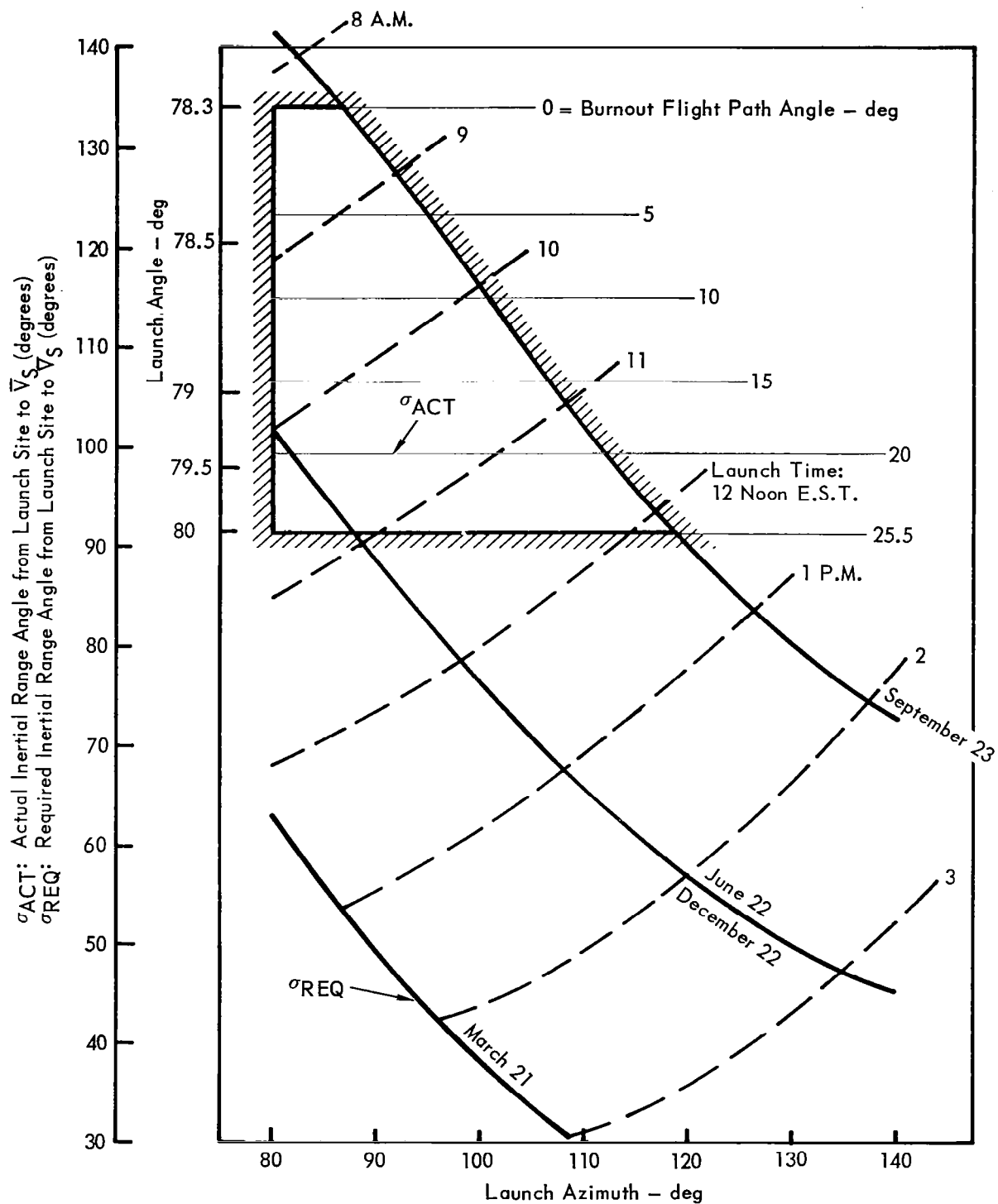


Figure 14. - Launch Conditions for Nominal Heliocentric Trajectory

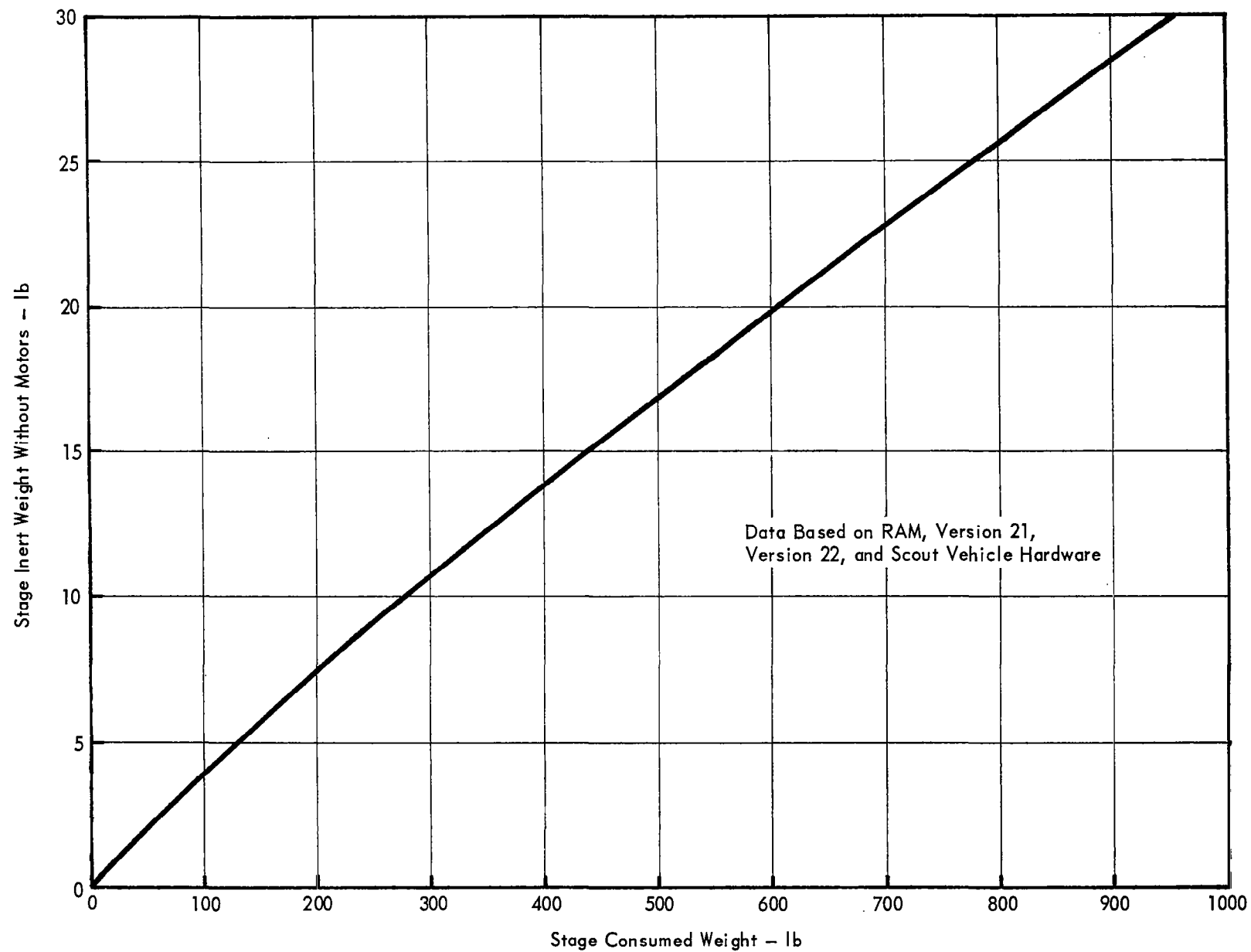


Figure 15.— Final Stage Weight Estimating Data

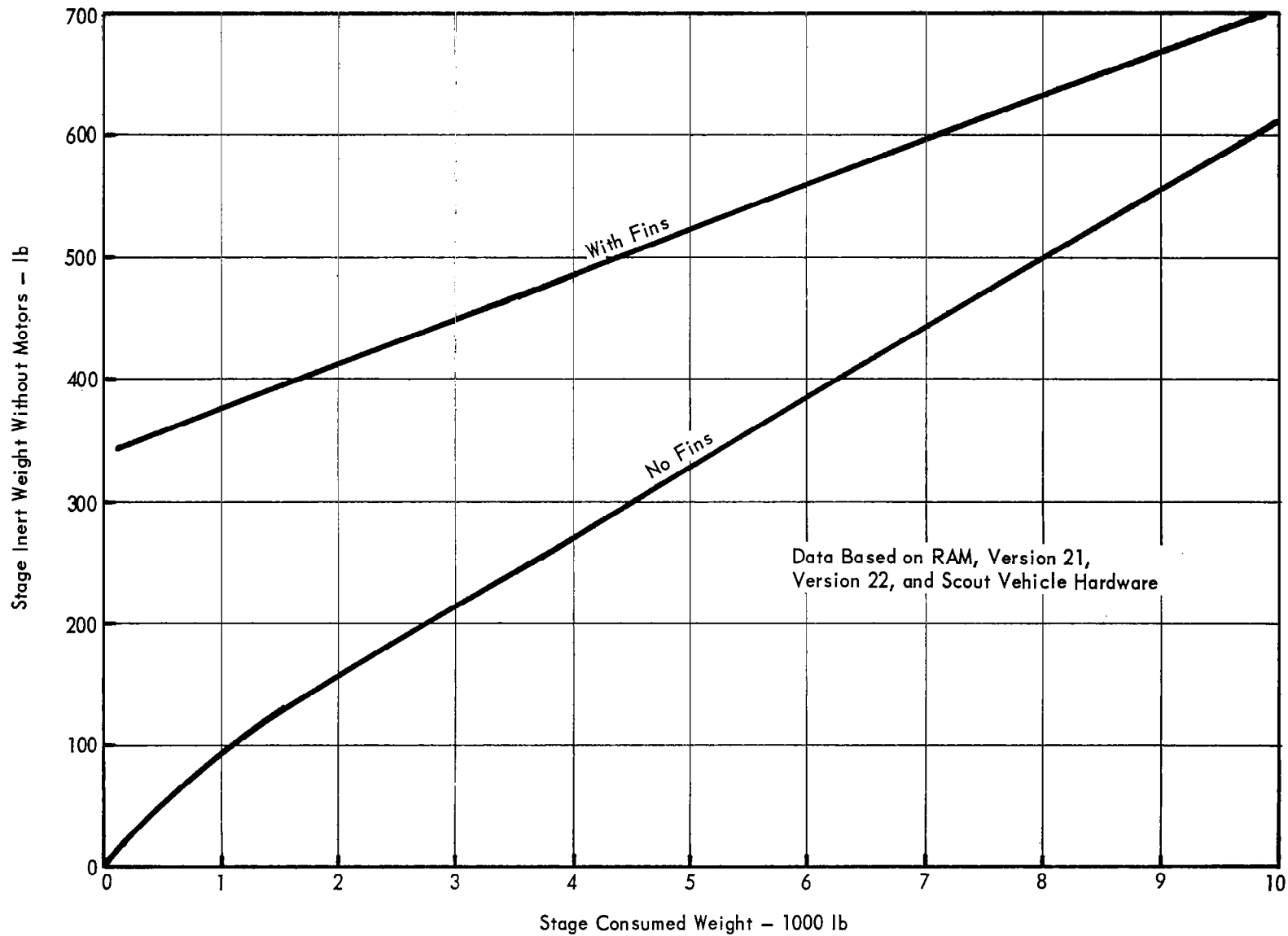


Figure 16. - Middle Stages Weight Estimating Data

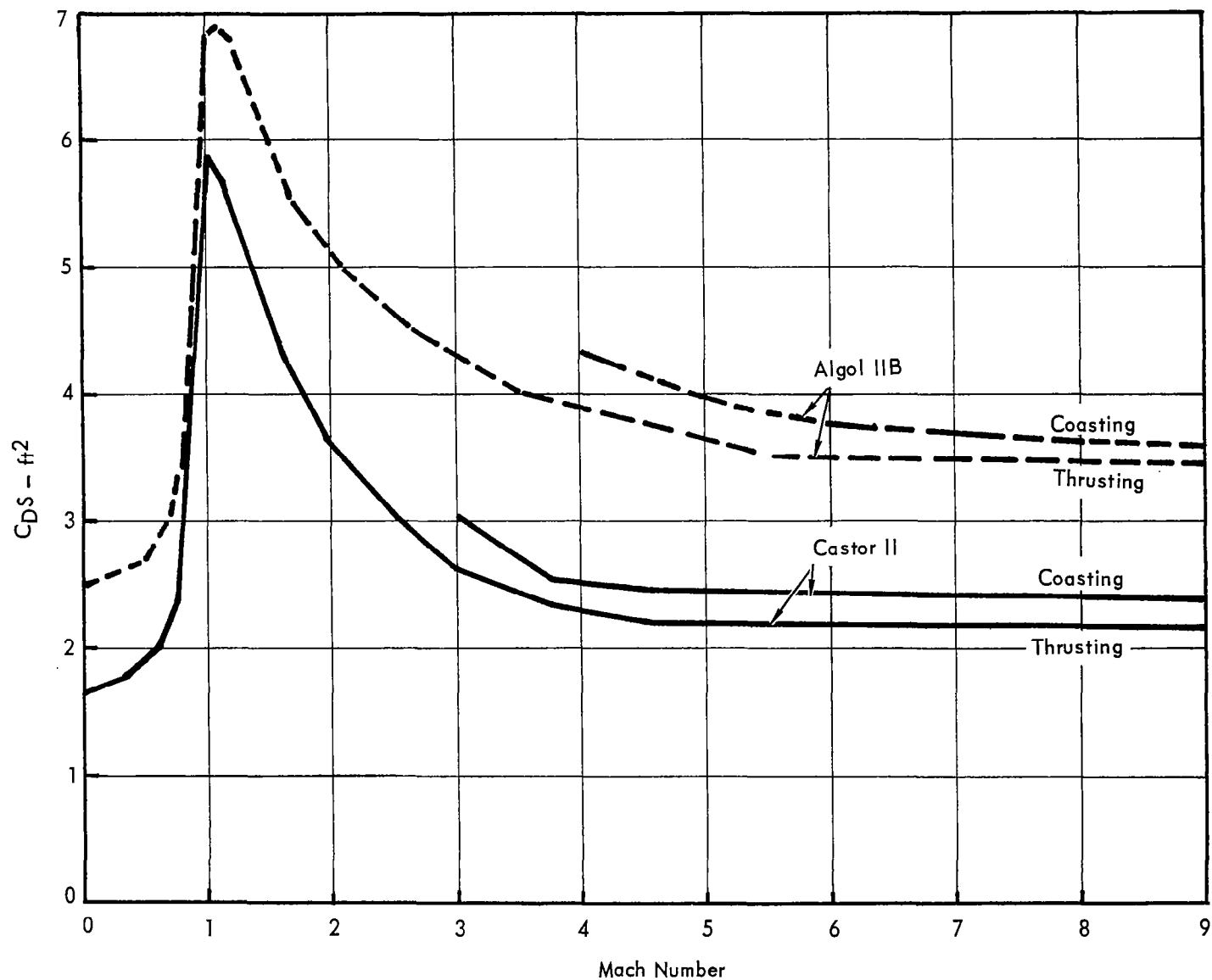


Figure 17. - Aerodynamic Zero Lift Drag Characteristics

Note: Conditions are at
Dynamic Pressure = 3.0 lb/ft²

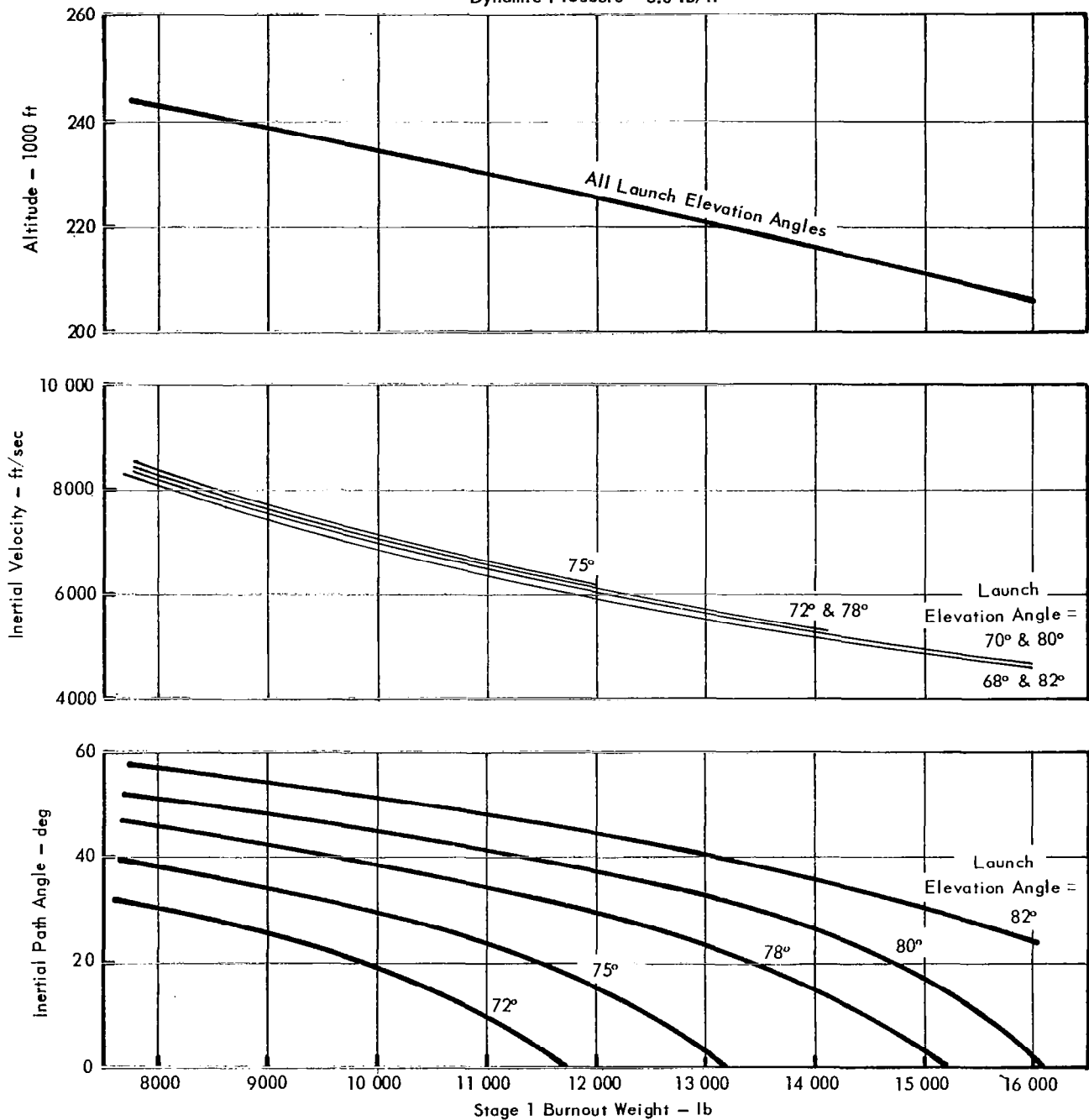


Figure 18. - Algal IIB Booster Performance

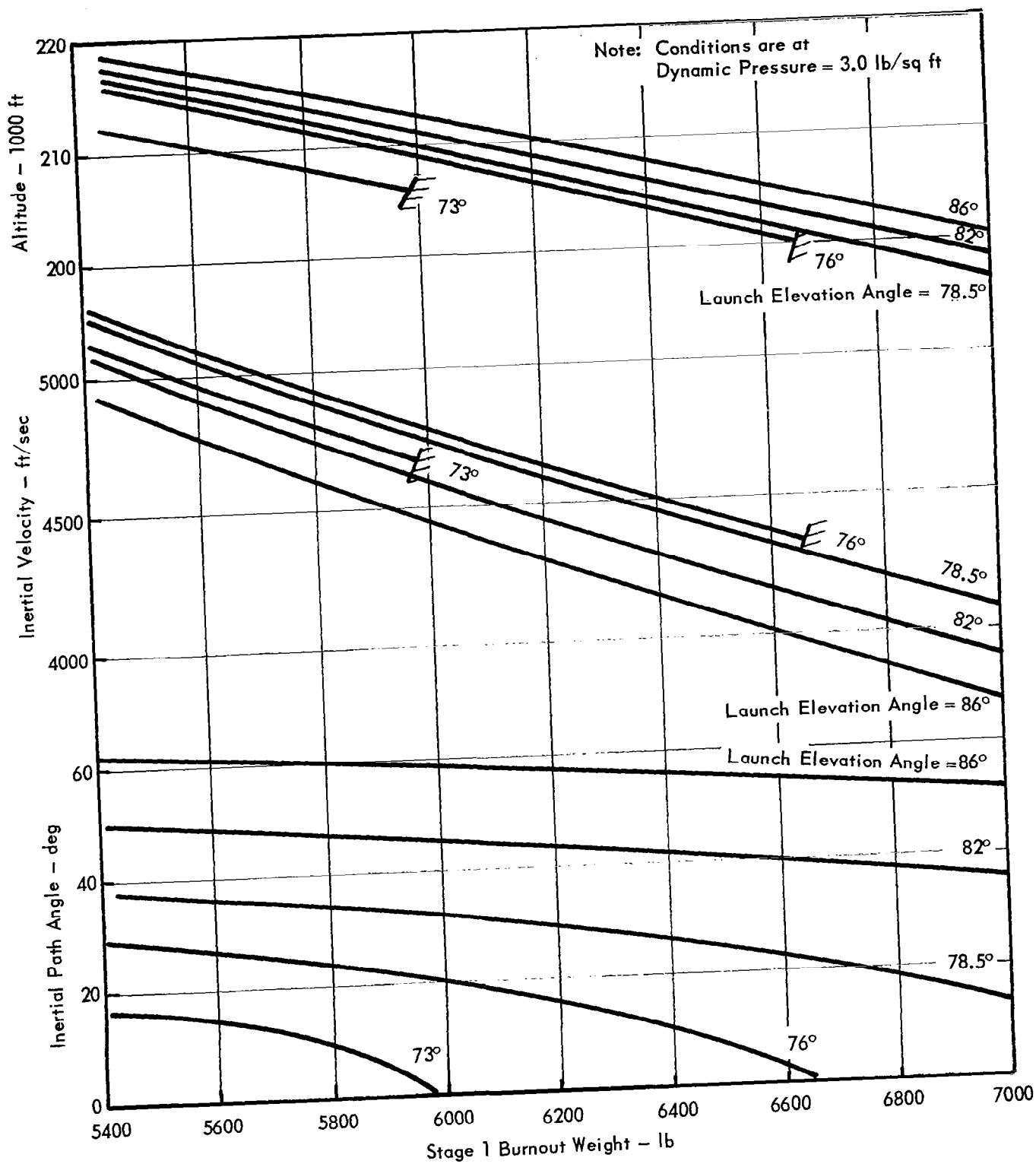


Figure 19. - Castor II Booster Performance

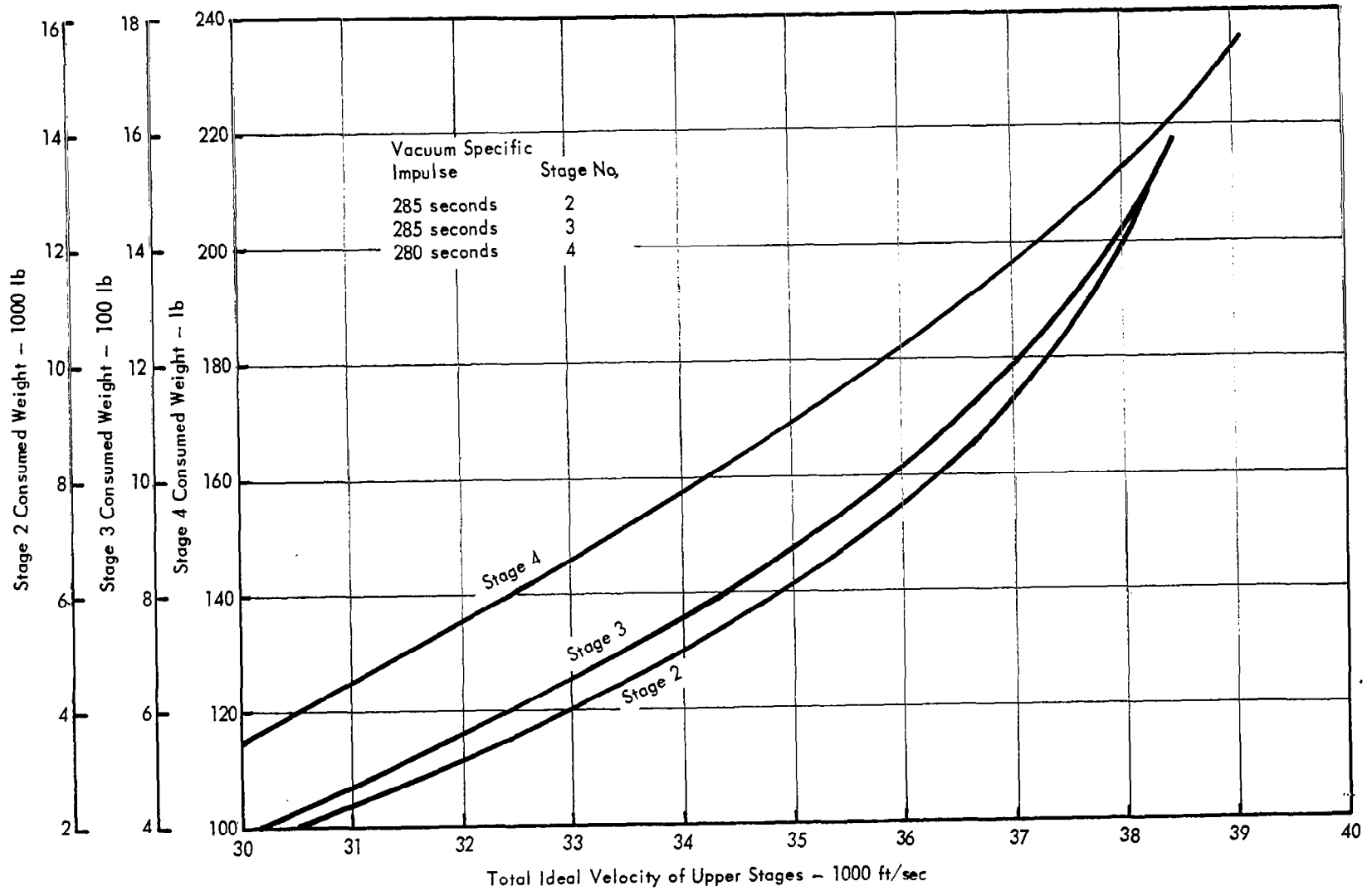


Figure 20. - Optimized Upper Stages for Consumed Weight Versus Ideal Velocity

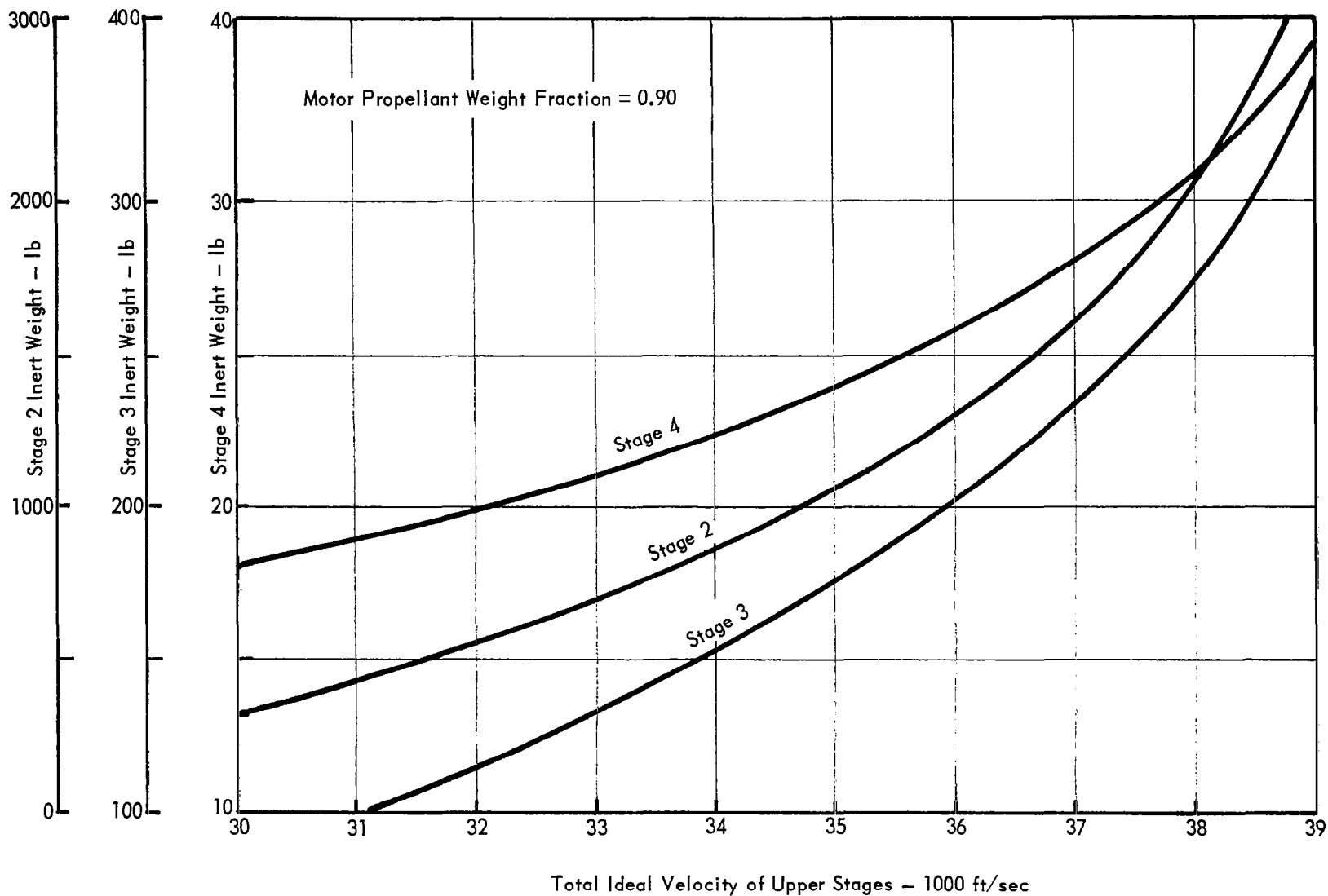


Figure 21. - Optimized Upper Stages for Inert Weight Versus Ideal Velocity

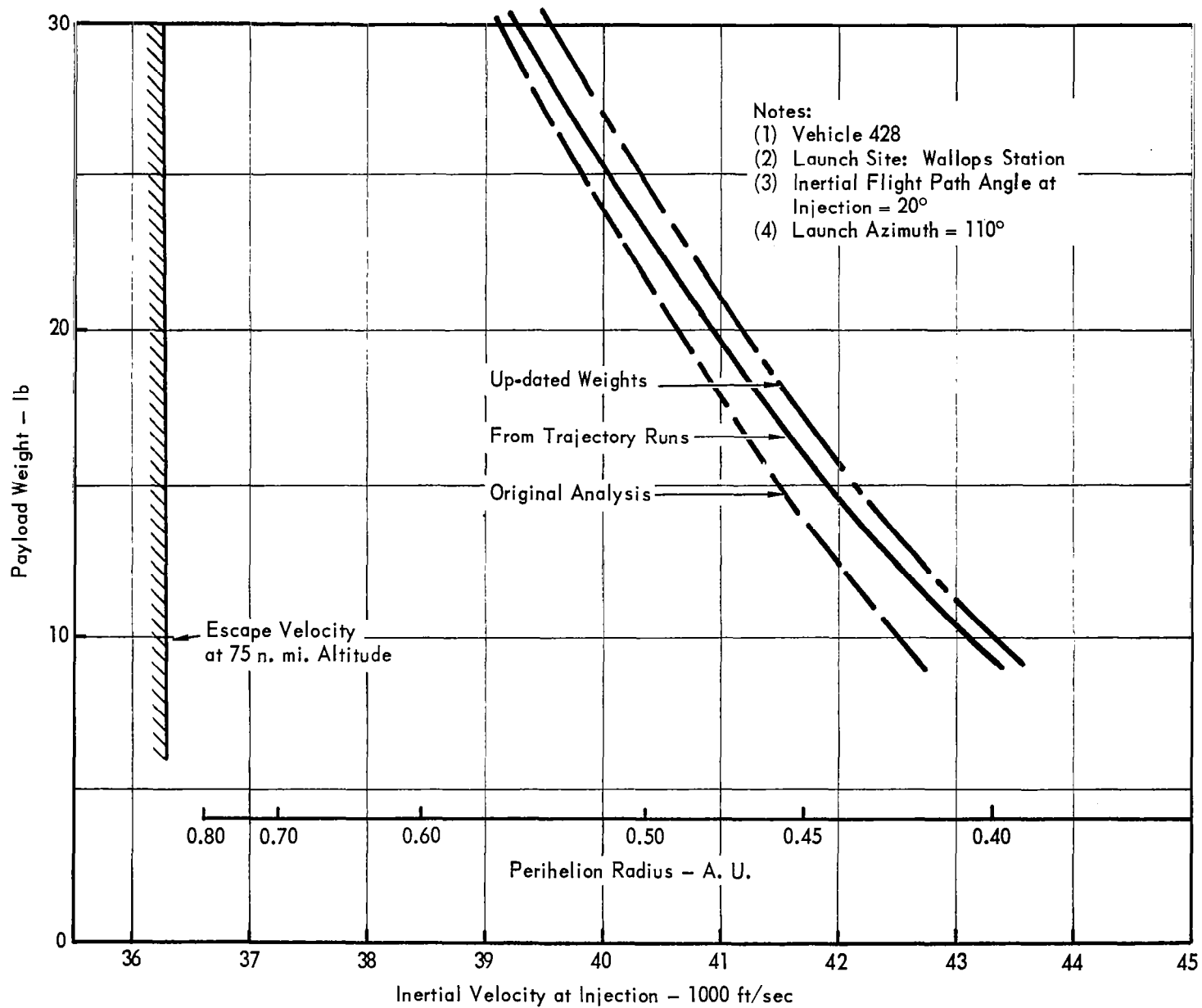


Figure 22. - Performance Calculations Compared with Computed Trajectories

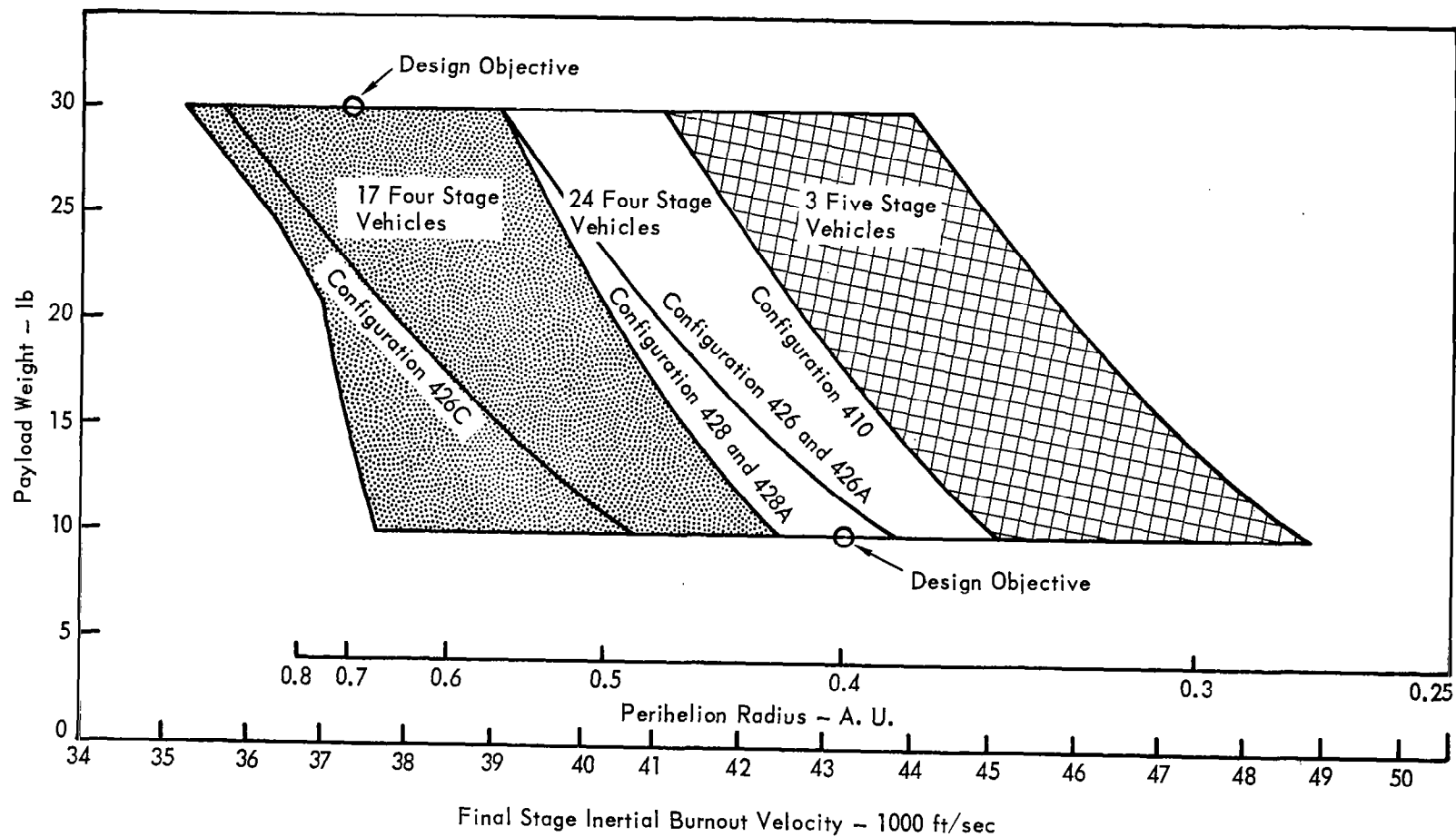


Figure 23. - Comparison of Candidate Vehicle Heliocentric Performance

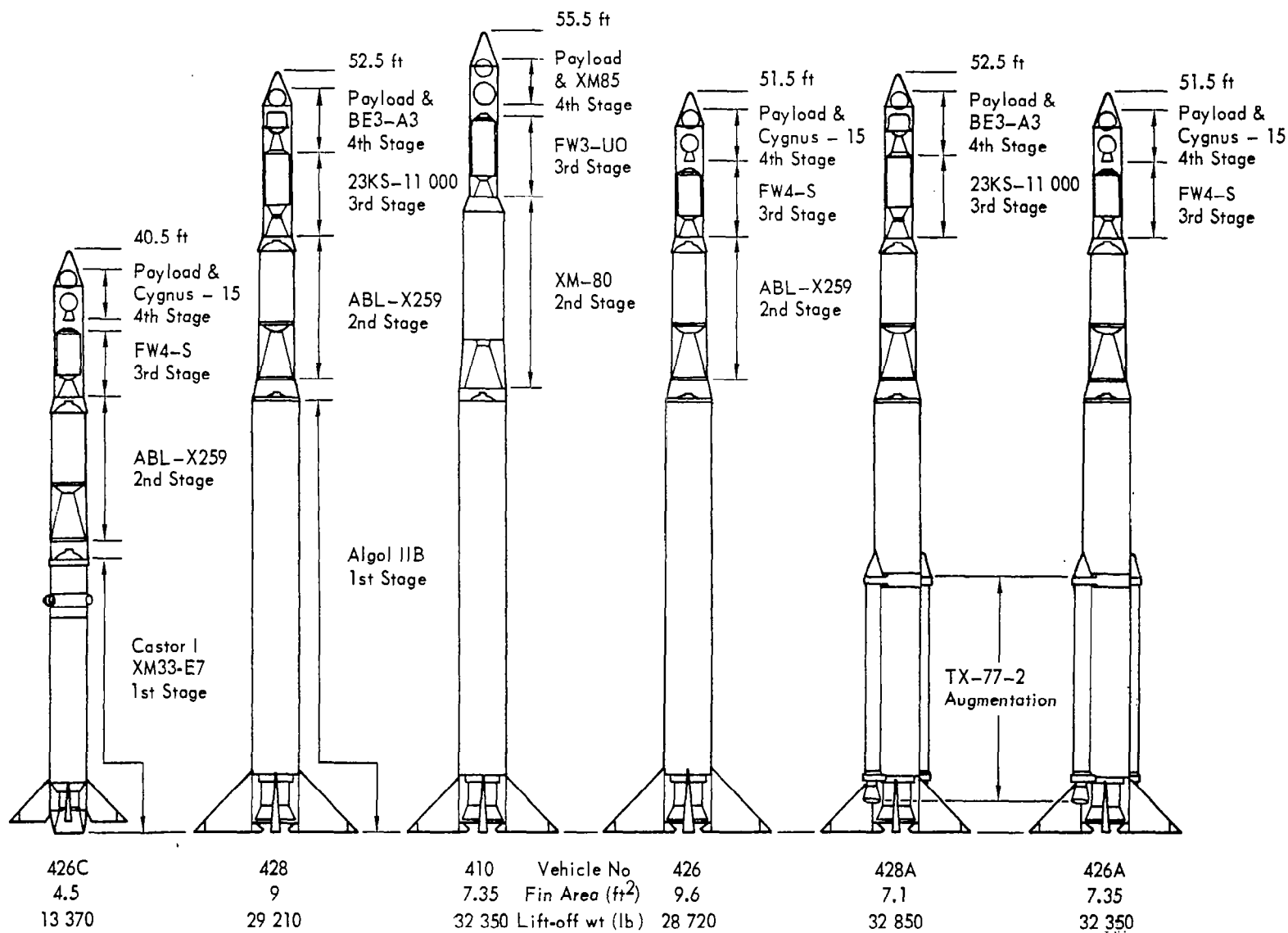


Figure 24. - Vehicle Candidate Configurations

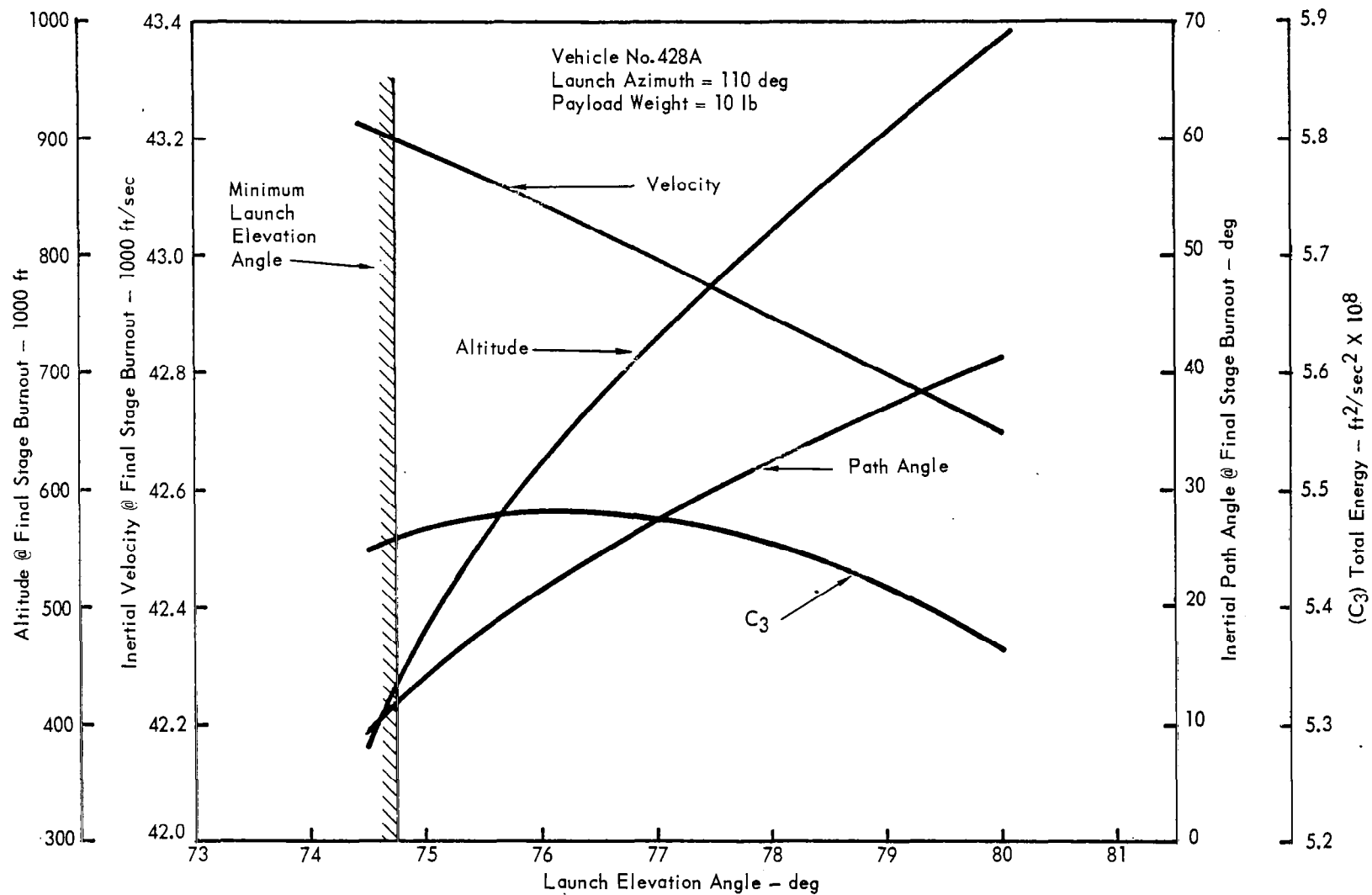


Figure 25. - The Effect of Launch Elevation Angle on Conditions at Final Stage Burnout

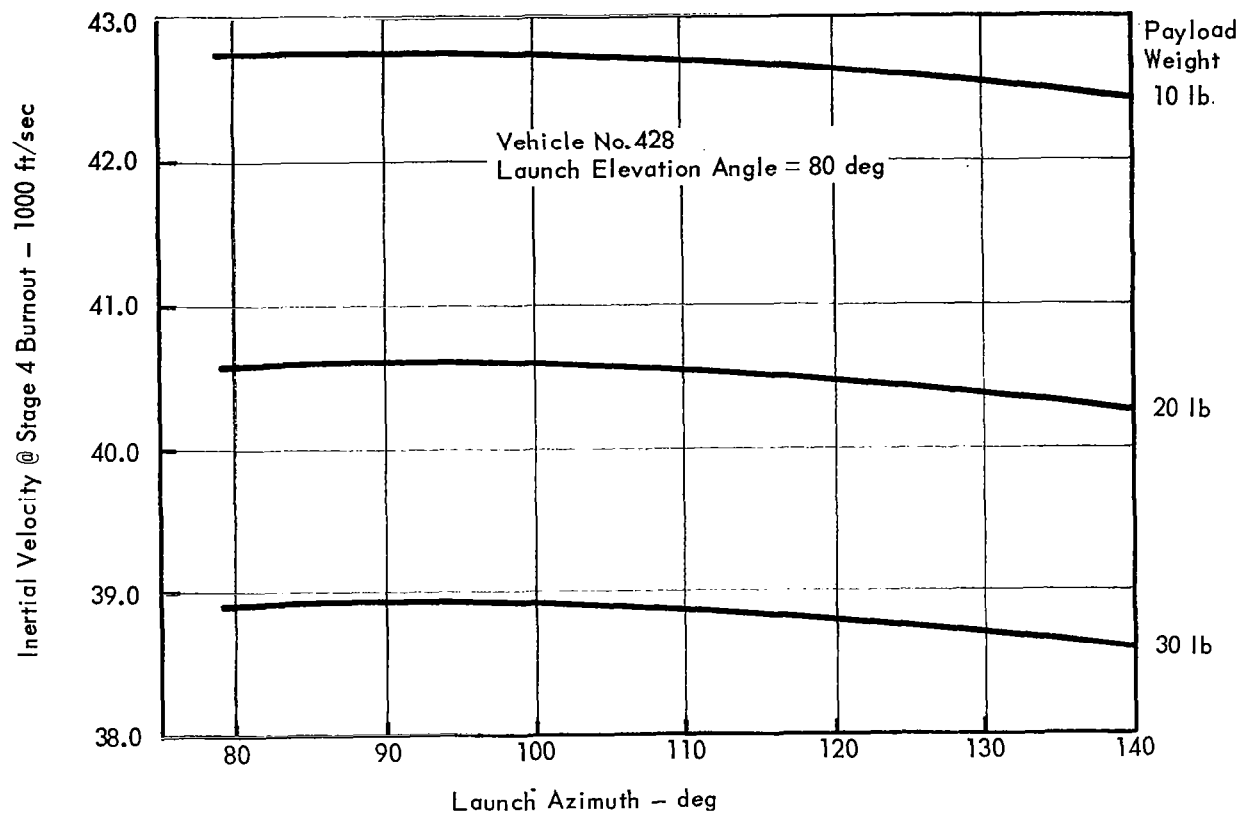


Figure 26. - The Effect of Launch Azimuth on Burnout Velocity

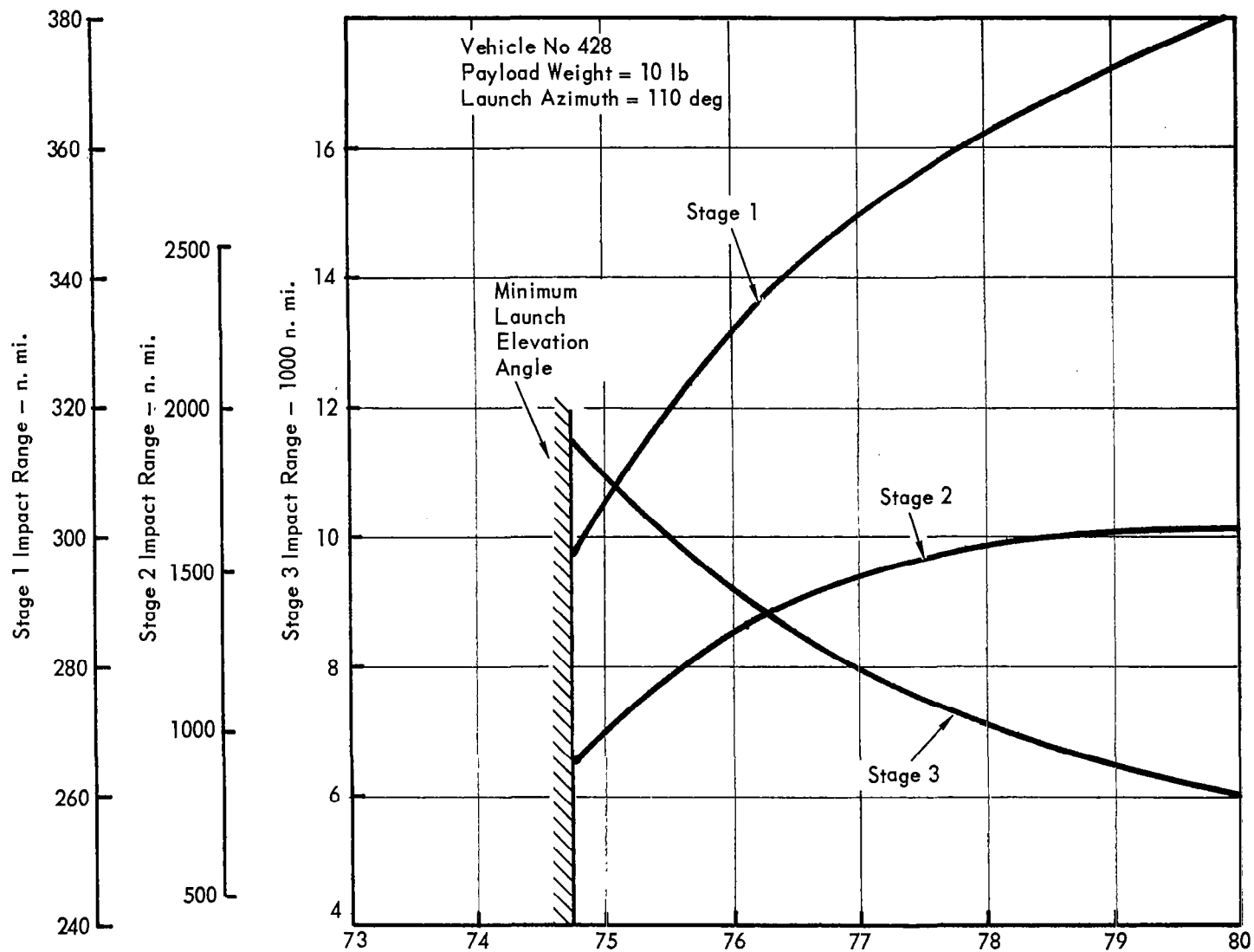


Figure 27. - Stage Impact Range Data

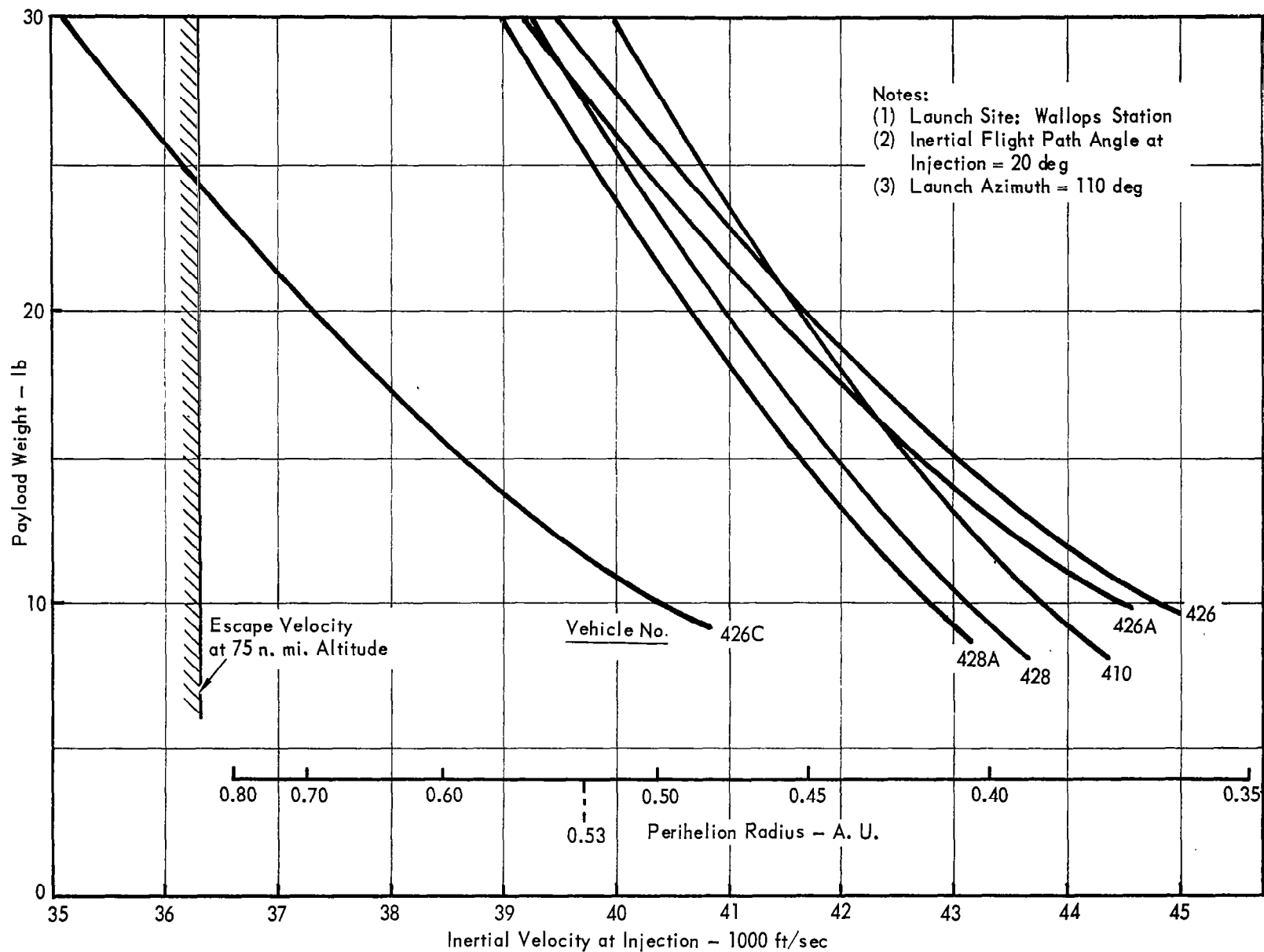


Figure 28. - Performance Comparison of Candidate Vehicles

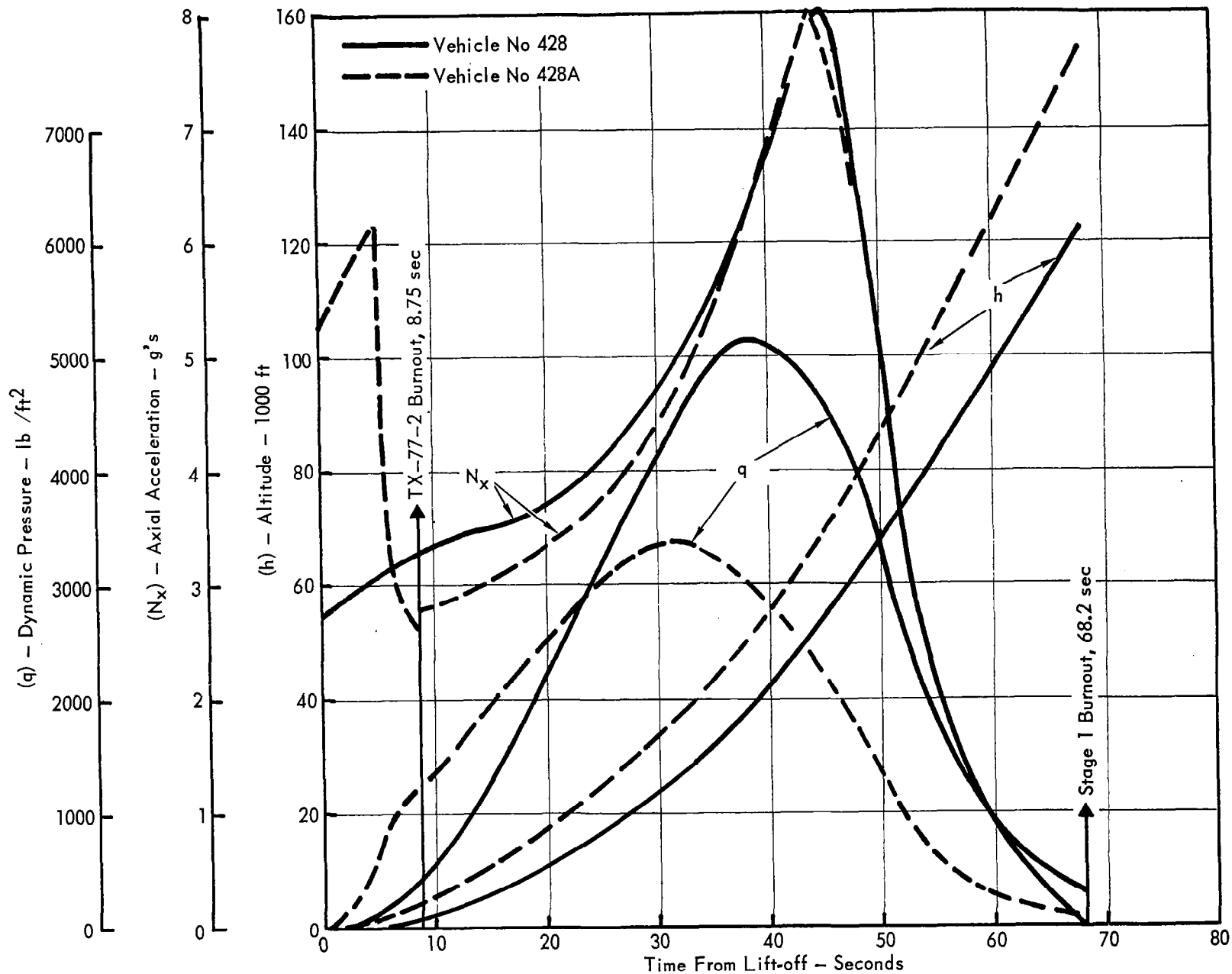


Figure 29. - Boost Time Histories of Augmented and Non-augmented Vehicles

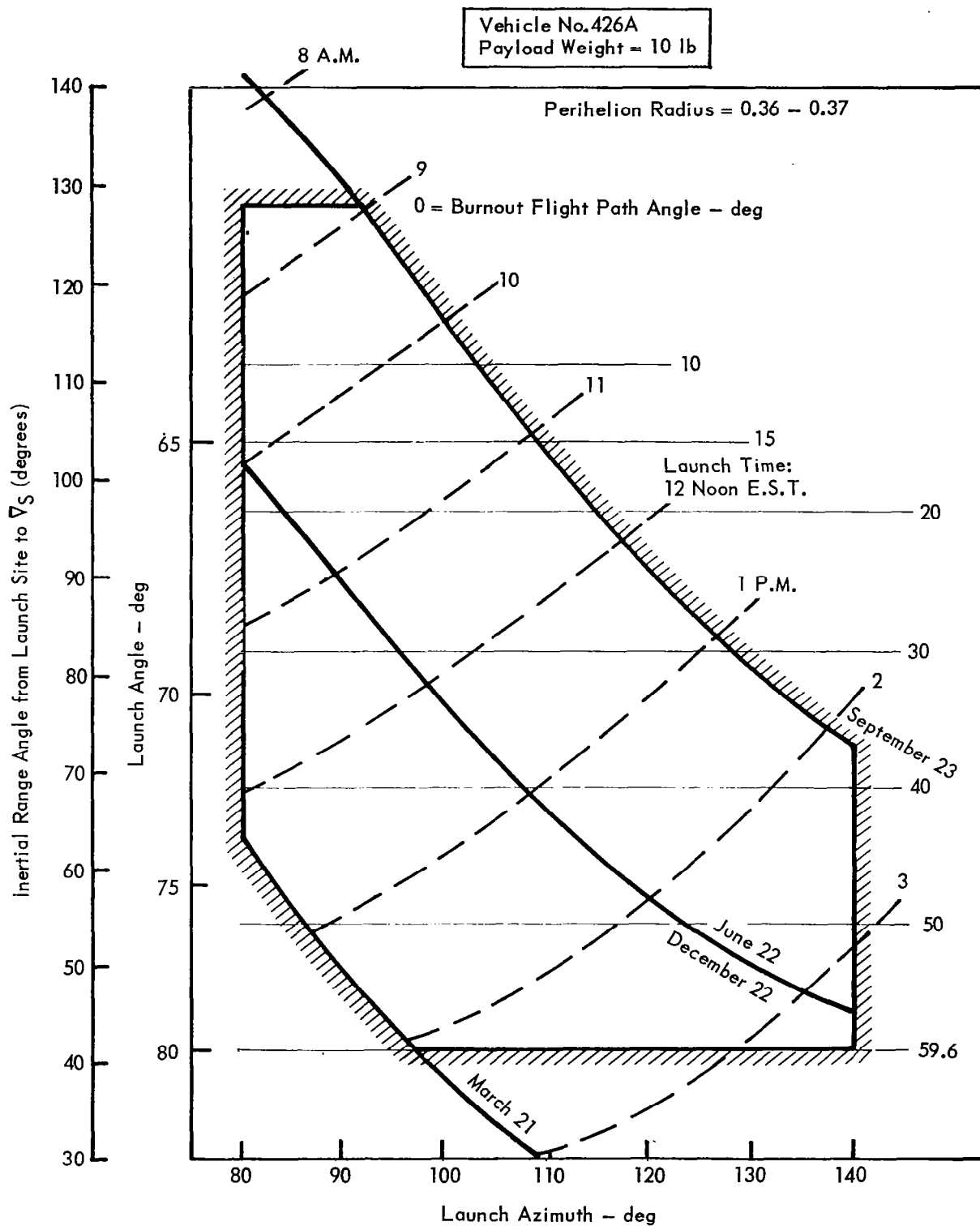


Figure 30. - Launch Conditions for Nominal Heliocentric Trajectory

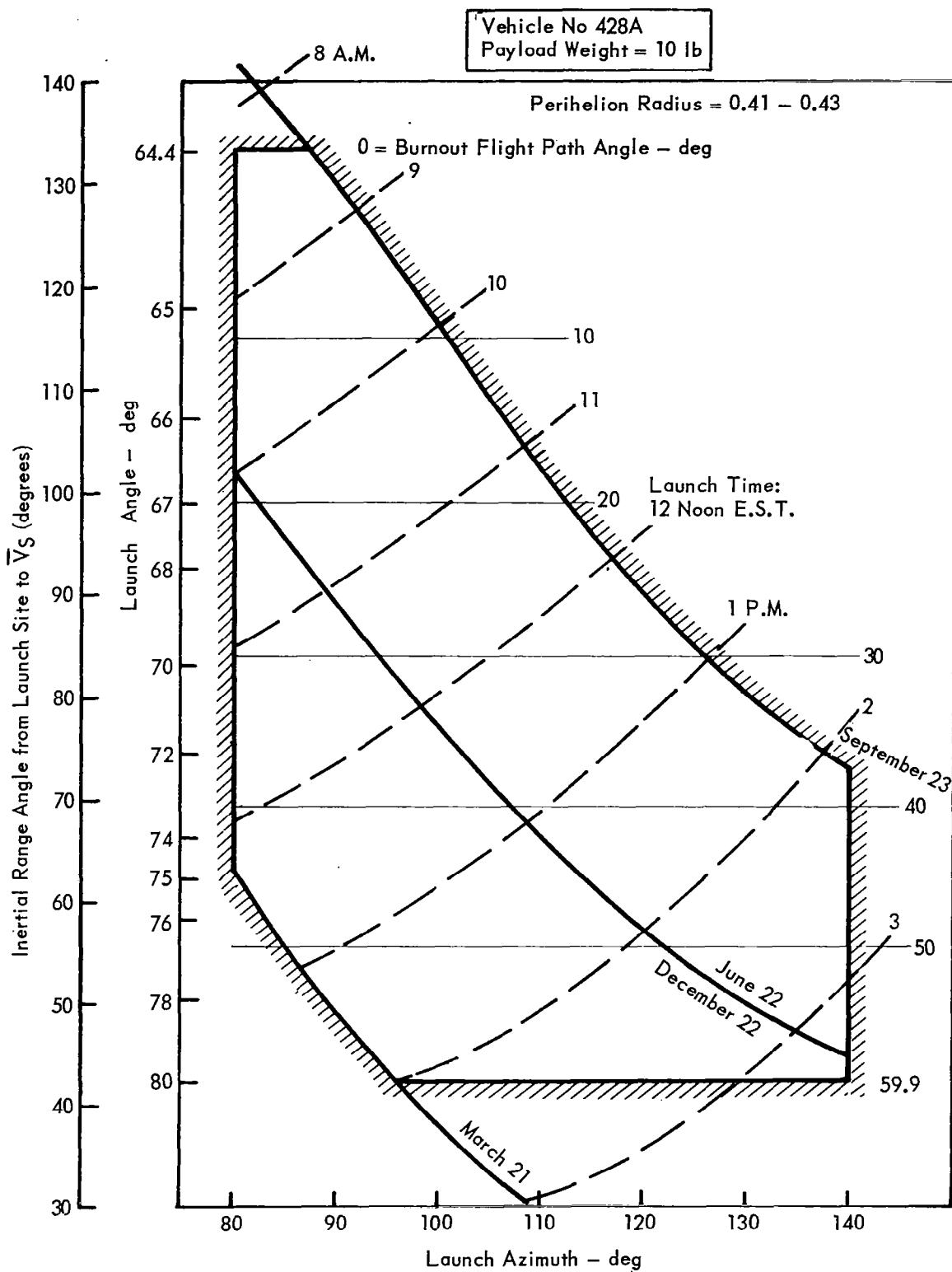


Figure 31. - Launch Conditions for Nominal Heliocentric Trajectory

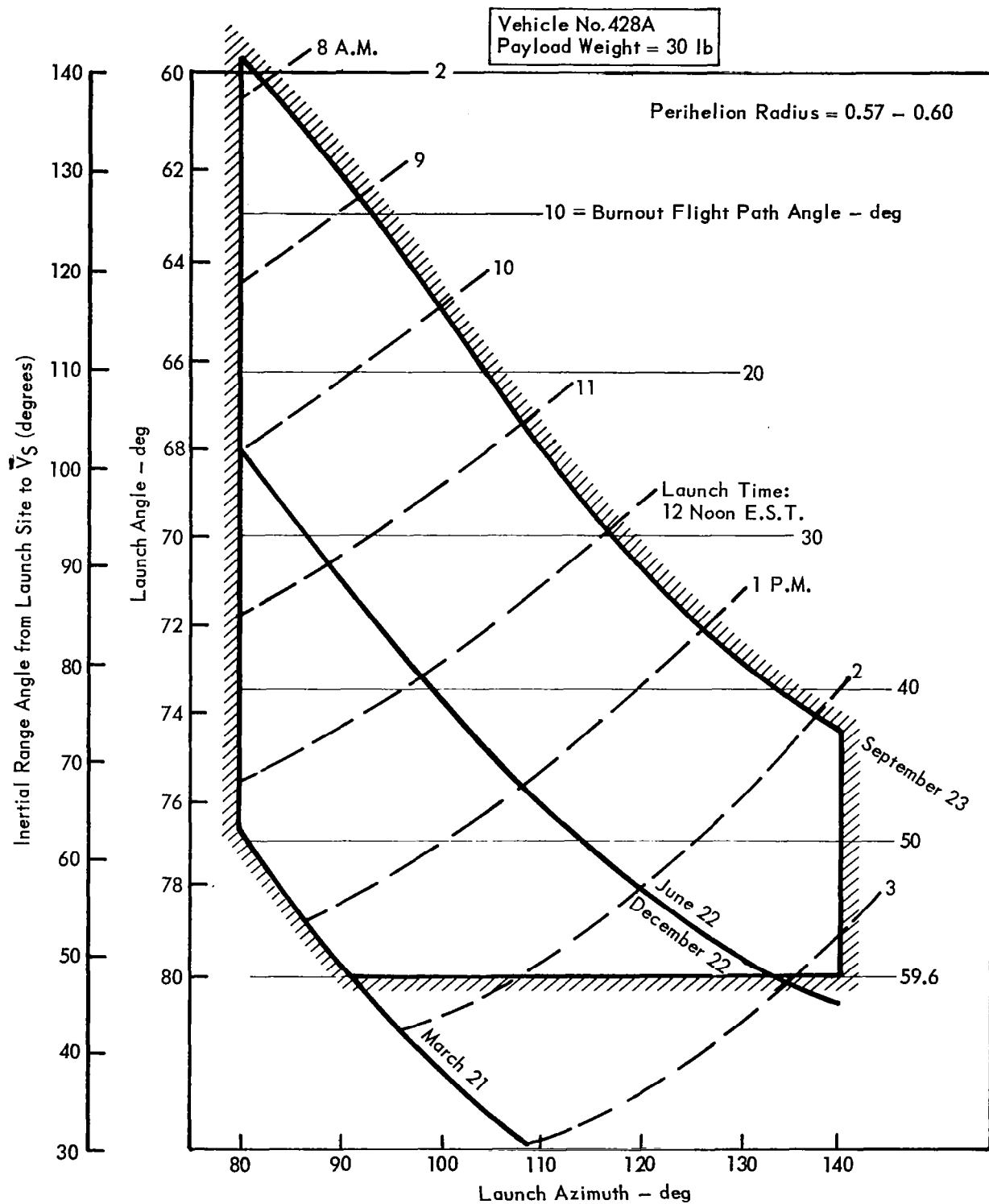


Figure 32. - Launch Conditions for Nominal Heliocentric Trajectory

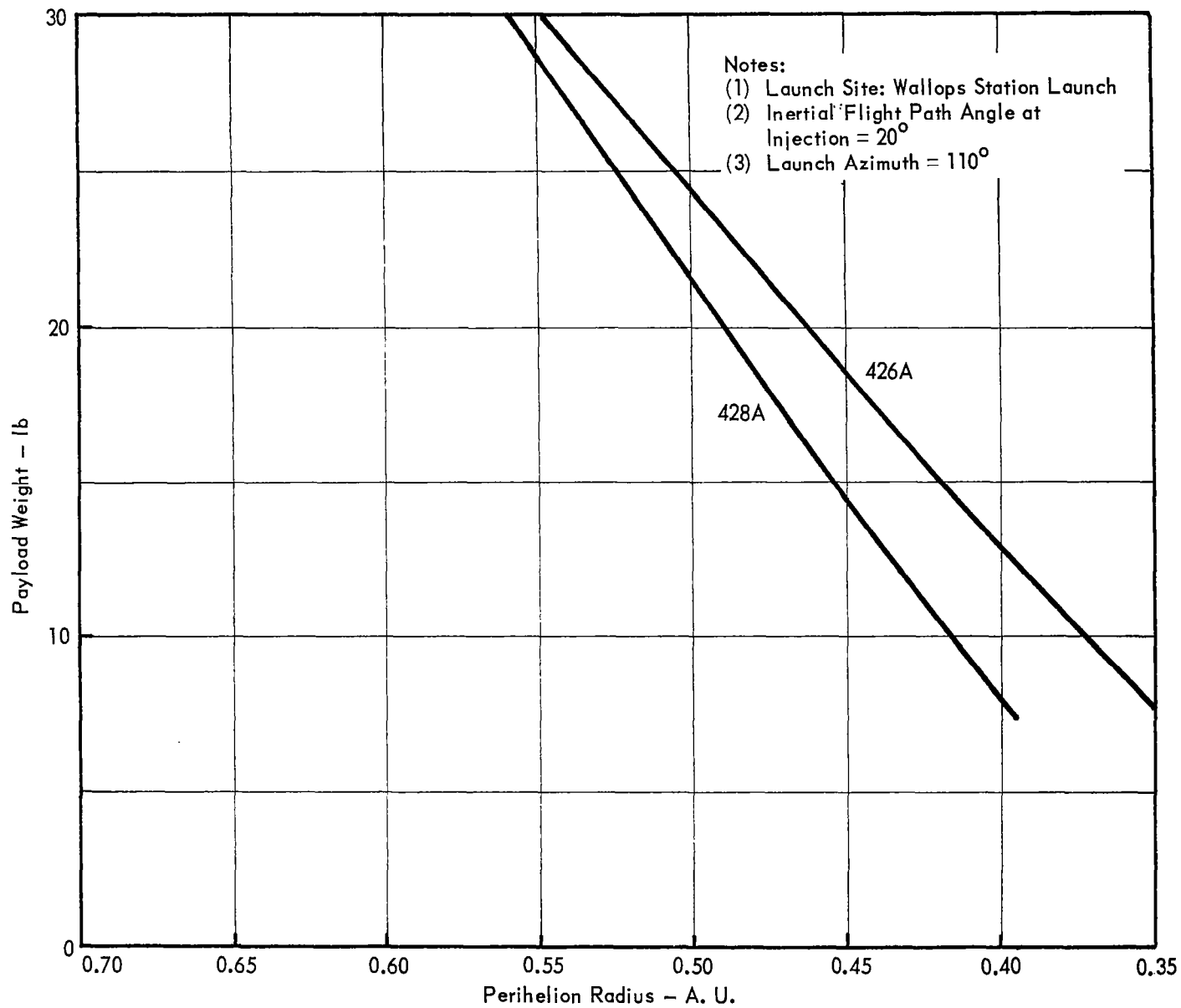


Figure 33. - Vehicle Candidate Performance

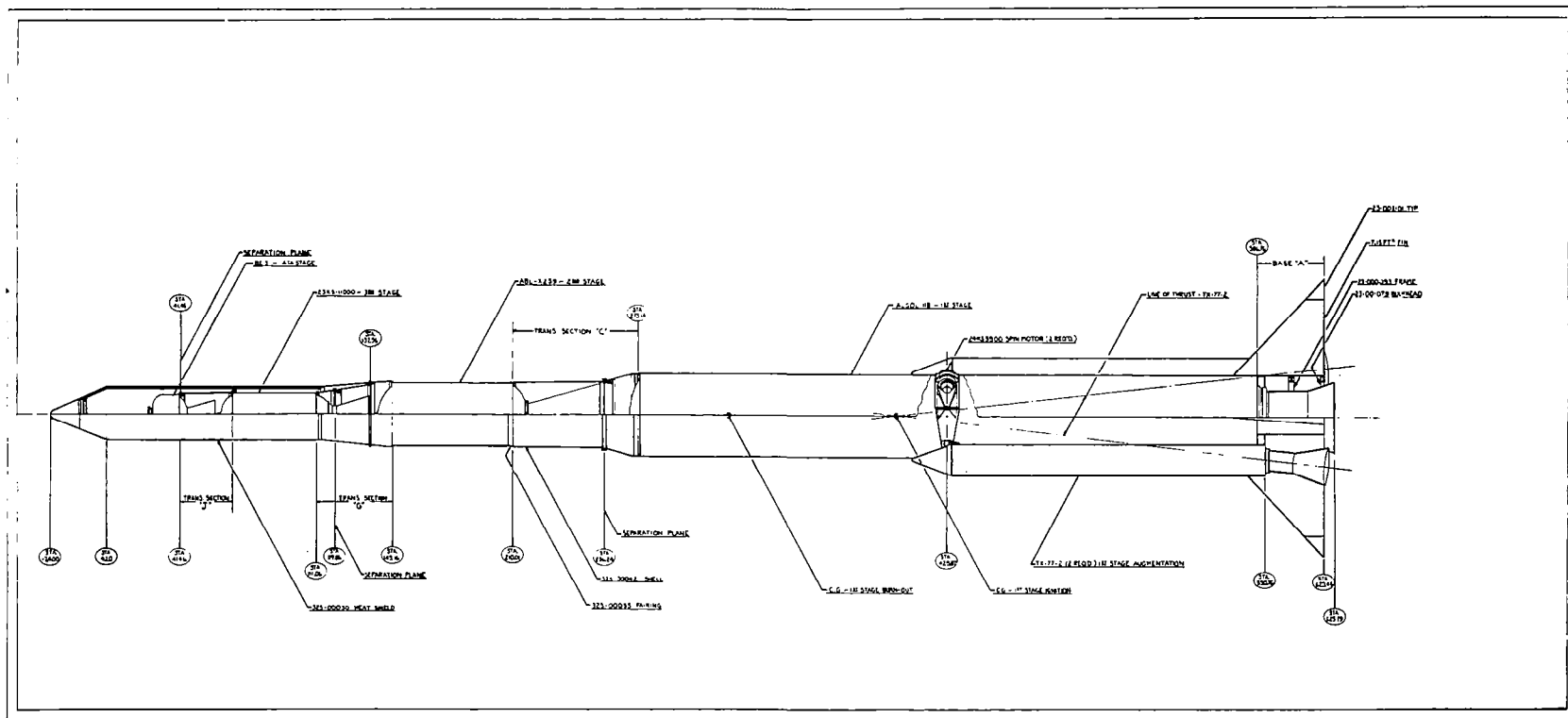


Figure 34. - 428A Launch Vehicle Configuration External Profile

Figure 35. – 428A Launch Vehicle Configuration Inboard Profile

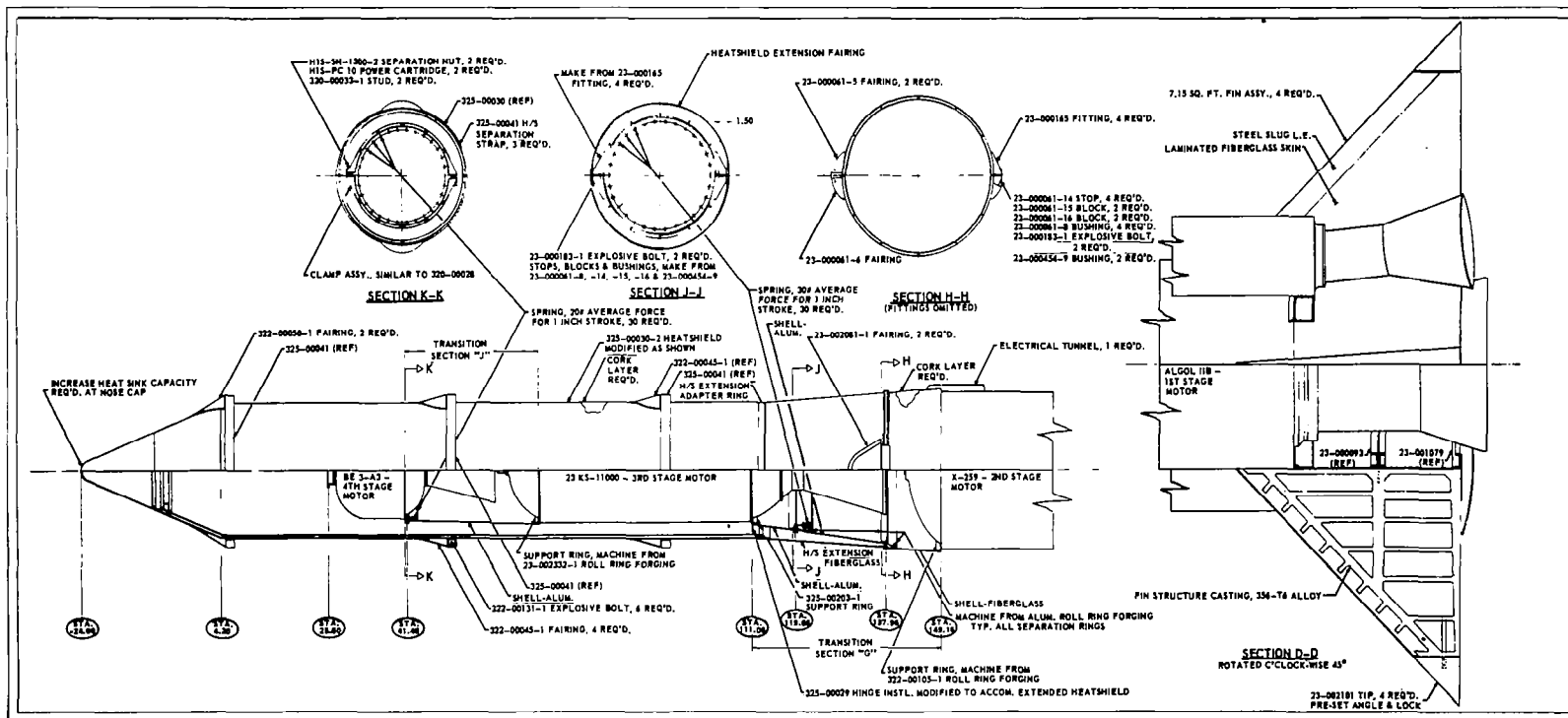


Figure 36. - 428A Launch Vehicle Configuration Inboard Profile

Figure 37. – 428 Launch Vehicle Configuration Electrical System Schematic Drawing

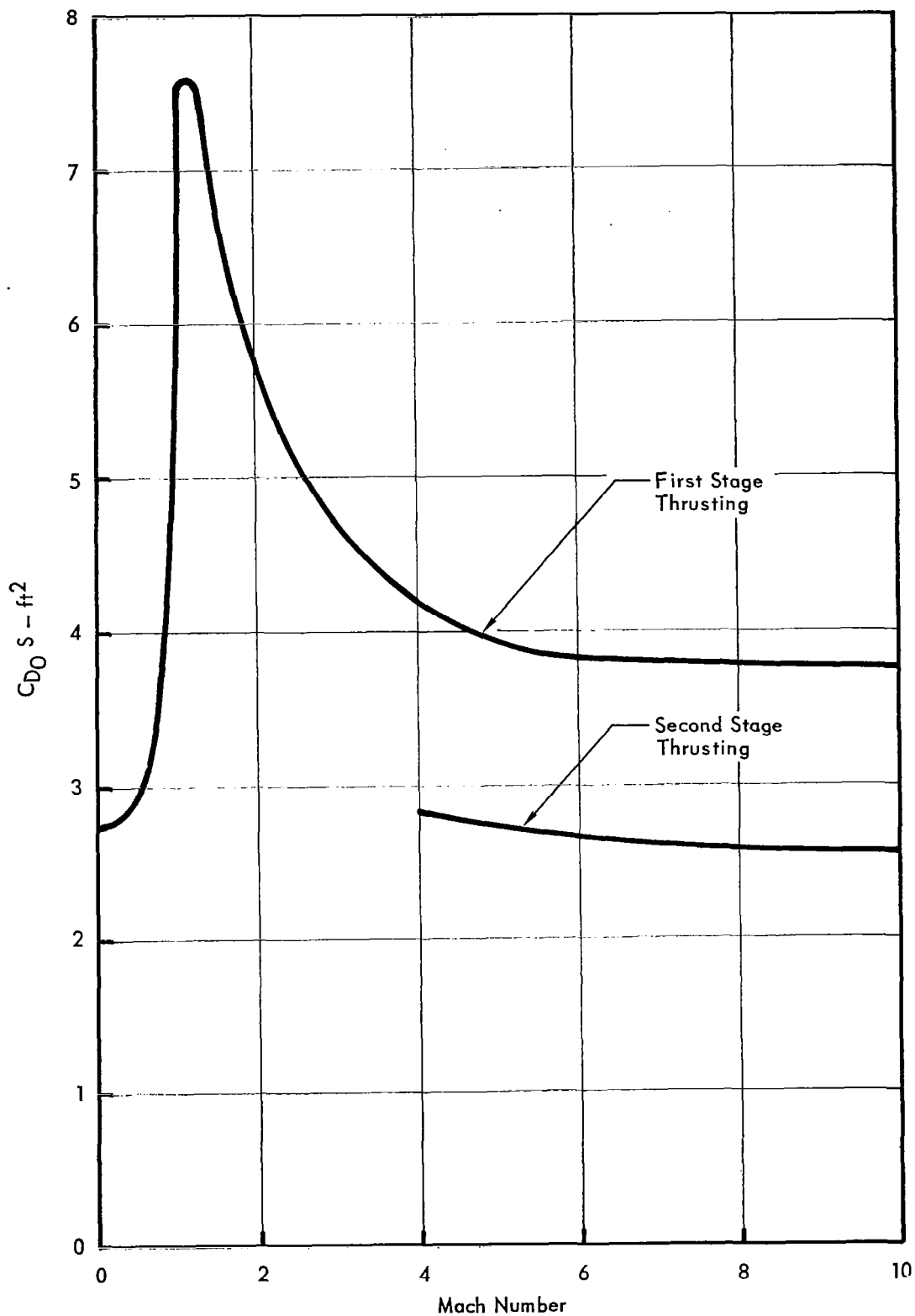


Figure 38. - The Variation of Zero Lift Drag Coefficient with Mach Number

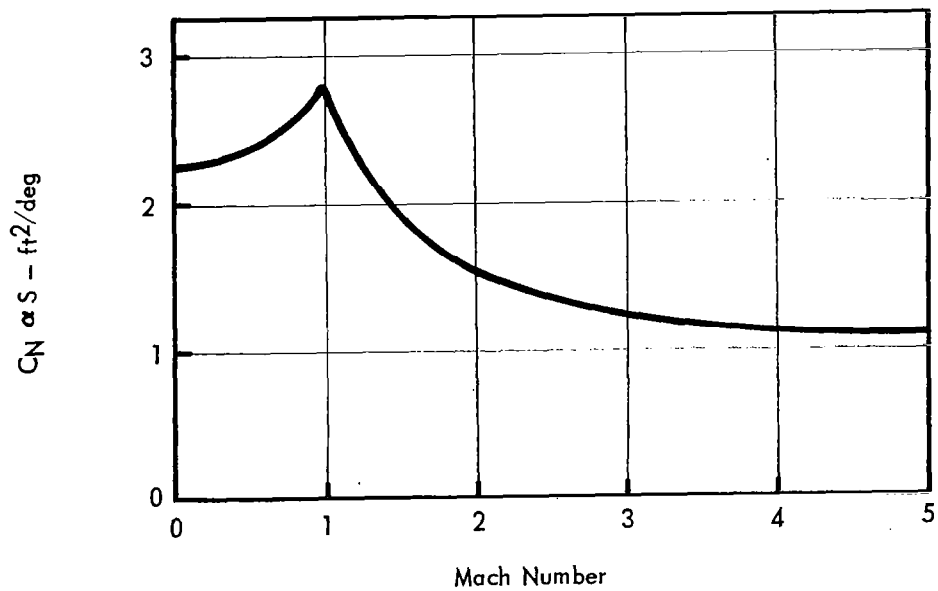
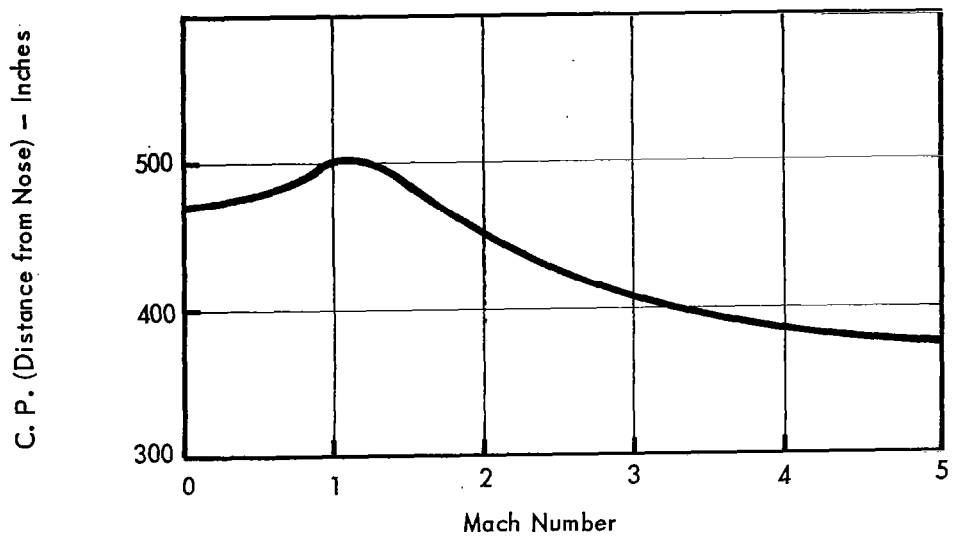


Figure 39. – The Variation of First Stage Center of Pressure and Normal Force Coefficient Derivative with Mach Number

$$\text{Moment Due to Pitch Rate} = \left[\frac{M}{q (\dot{\theta}/V)} \right] \times q \times \frac{\dot{\theta}}{V}$$

M – Pitching Moment – ft-lb

q – Dynamic Pressure – lb/sq ft

$\dot{\theta}$ – Pitch Rate – rad/sec

V – Velocity – ft/sec

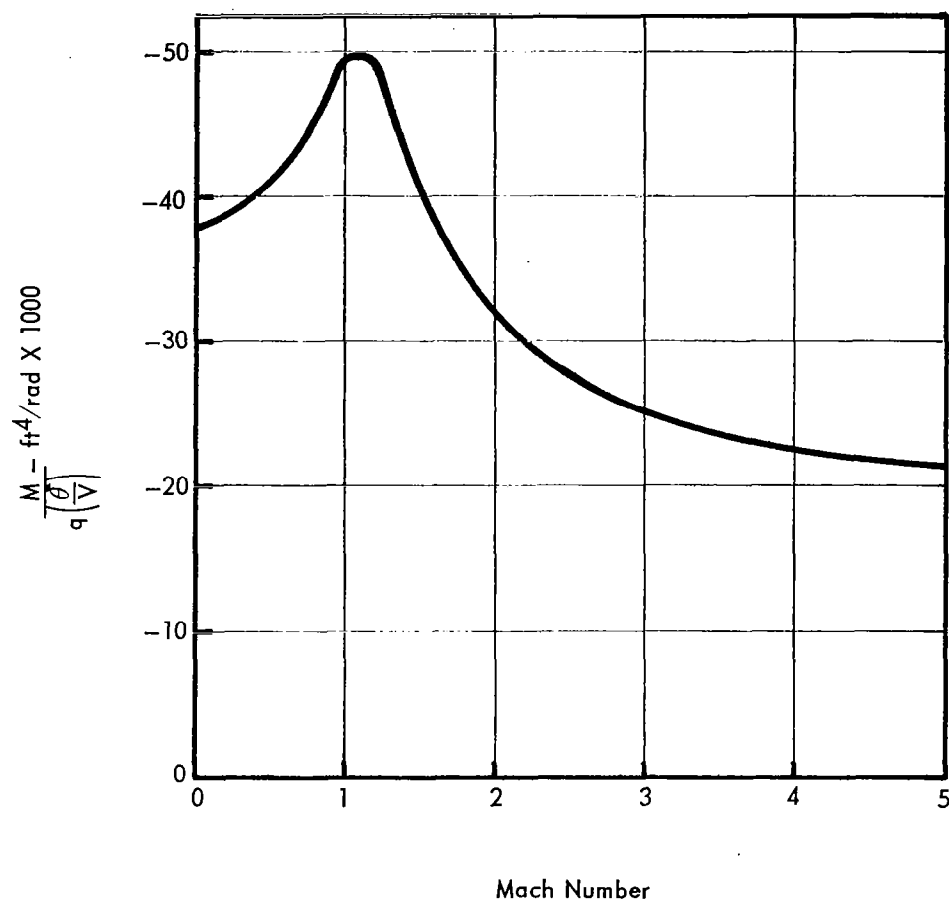


Figure 40. – The Variation of First Stage Pitch Damping Coefficient with Mach Number

$$\text{Roll Damping Moment} = \left[\frac{\ell_{\text{Damp}}}{q (P/V)} \right] \times q \times (P/V)$$

ℓ – Rolling Damping Moment – ft-lb

q – Dynamic Pressure – lb/sq ft

P – Spin Rate – rad/sec

V – Velocity – ft/sec

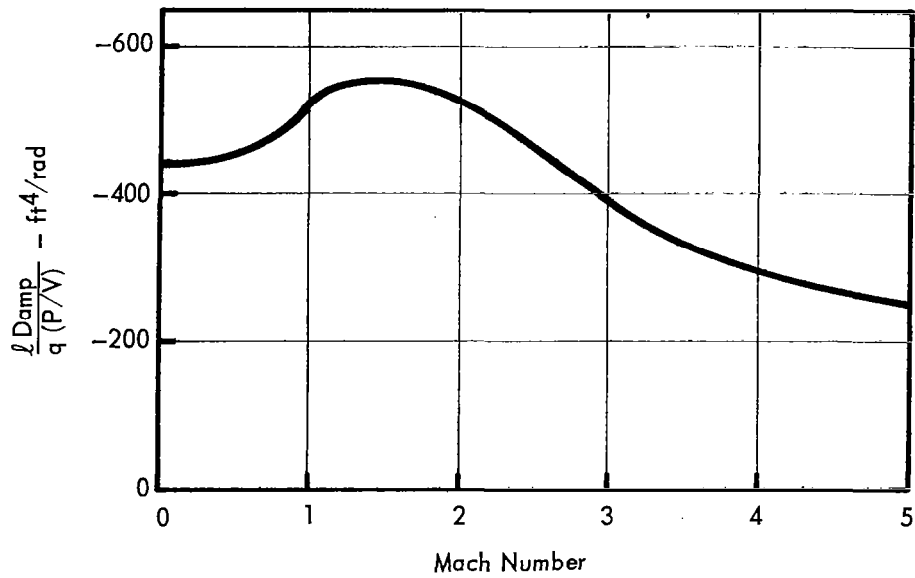


Figure 41. – The Variation of First Stage Roll Damping with Mach Number

$$\frac{\text{Rolling Moment Due to Fin}}{\text{Tip Deflection}} = \left[\frac{l_{\text{Tip}}}{q \delta_{\text{Tip}}} \right] \times q \times \delta_{\text{Tip}}$$

l_{Tip} – Rolling Moment – ft-lb
 q – Dynamic Pressure – lb/sq ft
 δ_{Tip} – Fin Tip Deflection – deg

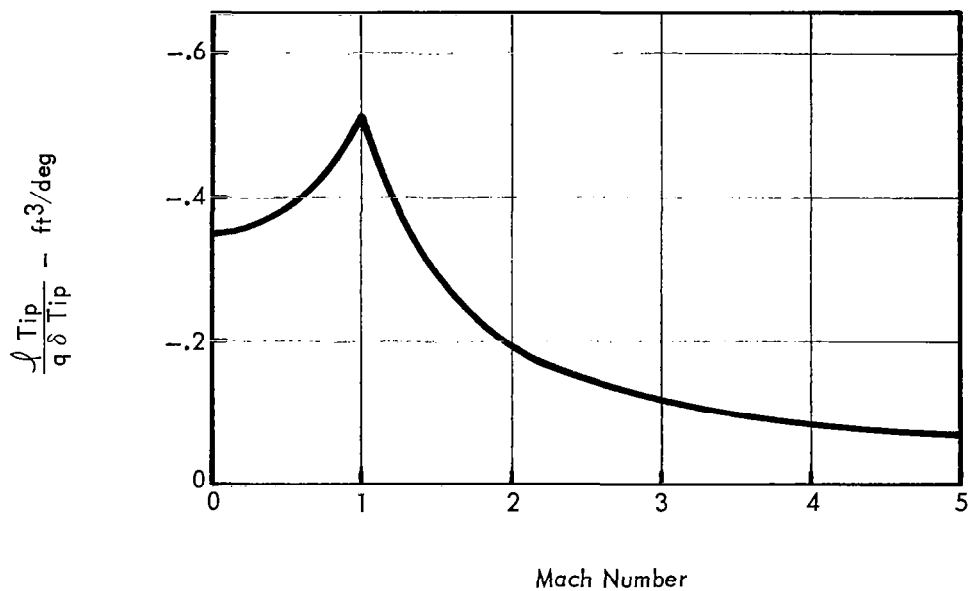


Figure 42. – The Variation of Fin Tip Rolling Effectiveness with Mach Number

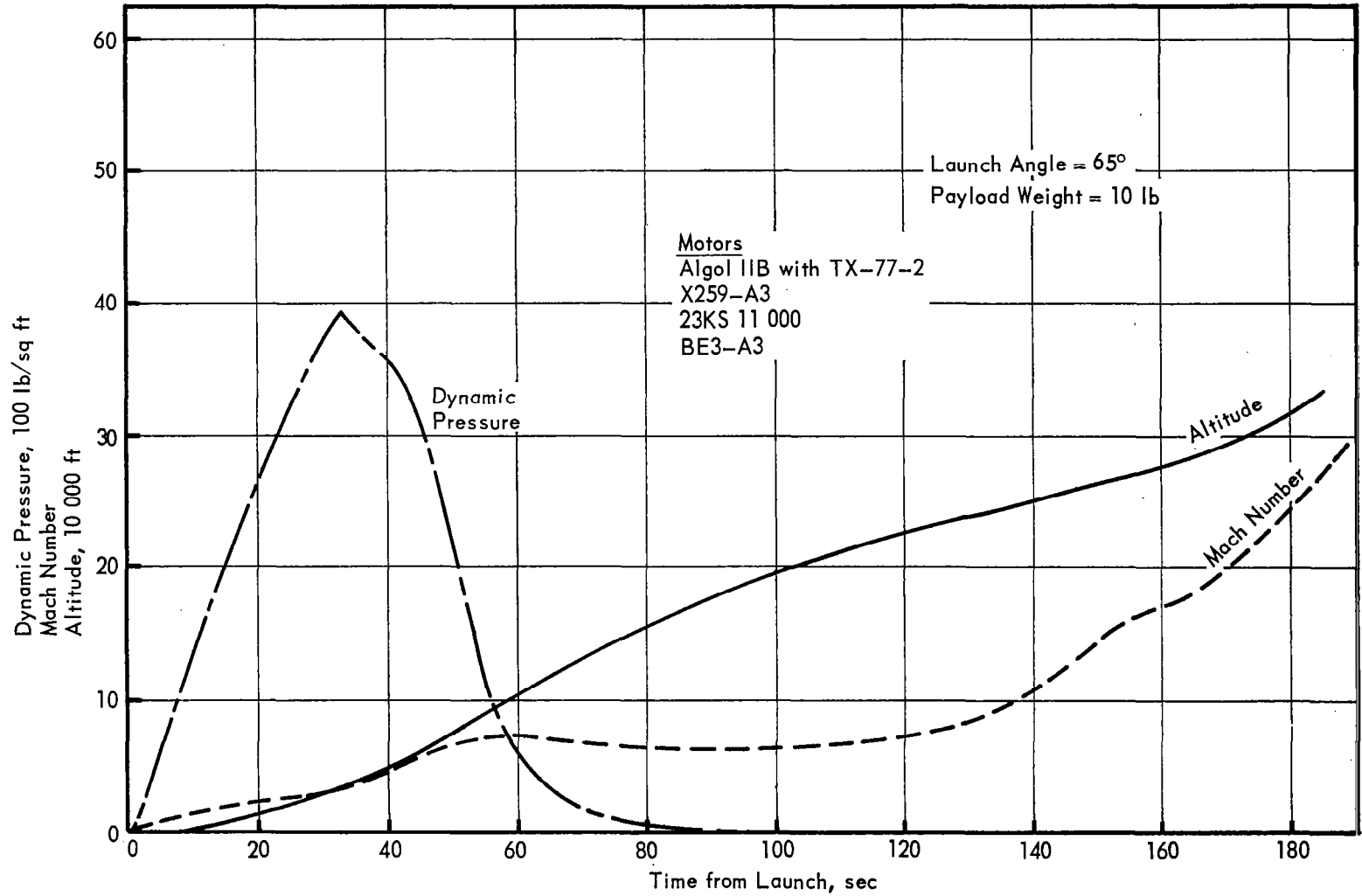


Figure 43. - 428A Vehicle Structural Design Trajectory

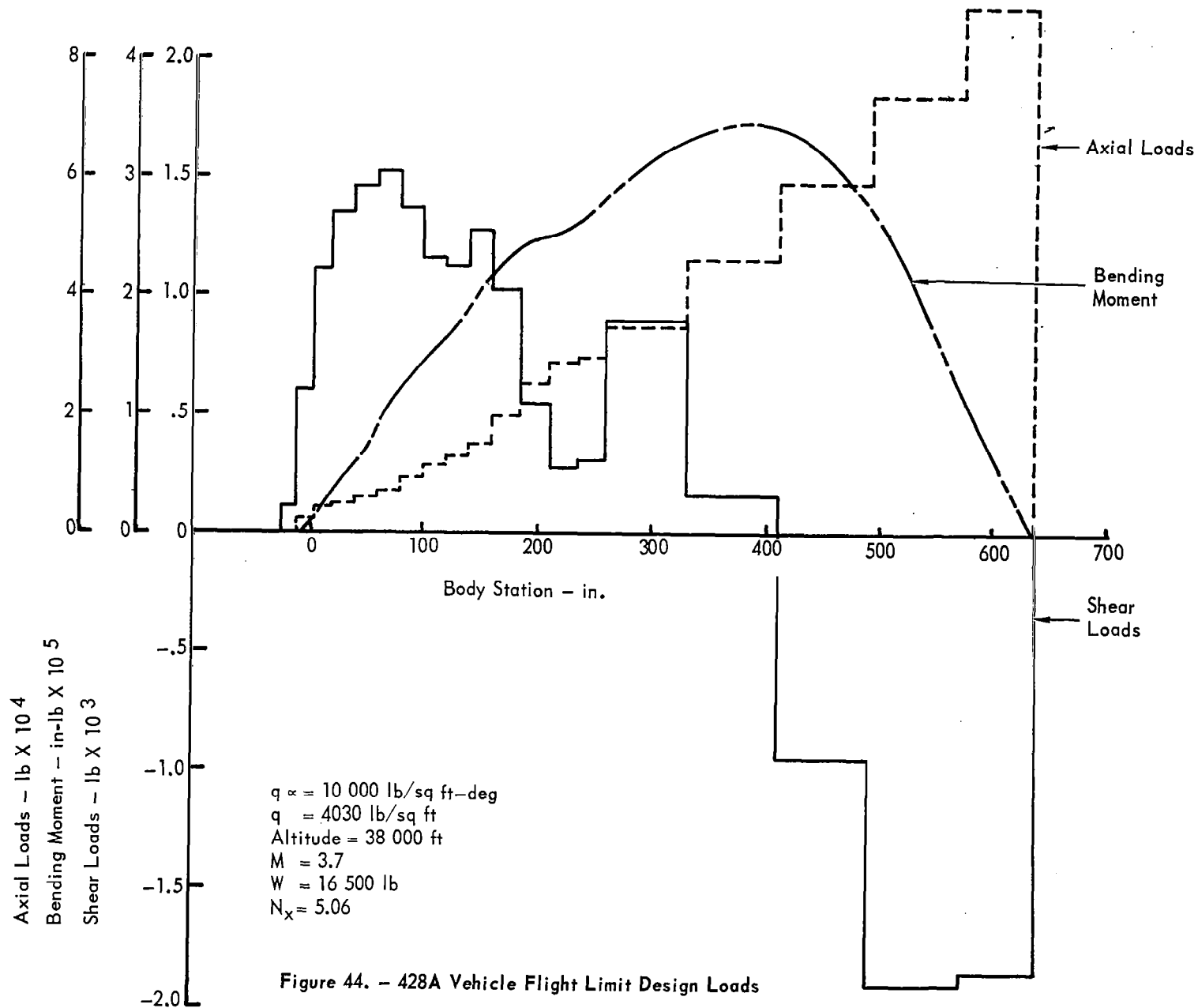


Figure 44. - 428A Vehicle Flight Limit Design Loads

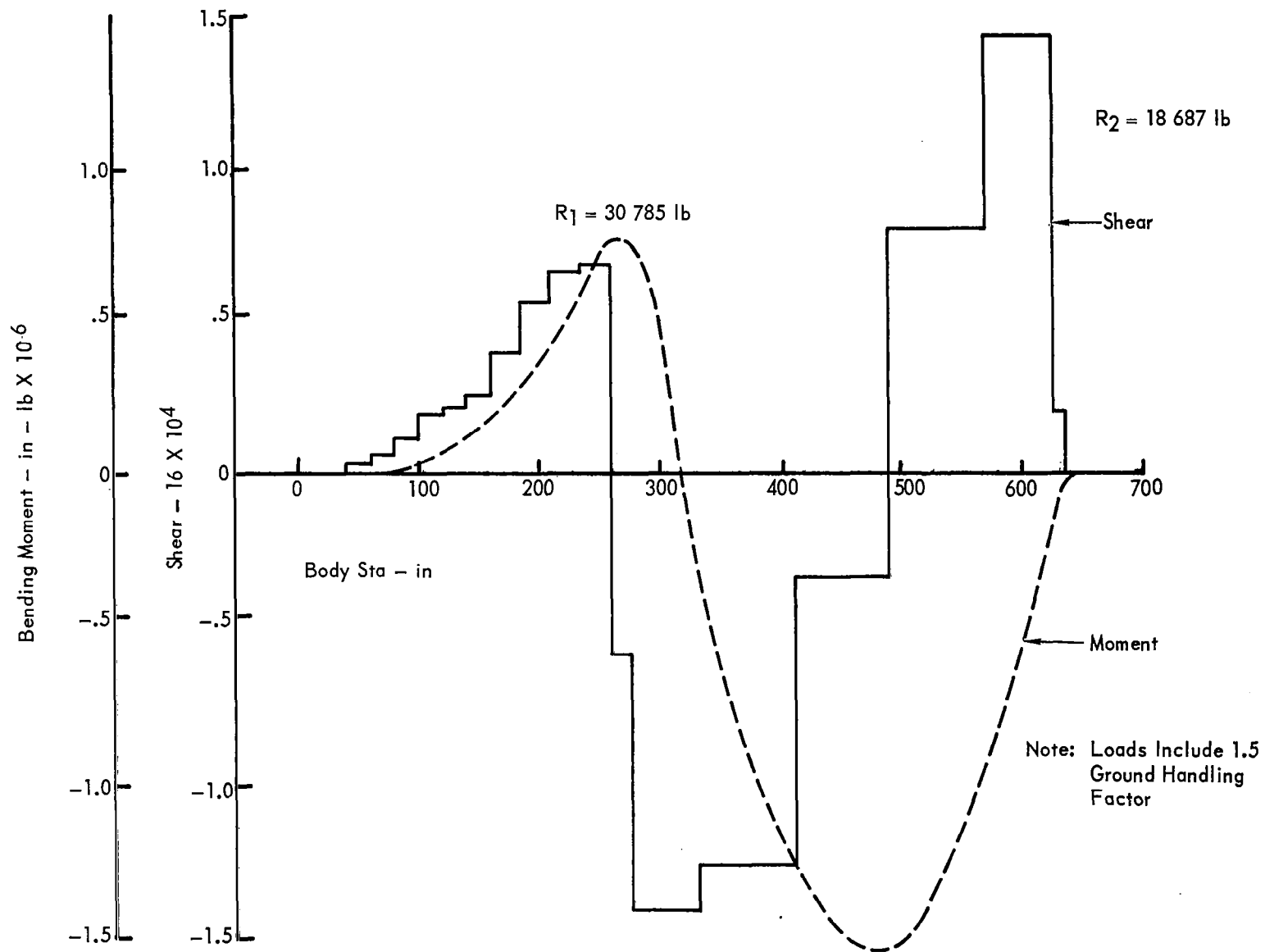


Figure 45. - 428A Vehicle Hoist Limit Design Loads

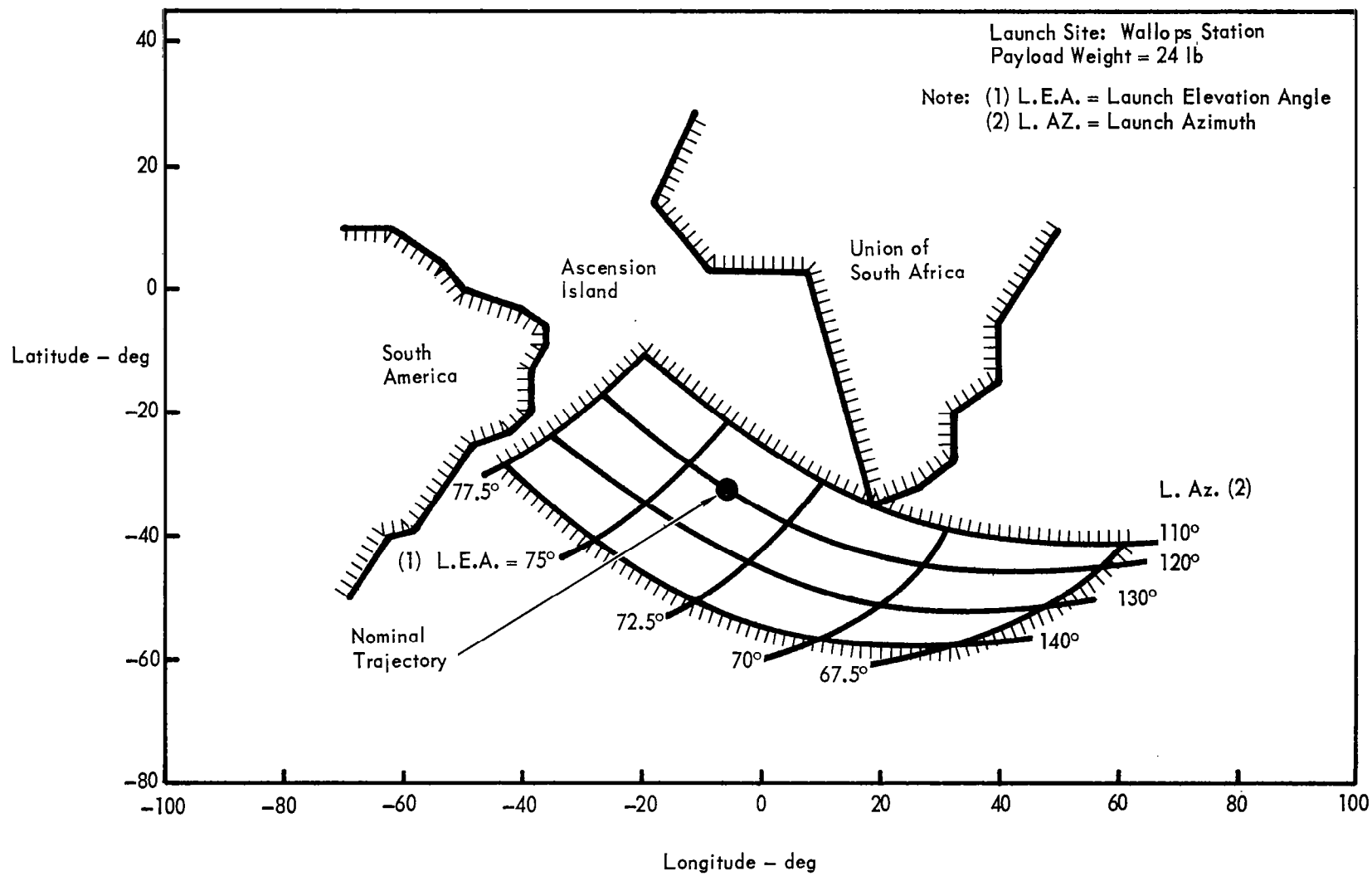


Figure 46. - Stage Three Impact Boundary

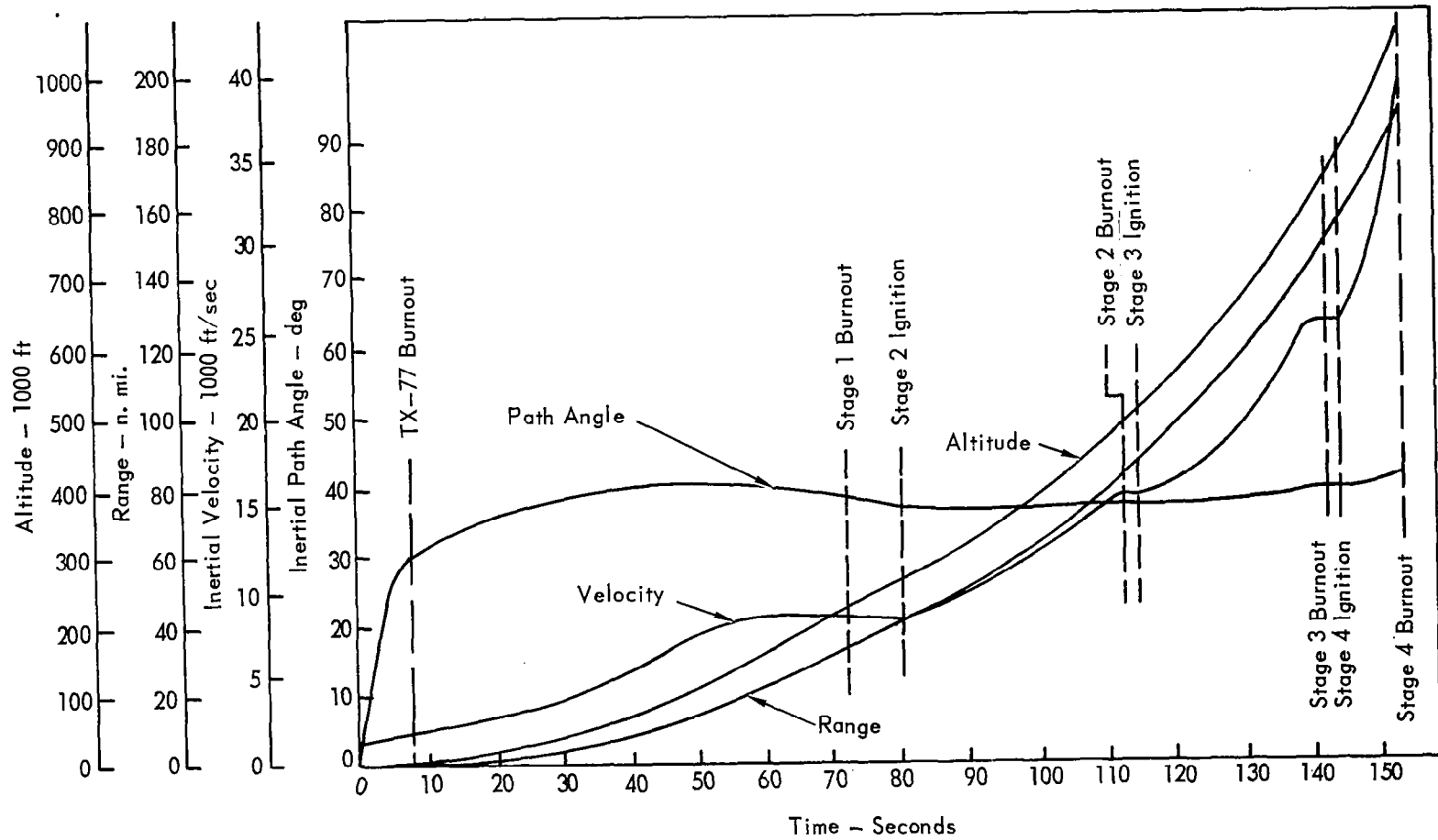


Figure 47. - Vehicle No 428A Nominal Trajectory Booster Time Histories

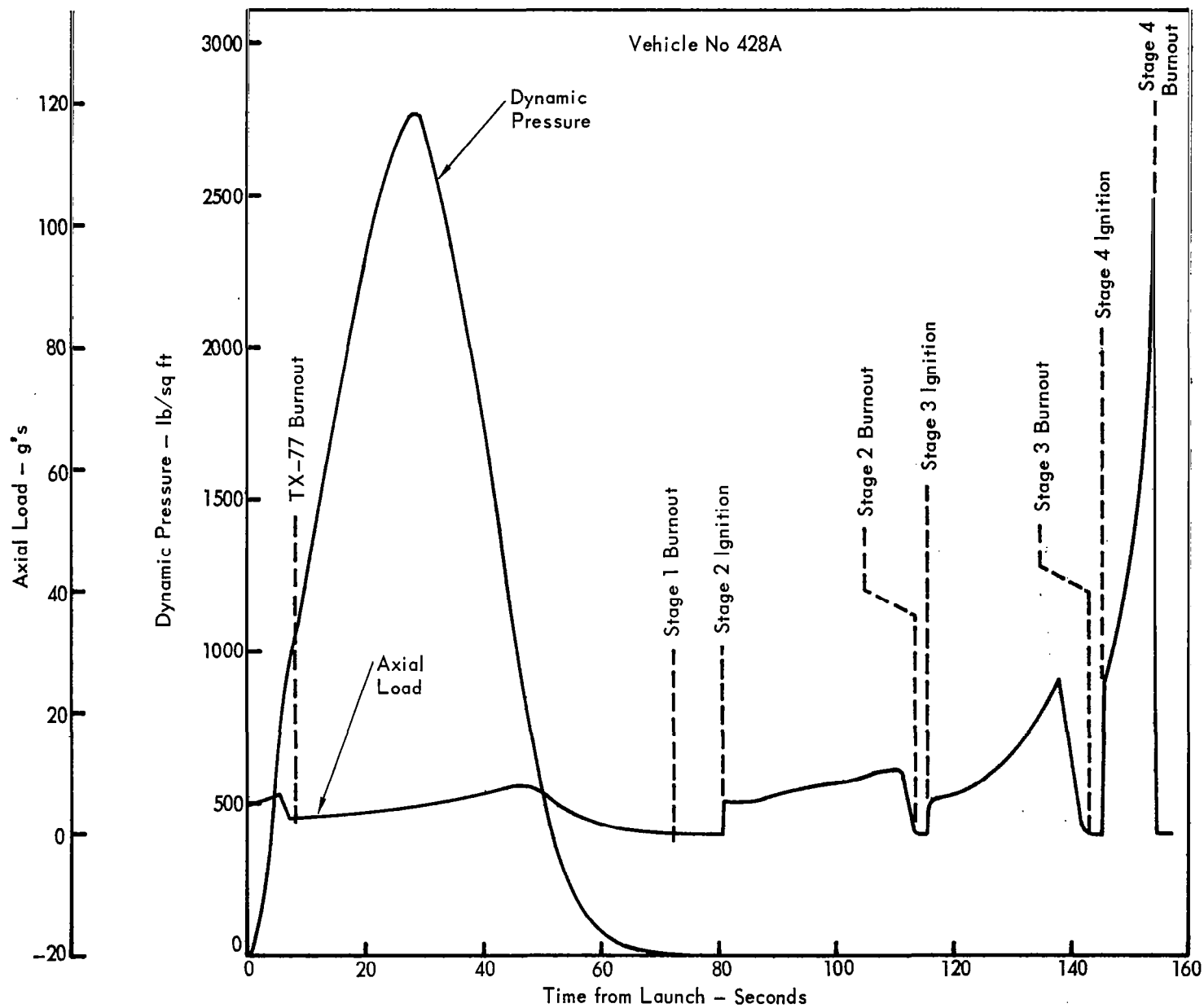


Figure 48. - Nominal Trajectory Axial Load and Dynamic Pressure Time Histories

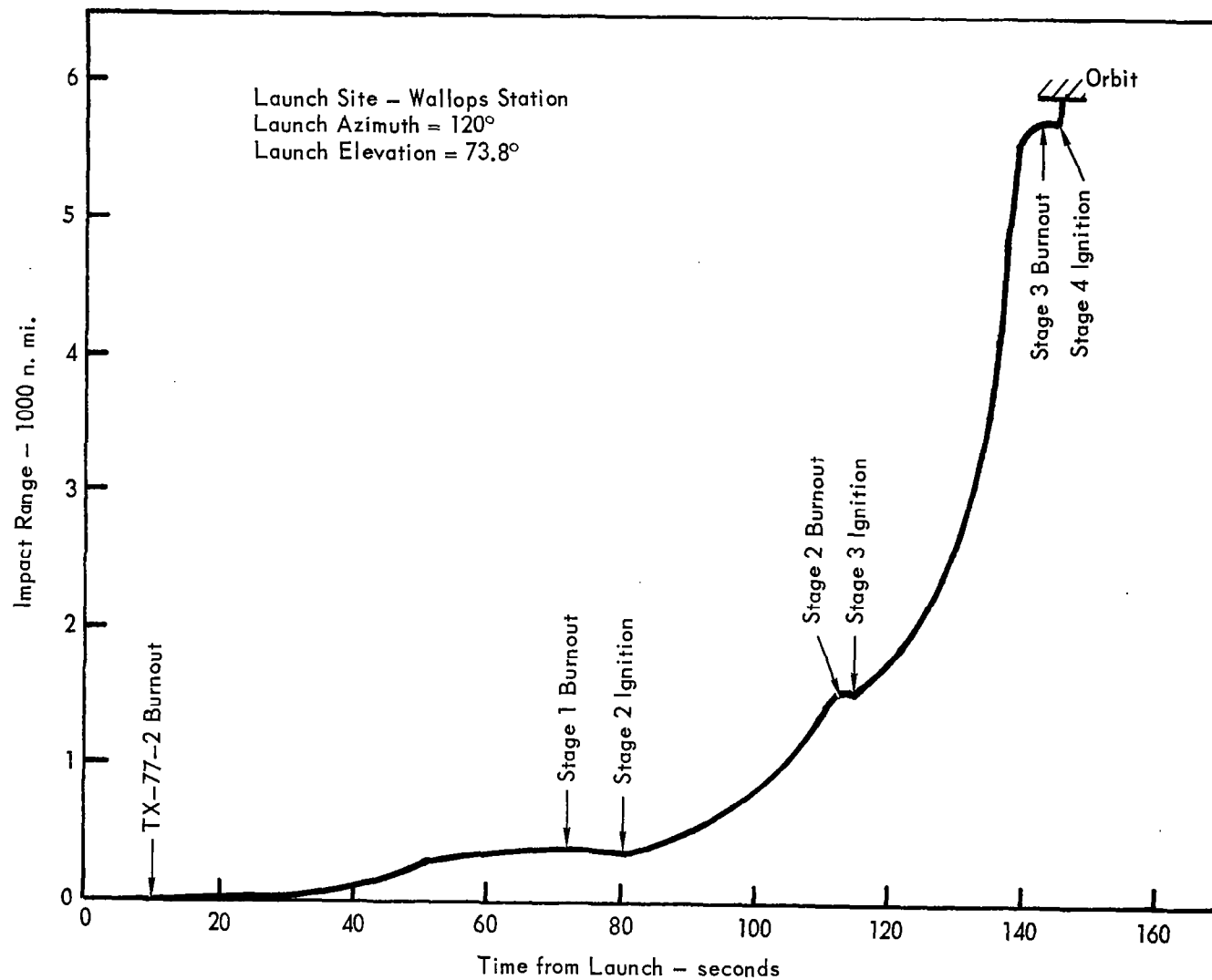


Figure 49. - Time History of Instantaneous Impact Range (Vehicle 428A)

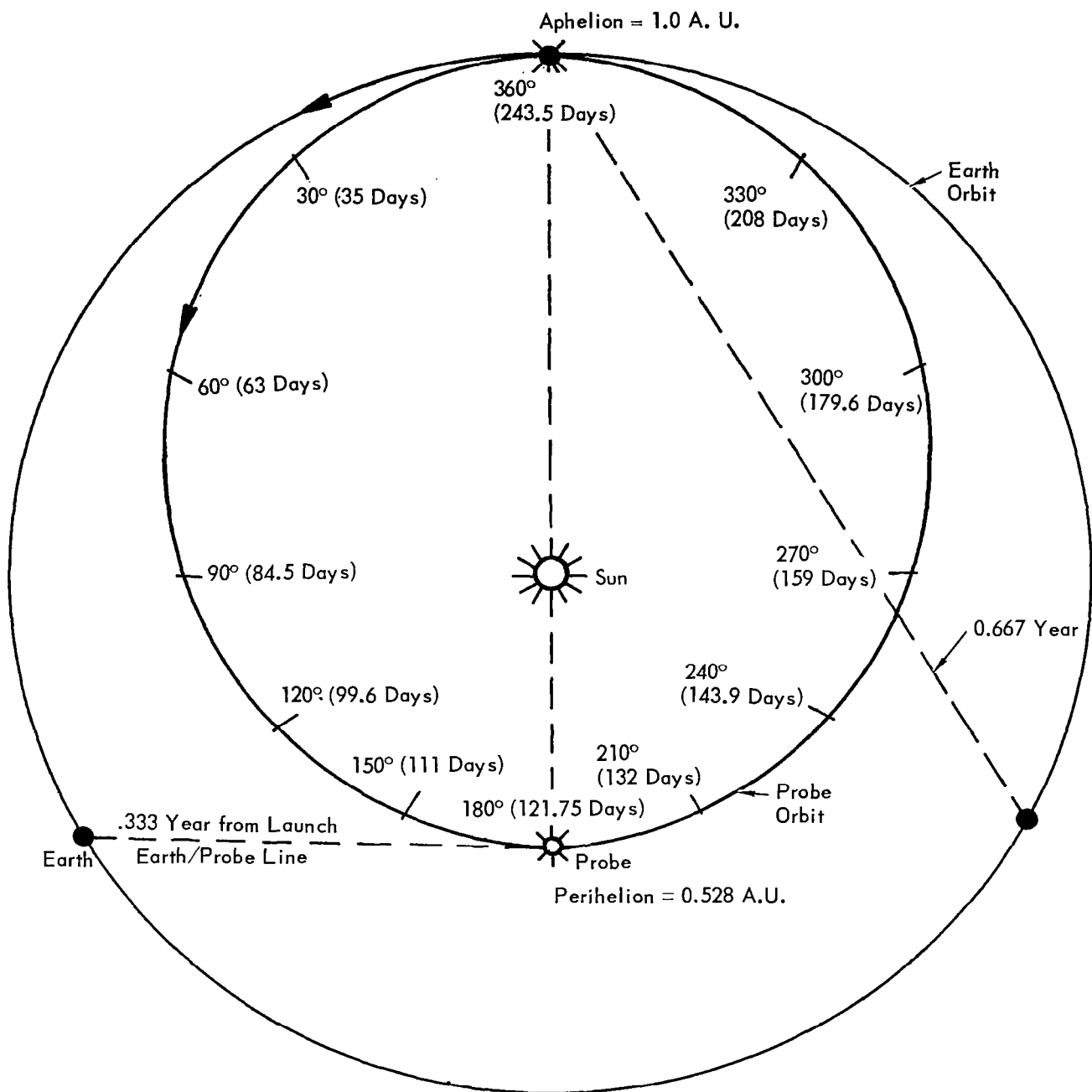


Figure 50. — Earth-Sun-Probe Time and Position for a 0.667 Year Period Solar Orbit

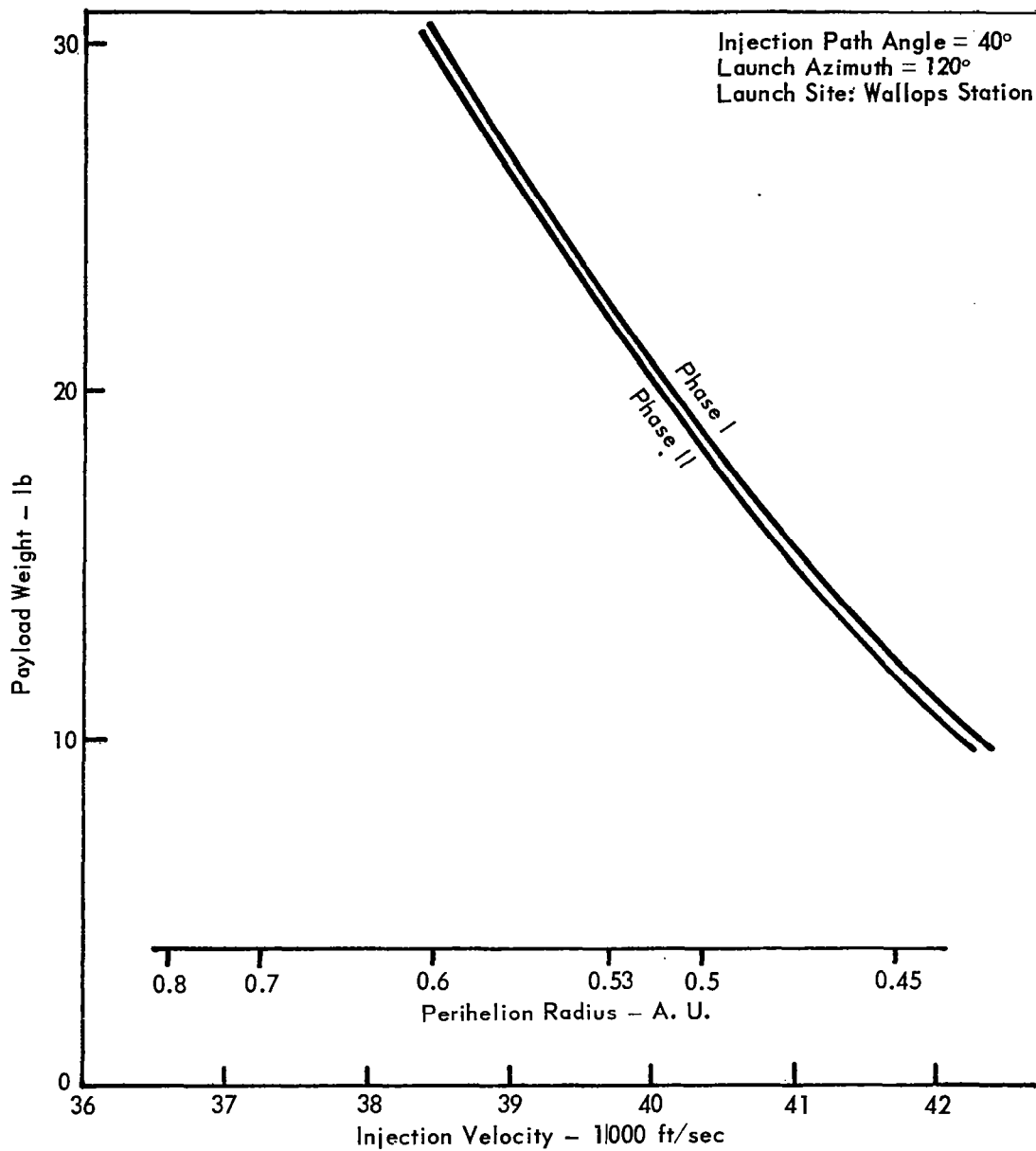


Figure 51. - Comparison of Performance Capability - Vehicle No. 428A

Notes:

- 1 Vehicle No 428A
- 2 Launch Elevation Angle = 73.8°
- 3 Launch Azimuth Angle = 120°
- 4 Payload Weight = 24 lb
- 5 Julian Date of Launch = 2 439 328.5 + 19.0 Hours Past Midnight, GMT
- 6 Civil Date of Launch = 22 July 1966 + 13.9618 Hours Past Midnight, EST
- 7 S.O.I. Crossing Occurs @ 2.0402 Days After Launch

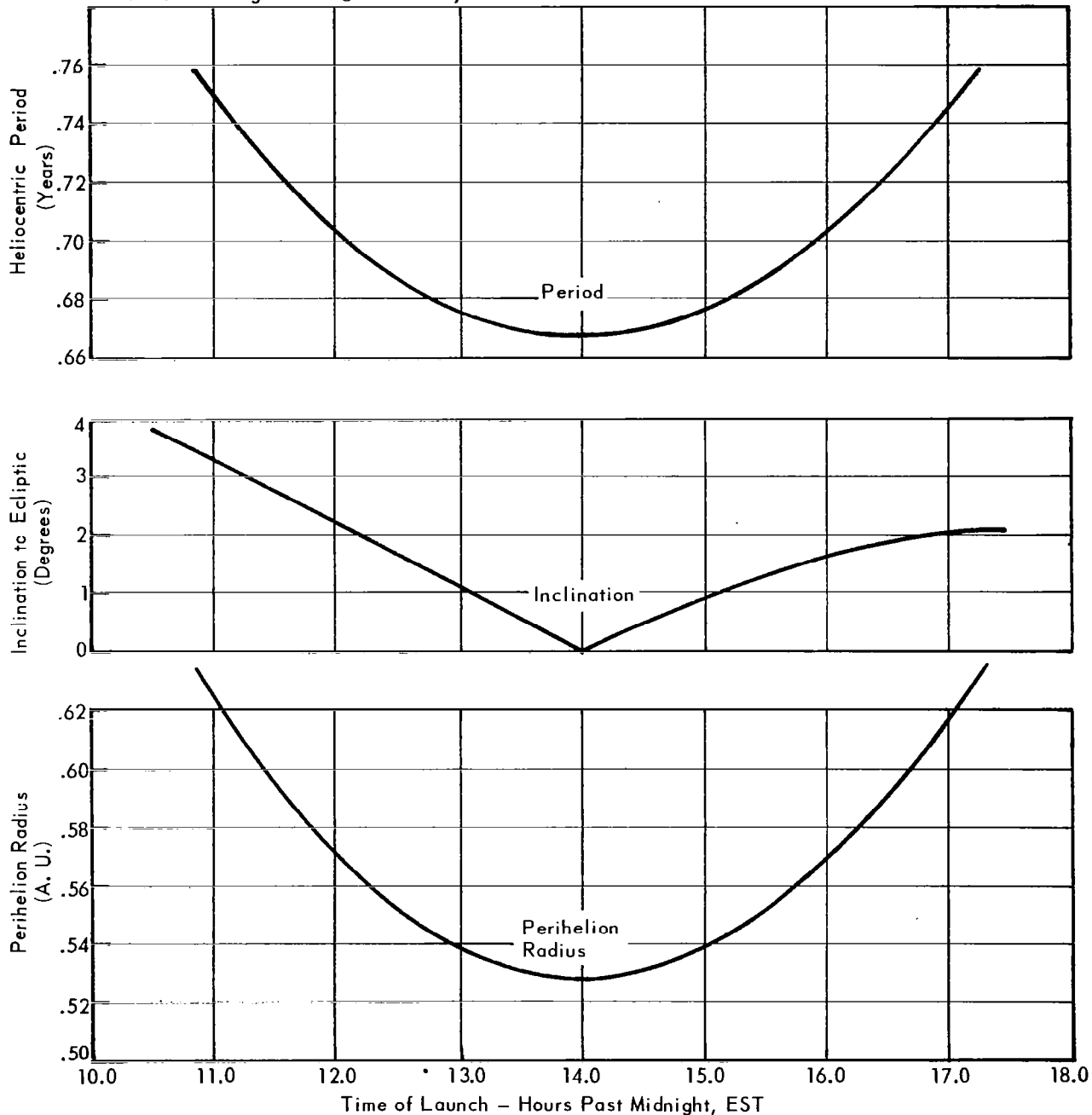


Figure 52. - 22 July Launch Window for the Nominal Trajectory - Constant Launch Conditions

Notes:

1. Vehicle No.428A
2. Launch Elevation Angle = 77.5 deg
3. Launch Azimuth Angle = 110 deg
4. Payload Weight = 24 lb
5. Julian Date of Launch = 2 439 204.5 = 0.0 Hours, GMT
6. Approximate Date of Vernal Equinox (20 March 1966)
7. S.O.I. Crossing Occurs @ 2.095437 Days After Launch

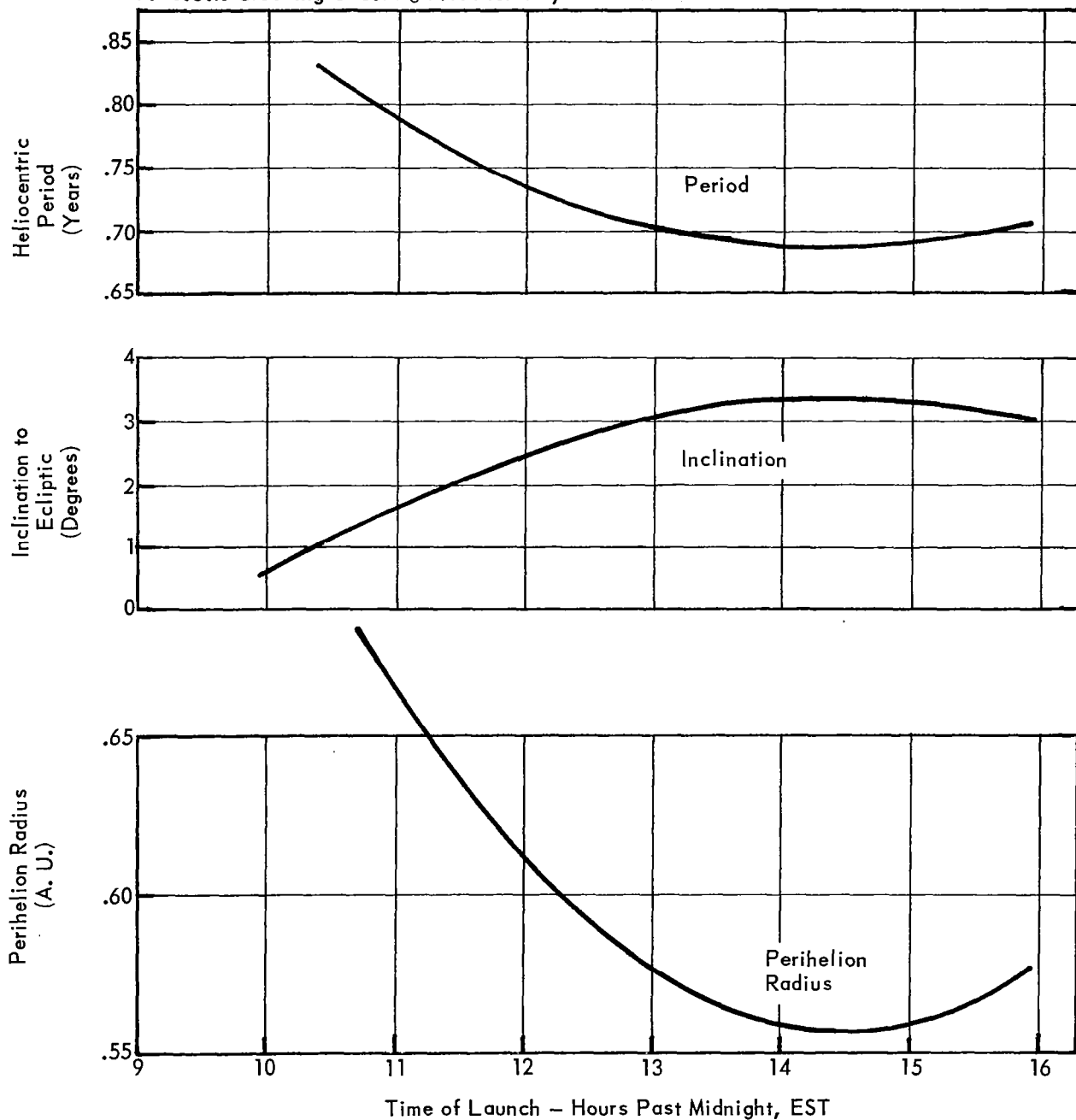


Figure 53. - 20 March Launch Window - Constant Launch Conditions

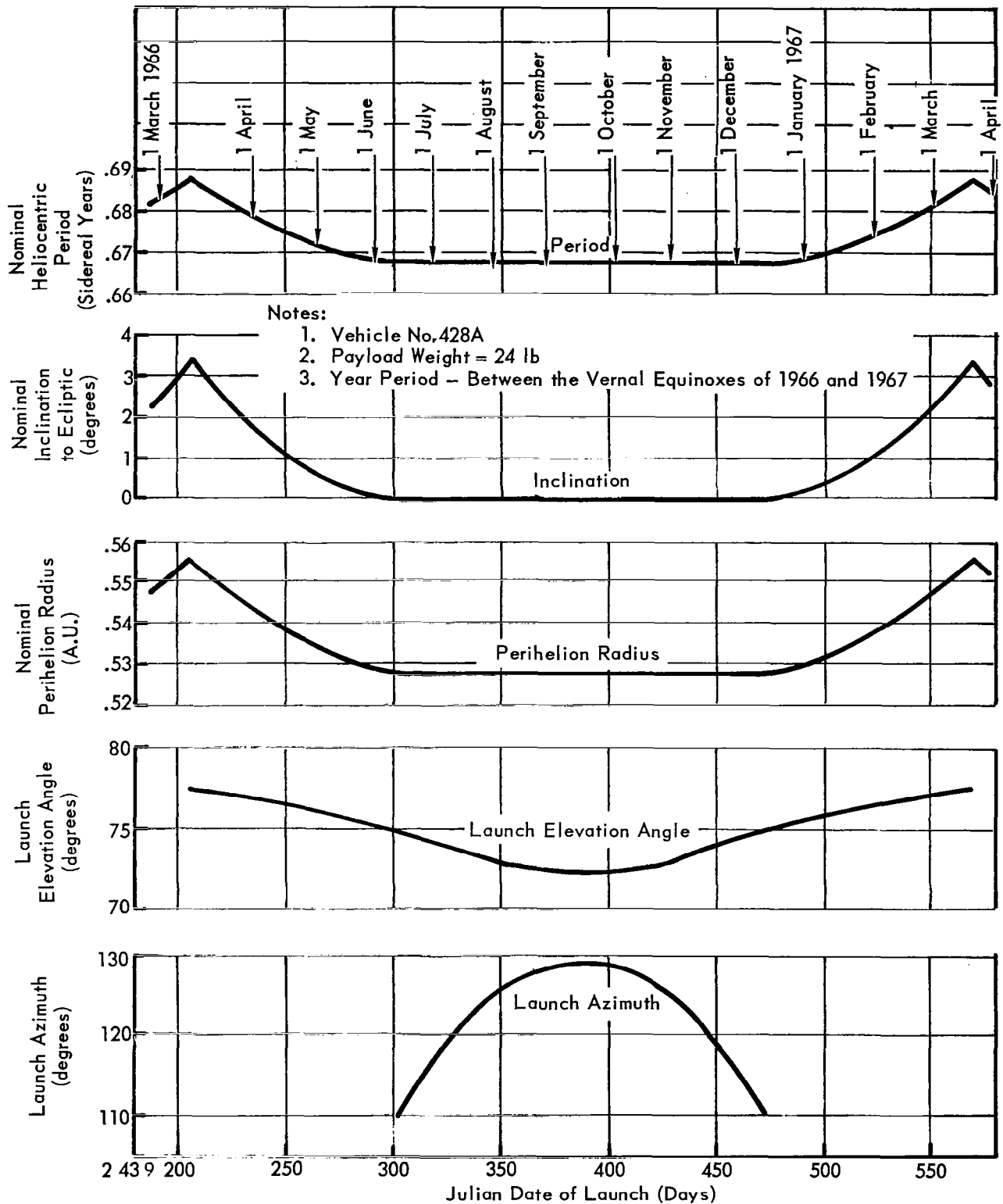


Figure 54. - Yearly Launch Window - Constant Daily Launch Conditions

Notes:

1. Vehicle No 428A

2. Nominal Conditions:

Launch Elevation Angle = 73.8°

Launch Azimuth Angle = 120°

Julian Date of Launch = 2 439 329.29 089 087 + 18.981 Hours Past Midnight, GMT

3. Payload Weight = 24 lb

4. Time to S.O.I. Crossing = Date of S.O.I. Crossing - Date of Launch

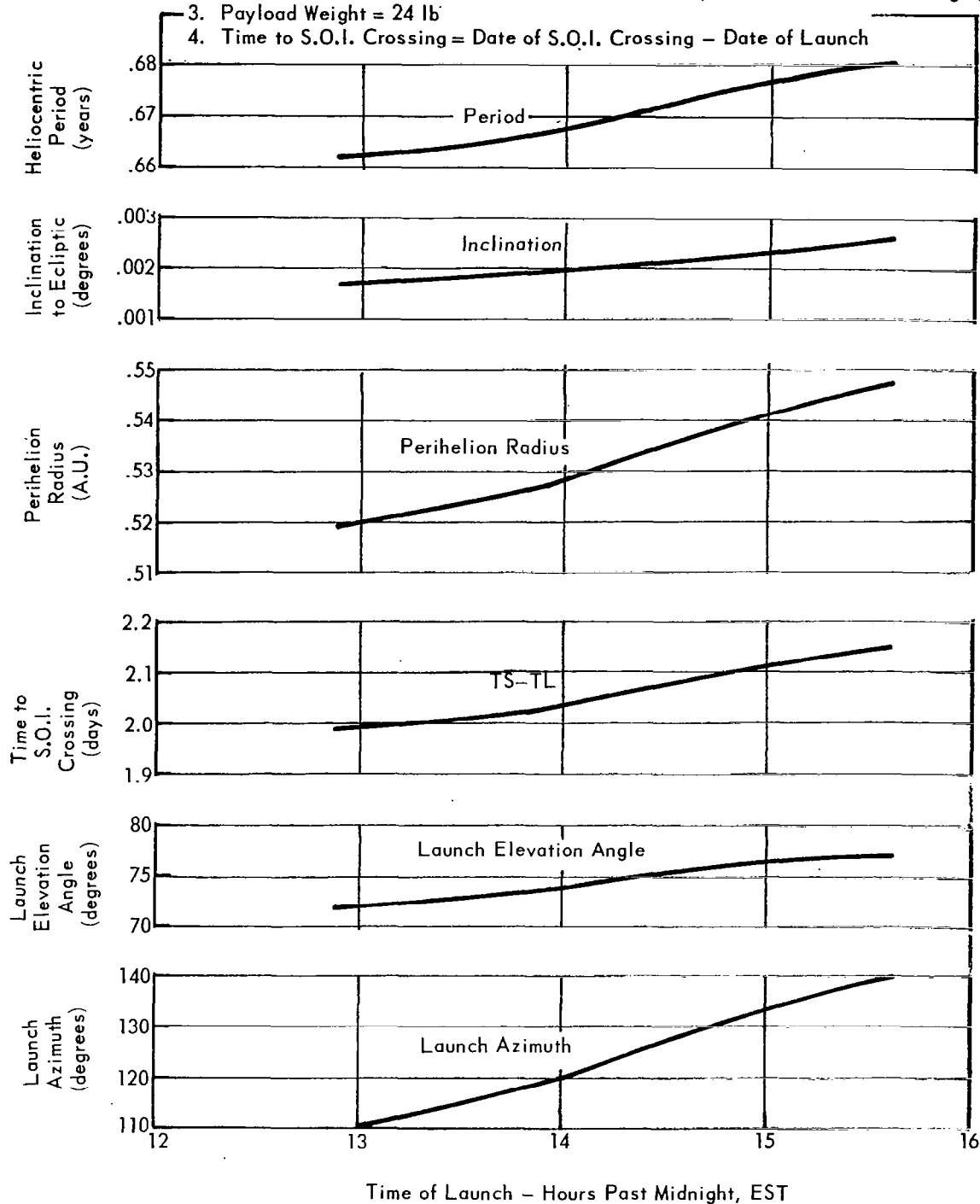


Figure 55. - 22 July Launch Window - Variable Launch Conditions

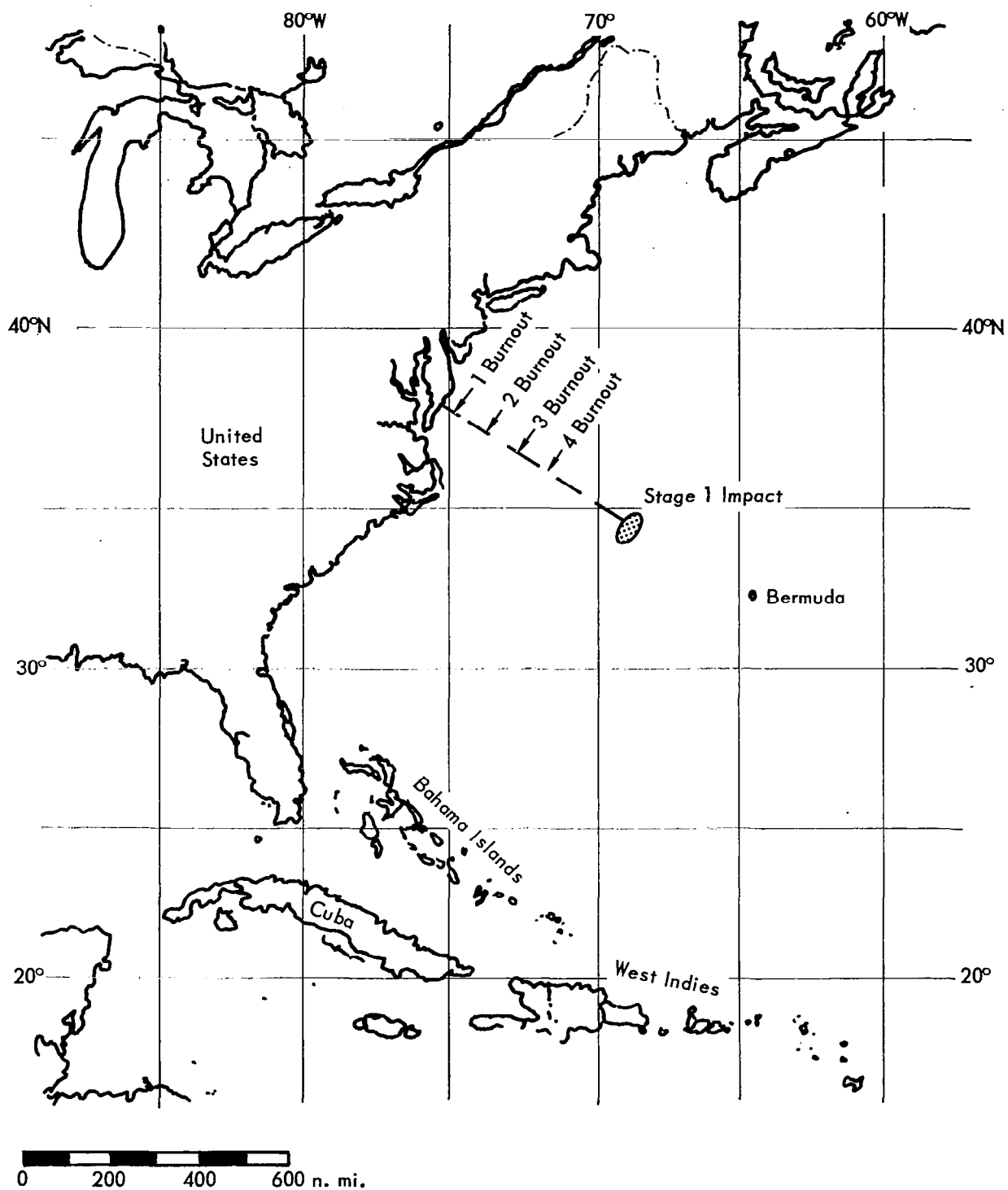


Figure 56. — Stage One Impact Dispersion

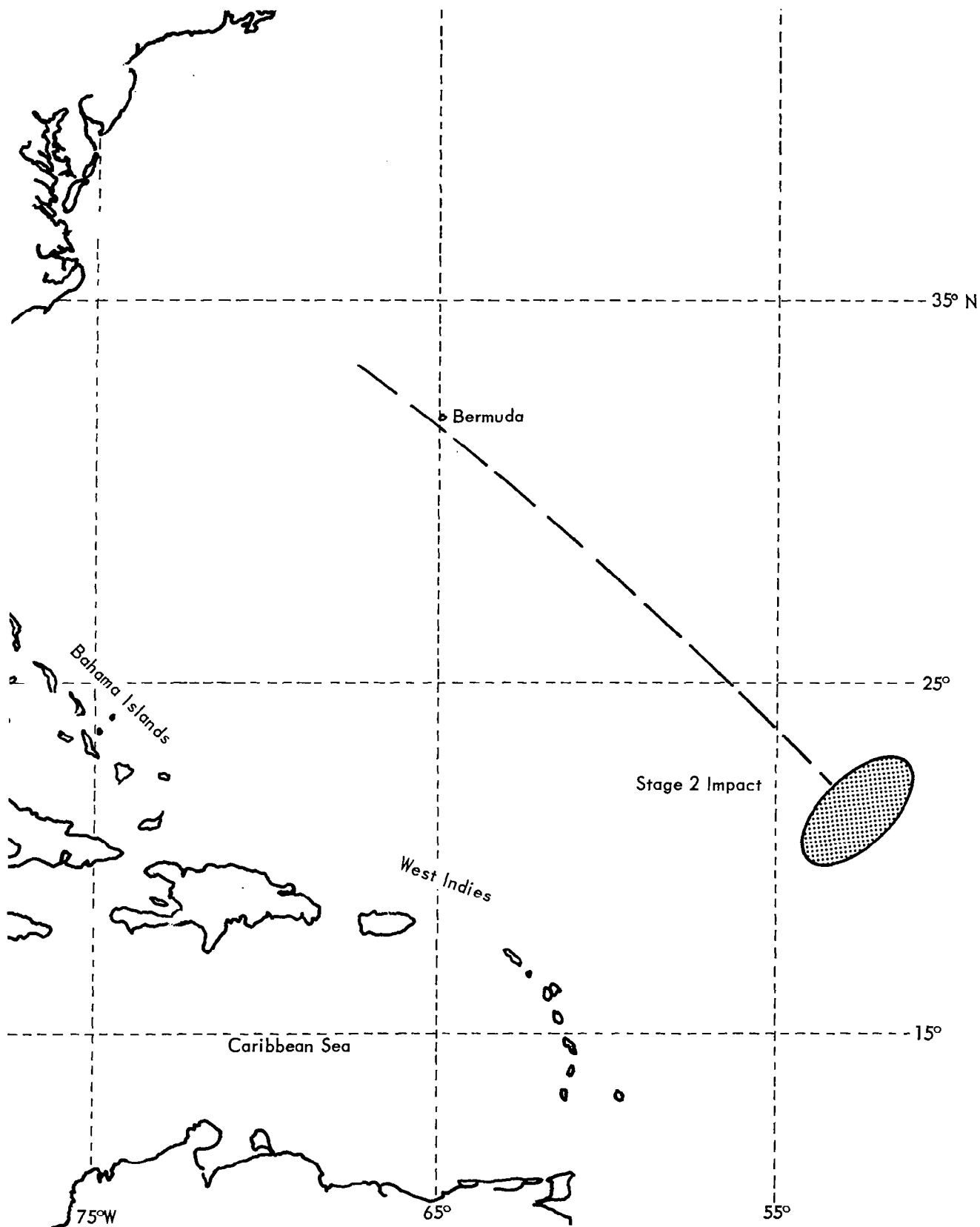


Figure 57. - Stage Two Impact Dispersion

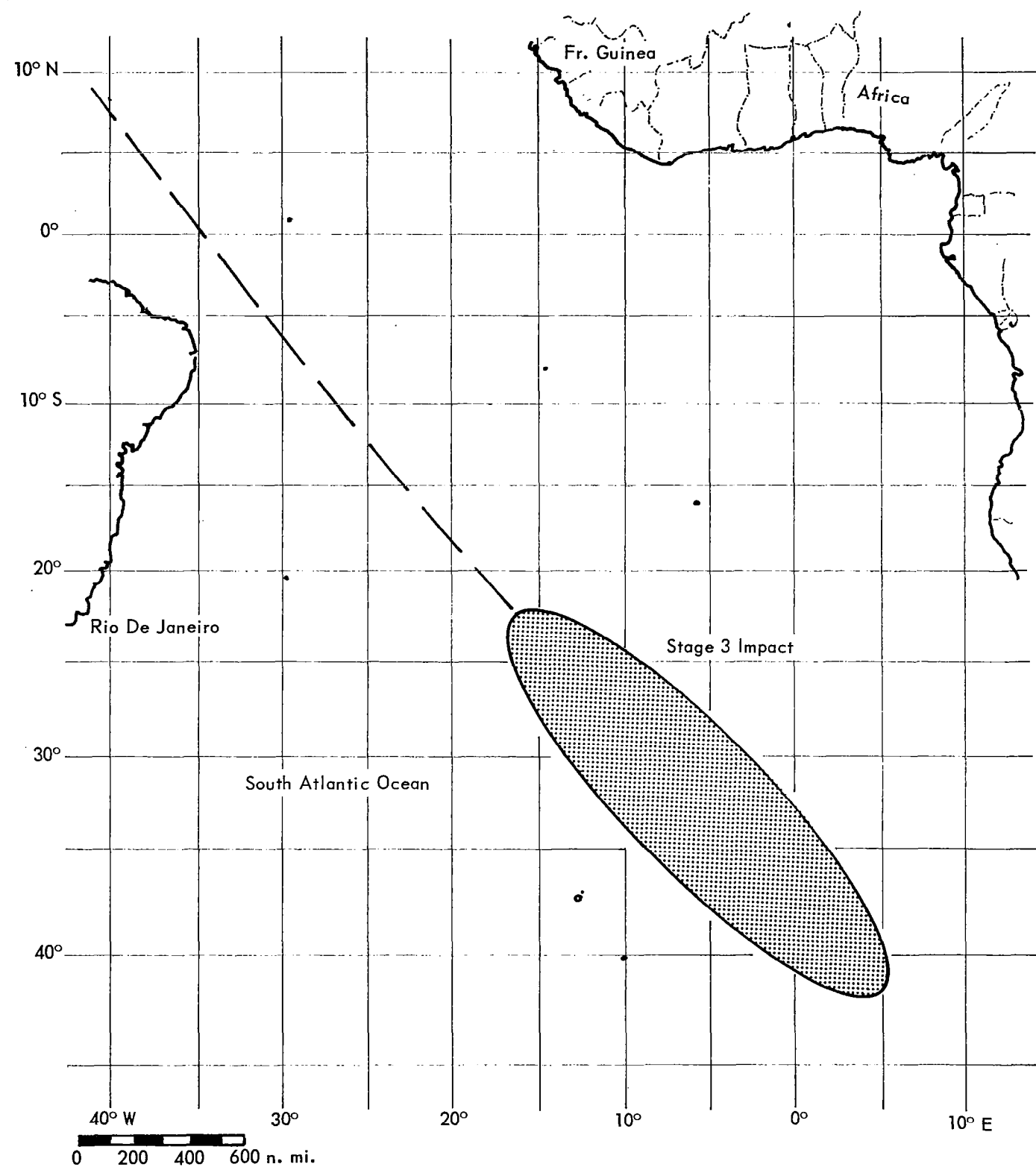


Figure 58. — Stage Three Impact Dispersion

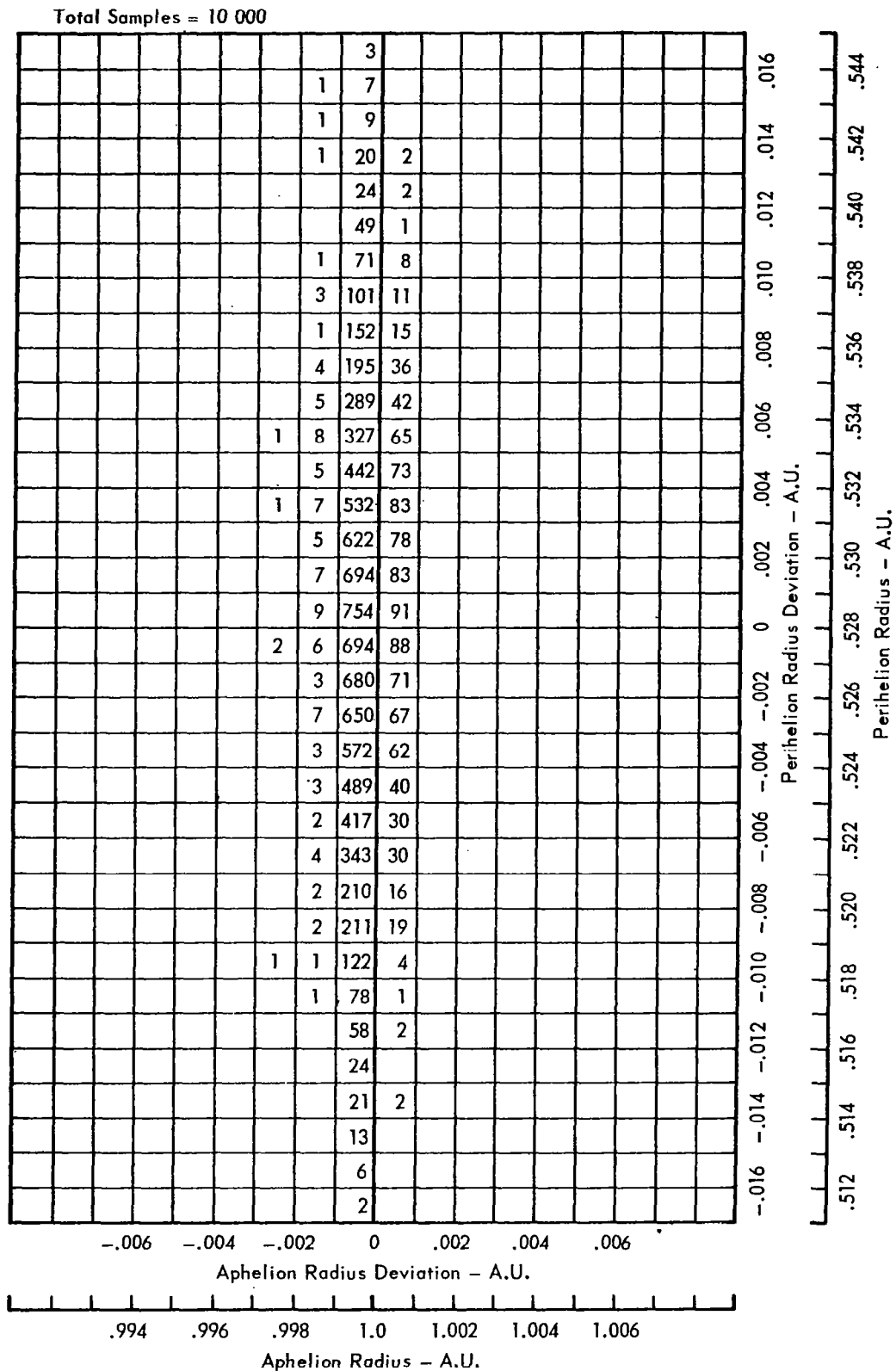


Figure 59. - Joint Density Function of Aphelion and Perihelion Deviations

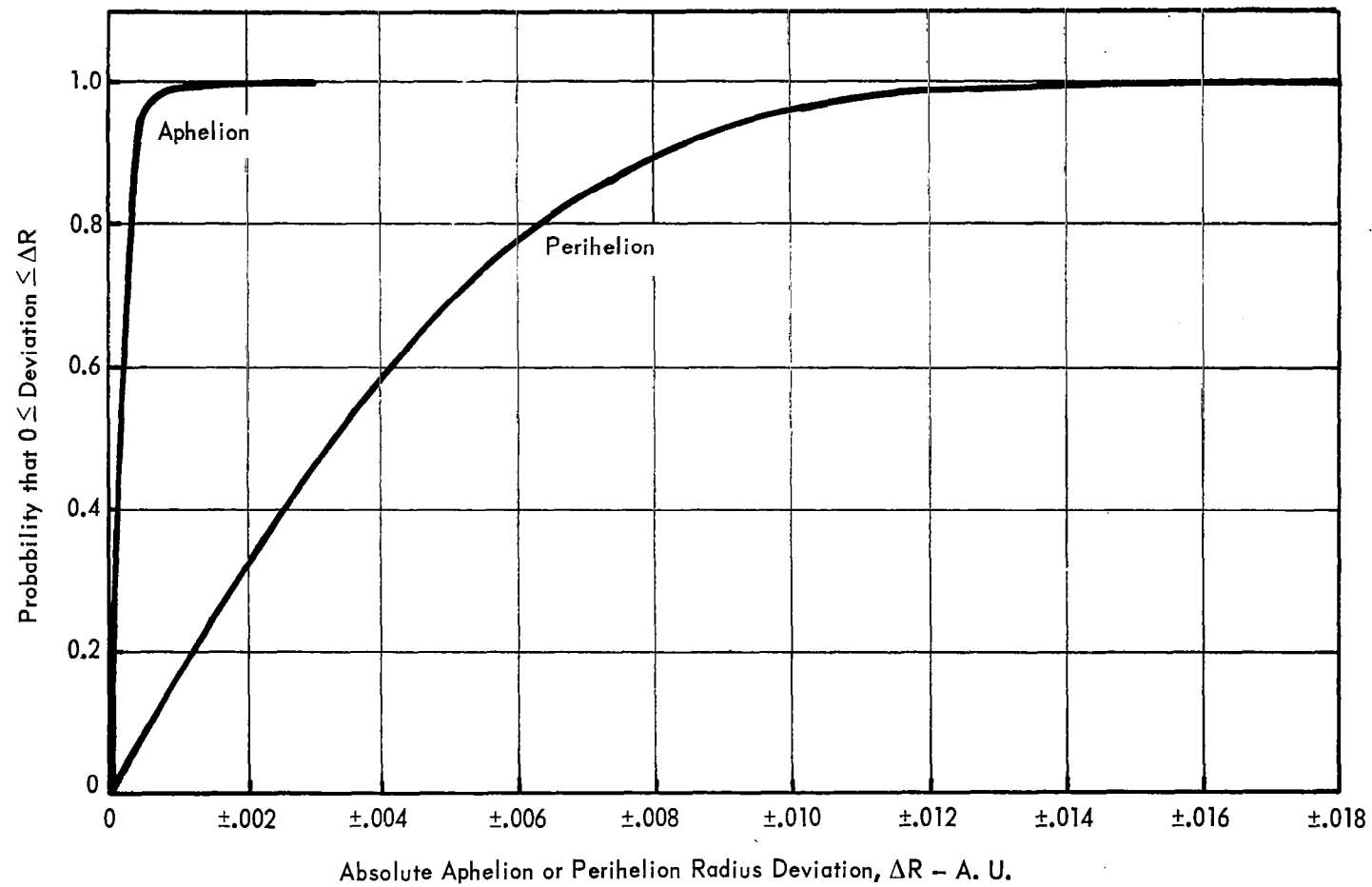


Figure 60. - Probability of Aphelion and Perihelion Deviations

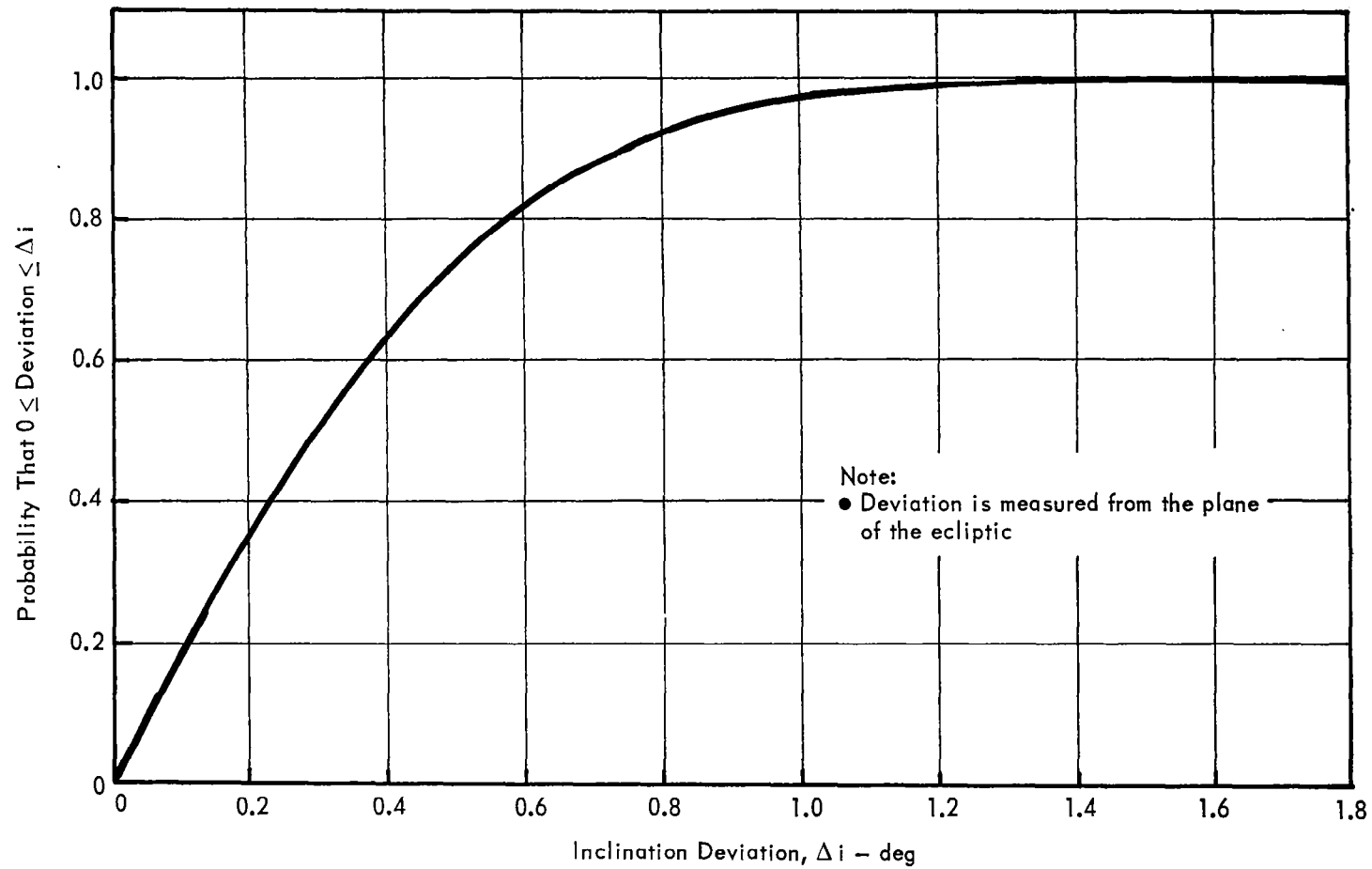


Figure 61. - Probability of Inclination Deviation

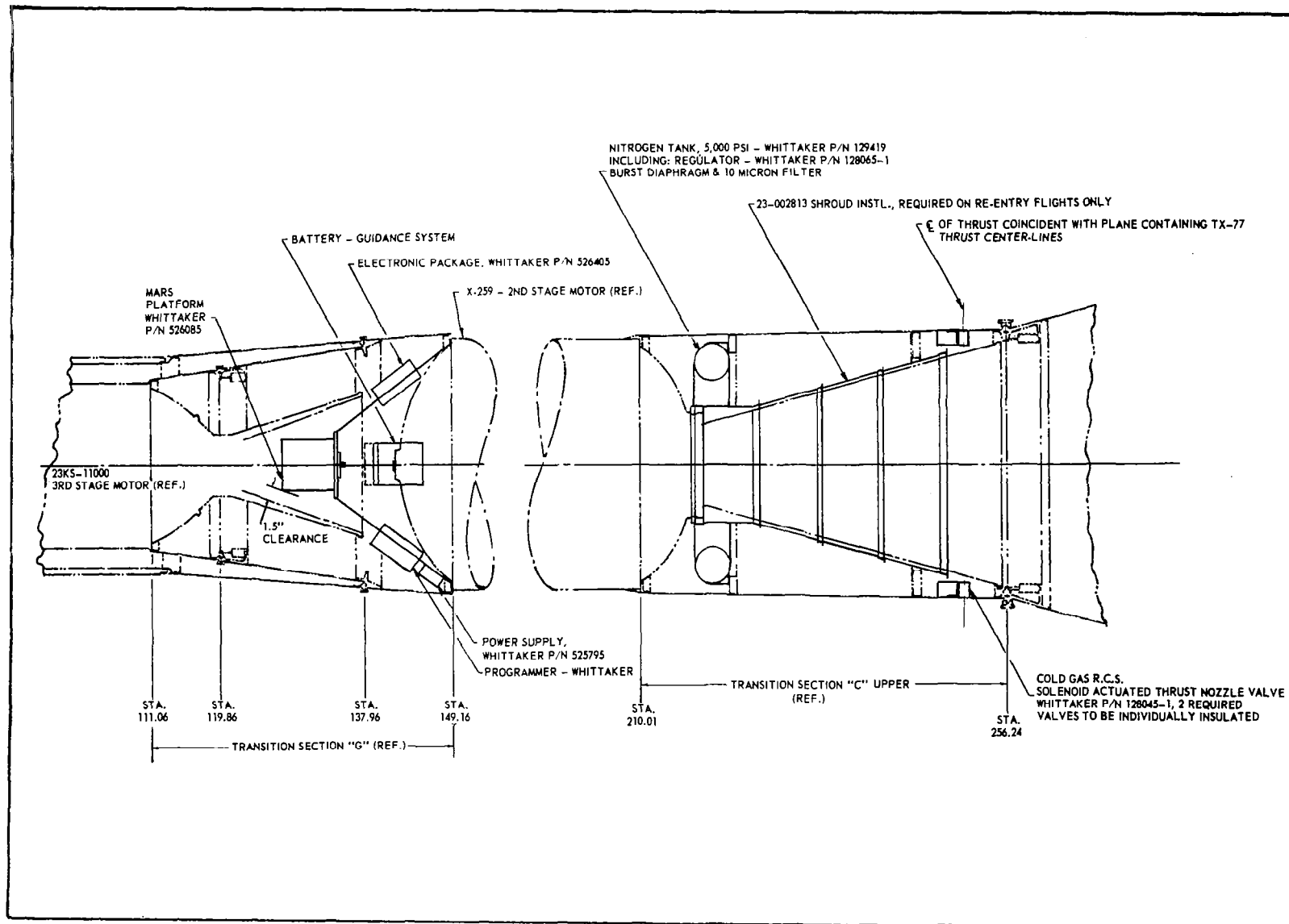


Figure 62. - Attitude Control System Installation, 428A Re-entry Configuration

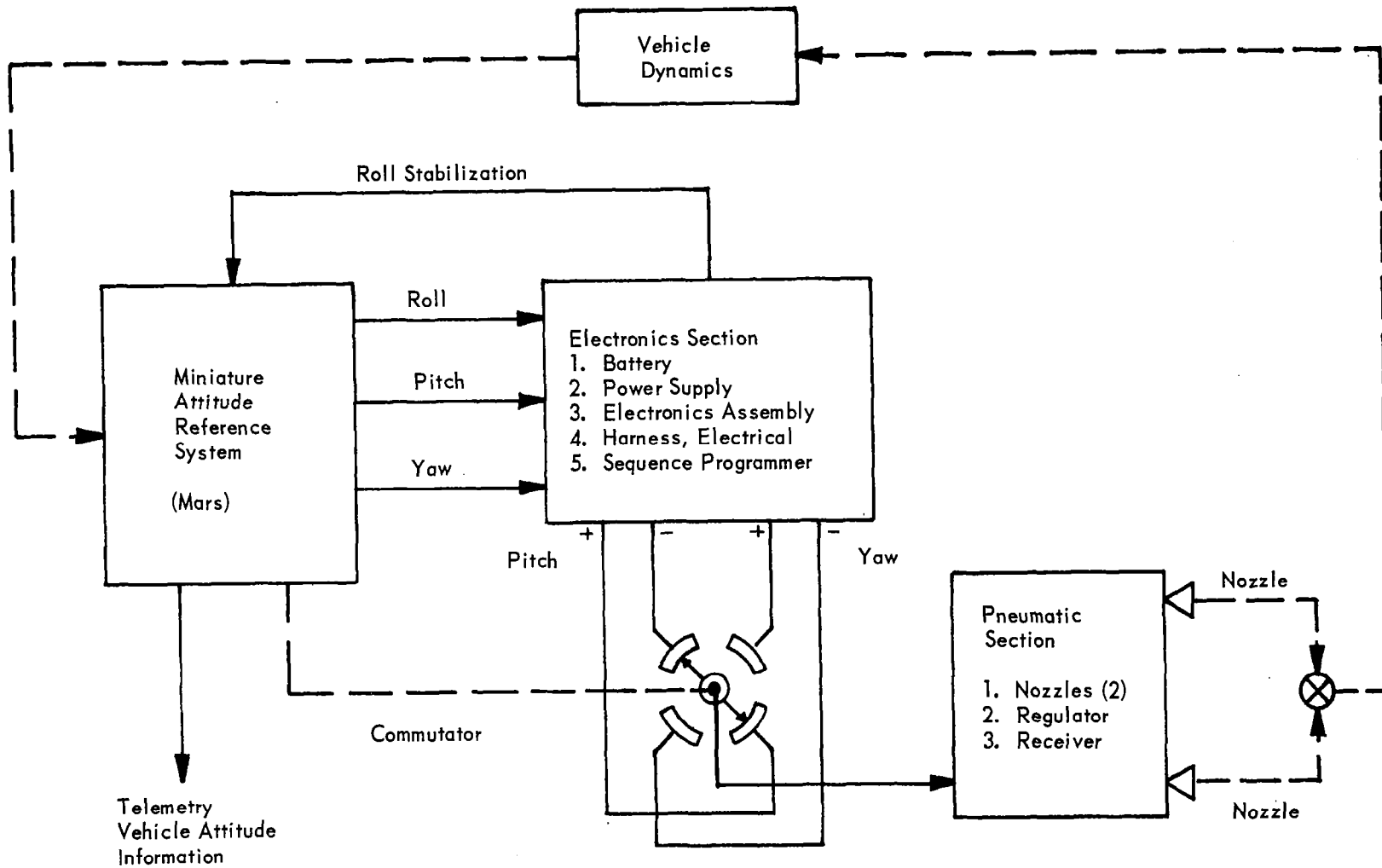


Figure 63. – Basic Block Diagram of Control System Operation

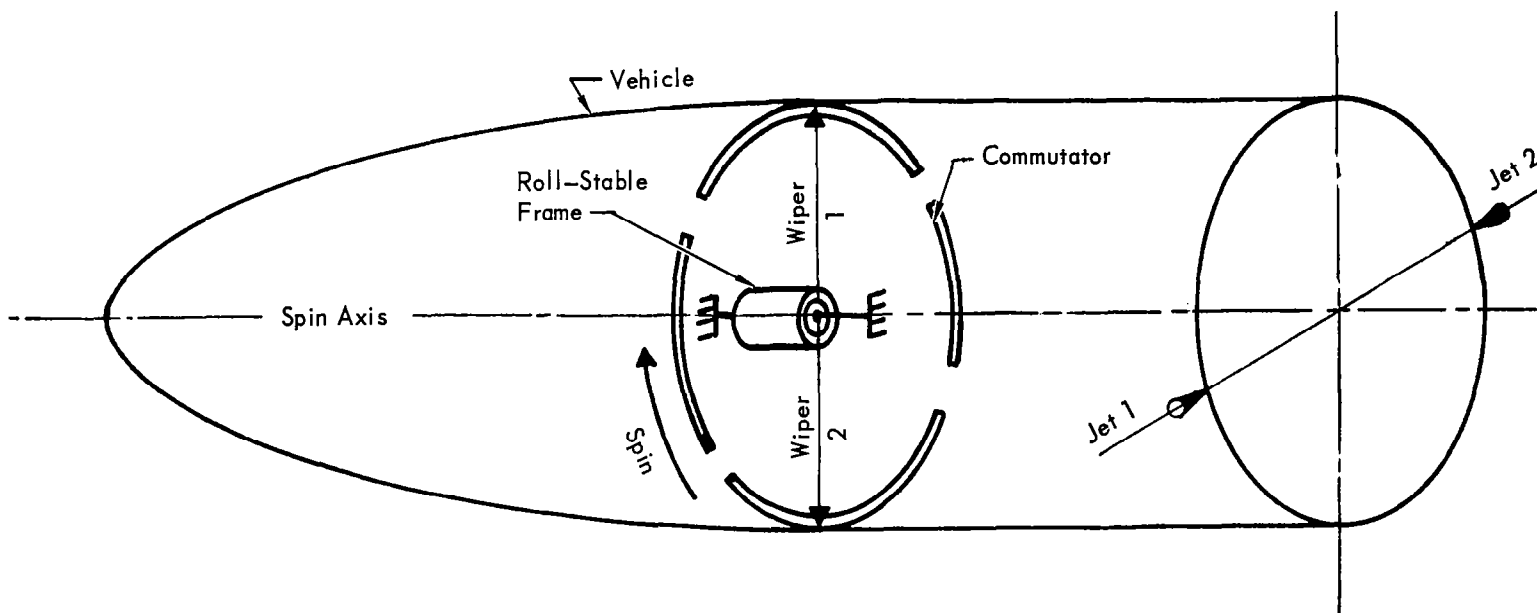
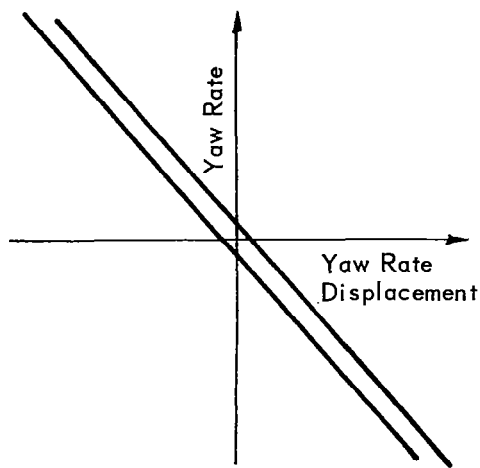
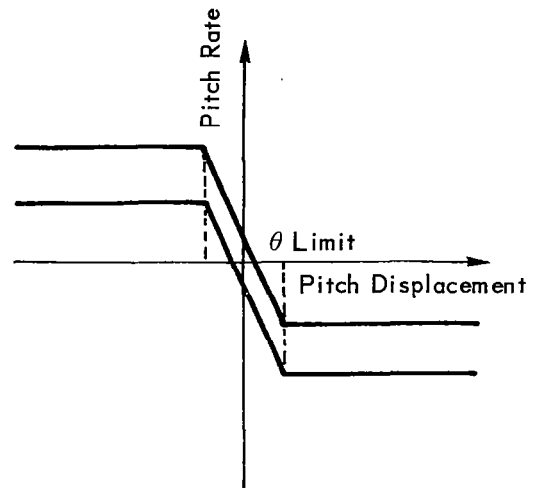


Figure 64. - Attitude Control System Configuration



Yaw Phase Plane



Pitch Phase Plane

Figure 65. - Attitude Control System Pitch and Yaw Deadbands

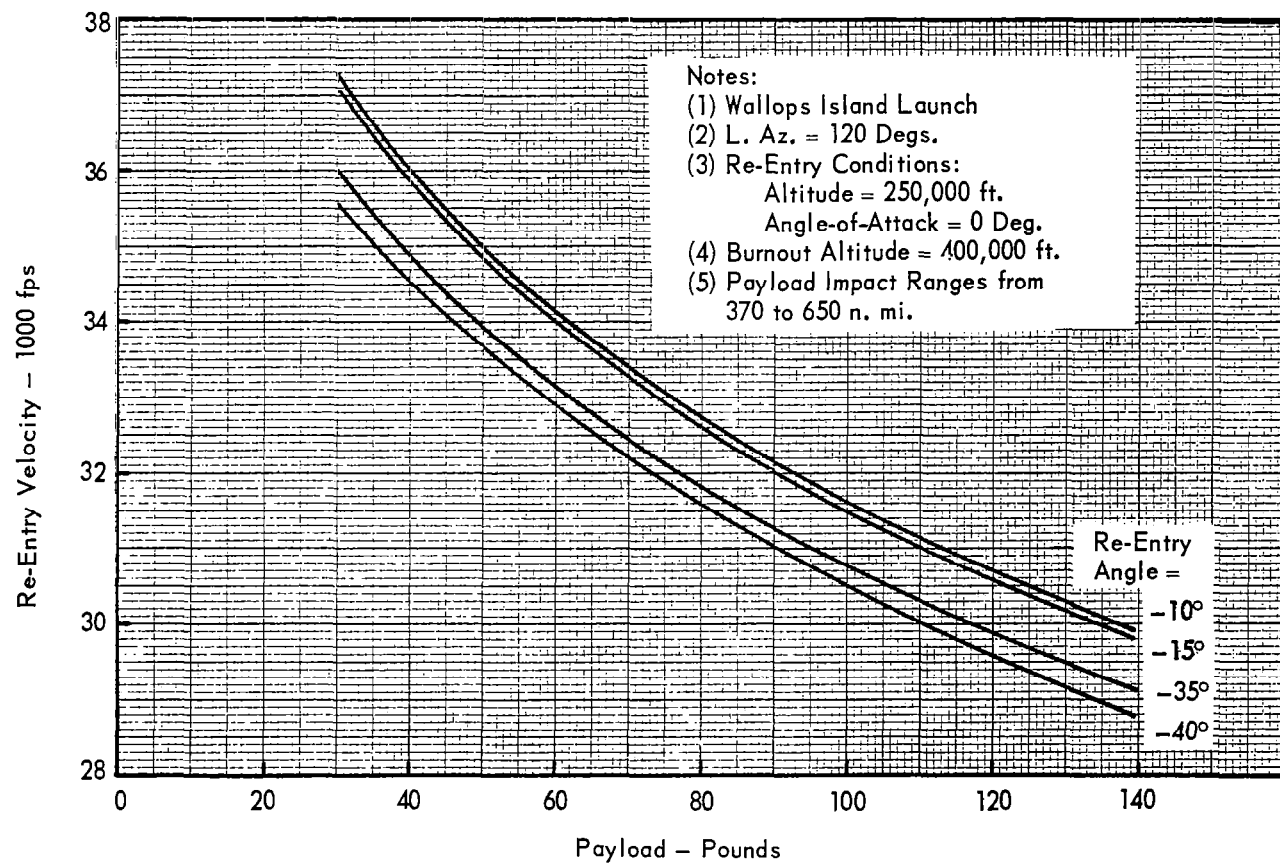


Figure 66. - 428A Re-Entry Performance Capability for One-Up, Three-Down Flight Mode

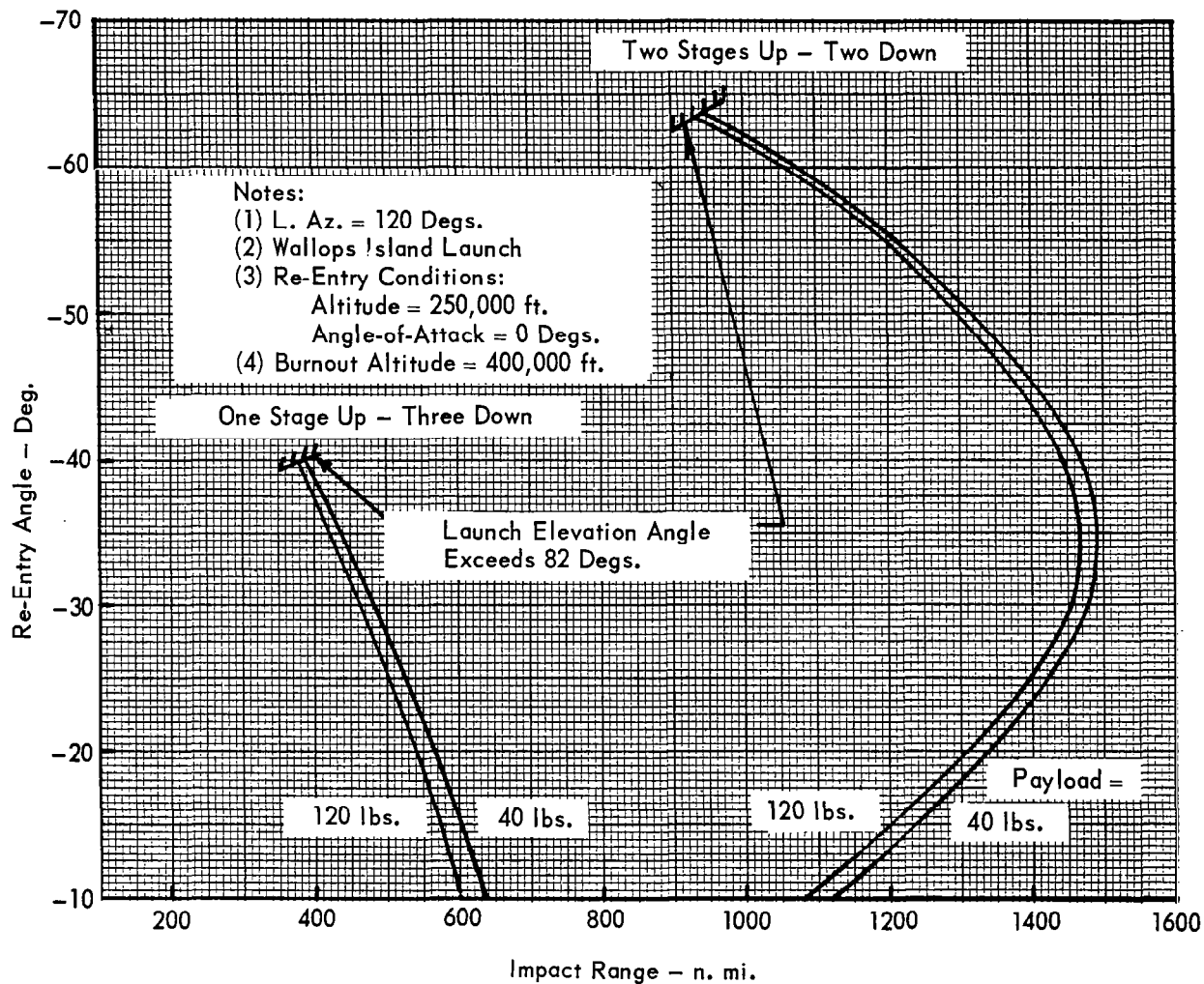


Figure 67. - 428A Re-Entry Range Variation as a Function of Re-Entry Angle

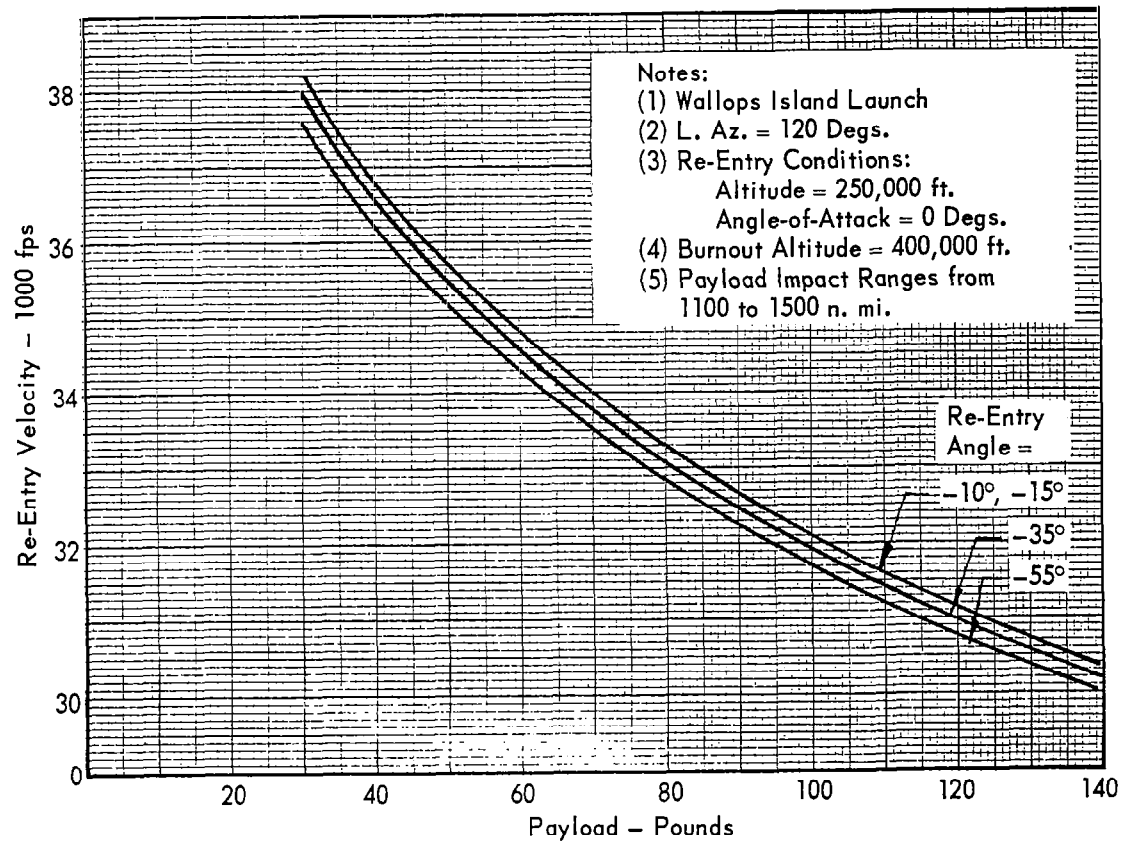


Figure 68. - 428A Re-Entry Performance Capability for Two-Up, Two-Down Flight Mode

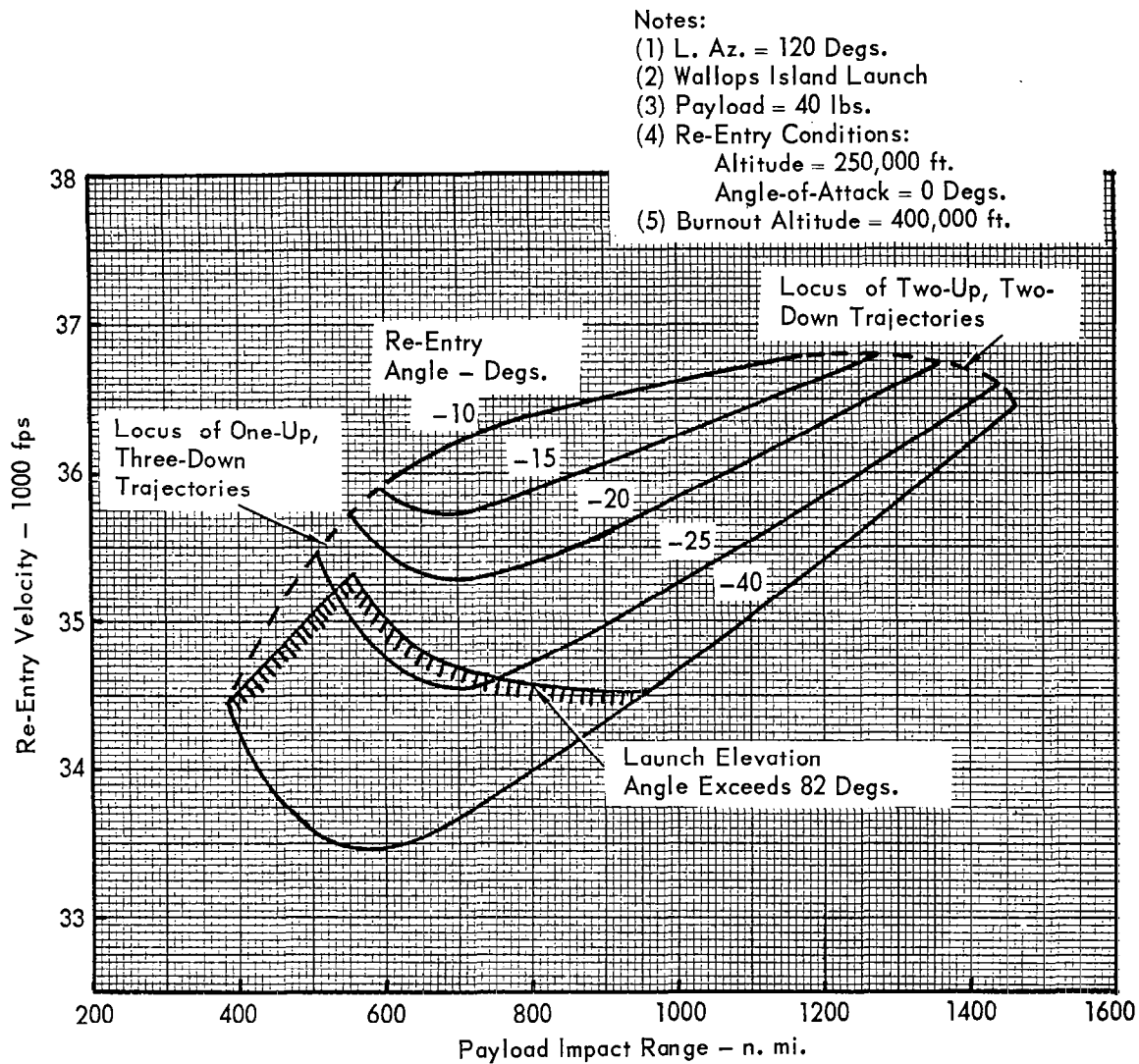


Figure 69. - 428A Re-Entry Performance Envelope at Constant Payload Weight

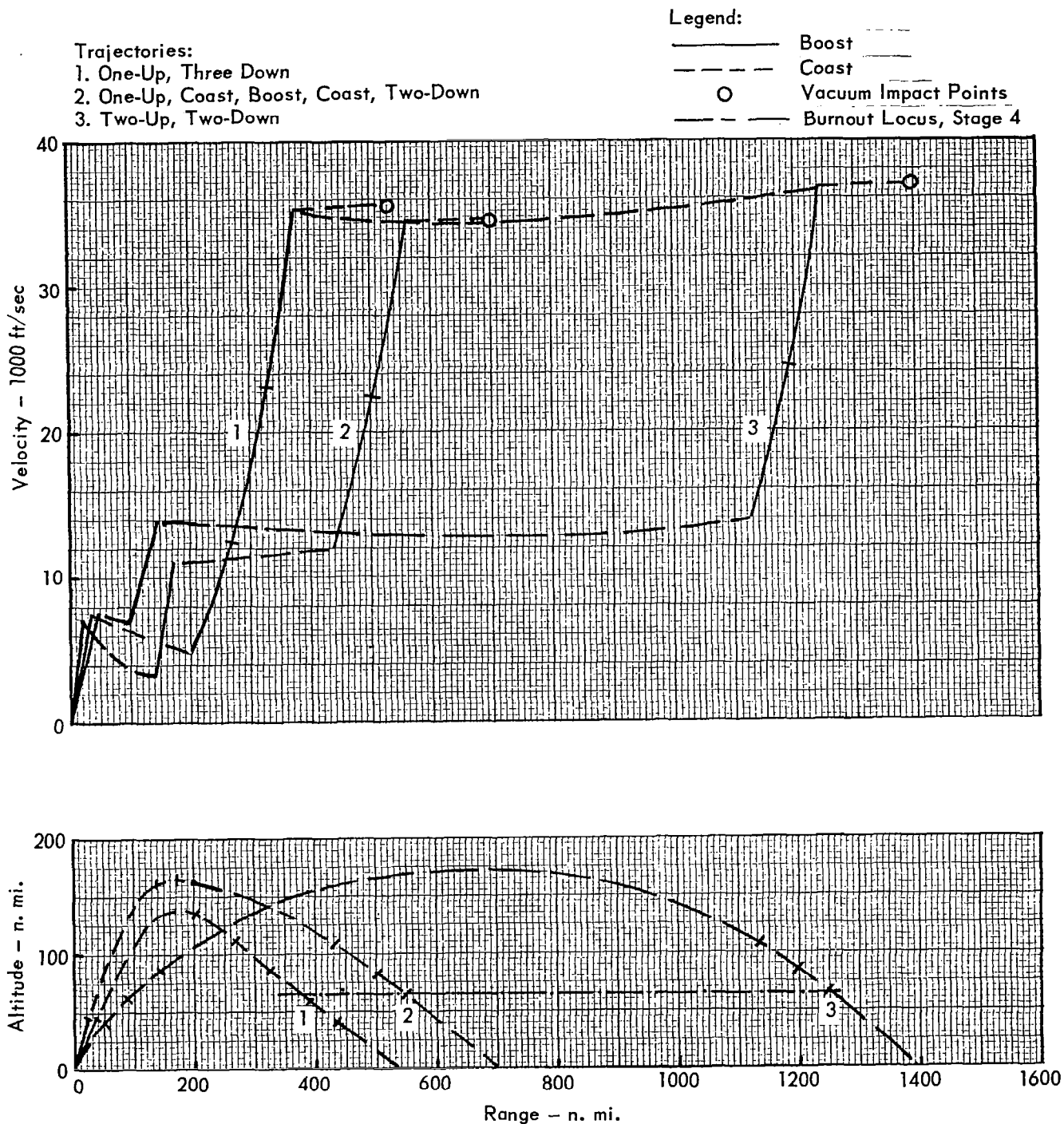


Figure 70. - 428A Re-Entry Missions - Altitude - Range and Velocity - Range Flight Profiles for Constant Re-Entry Angle

Notes:

- (1) L. Az. = 120 Deg.
- (2) Wallops Island Launch
- (3) Variable Range at Re-Entry

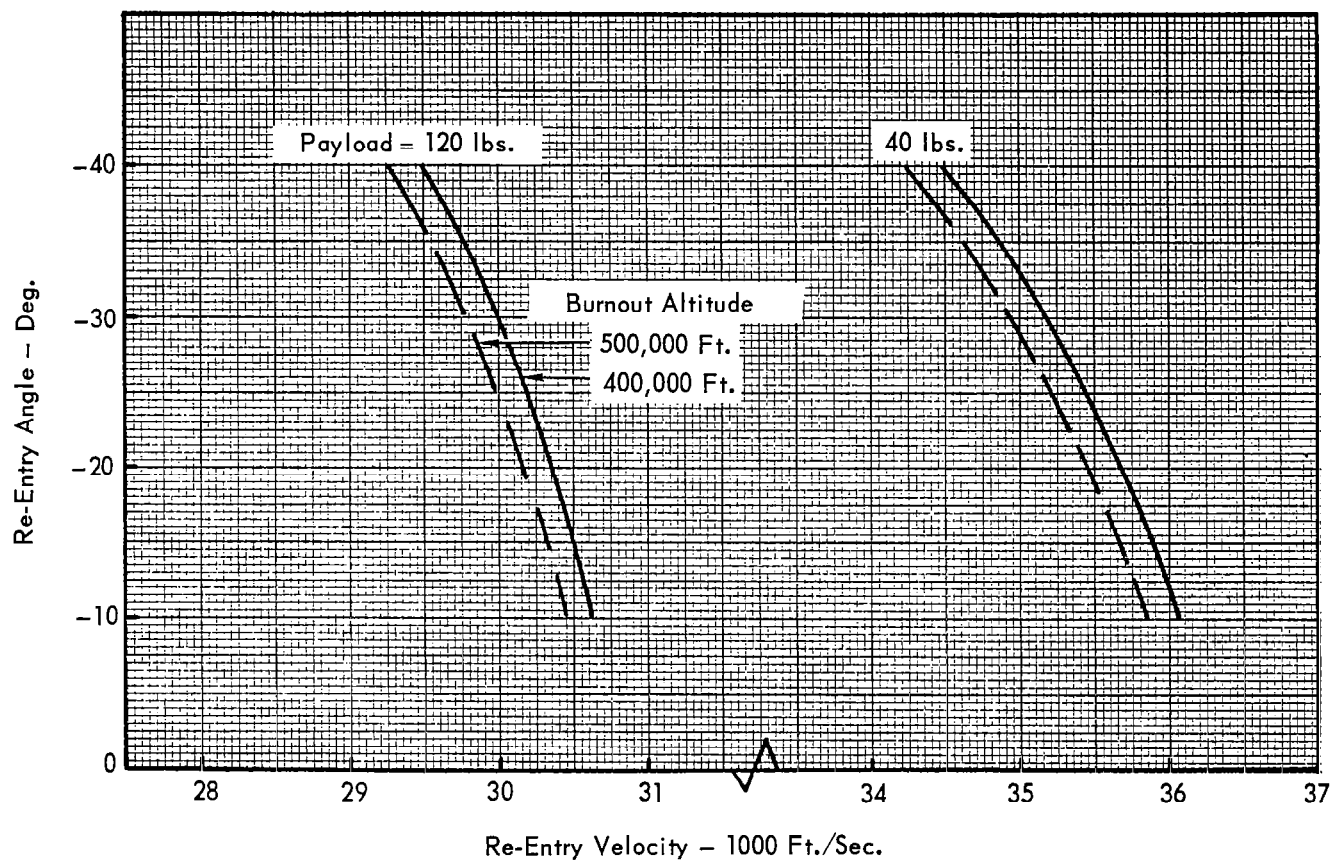


Figure 71. - 428A Re-Entry Missions - The Effects of Burnout Altitude on Velocity

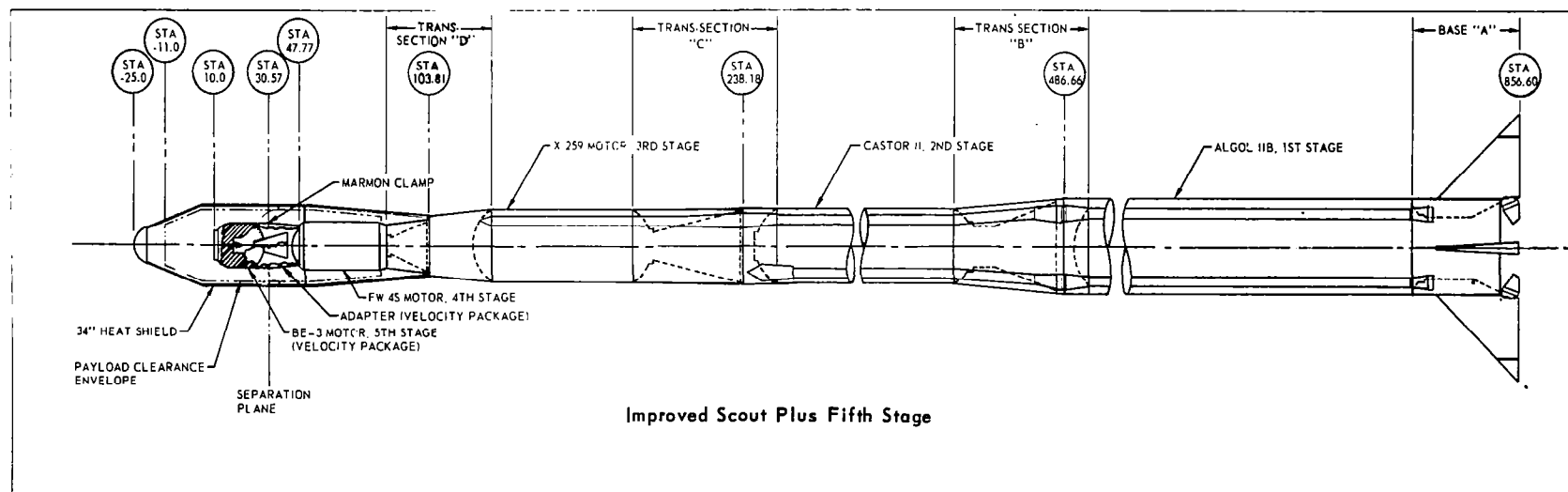
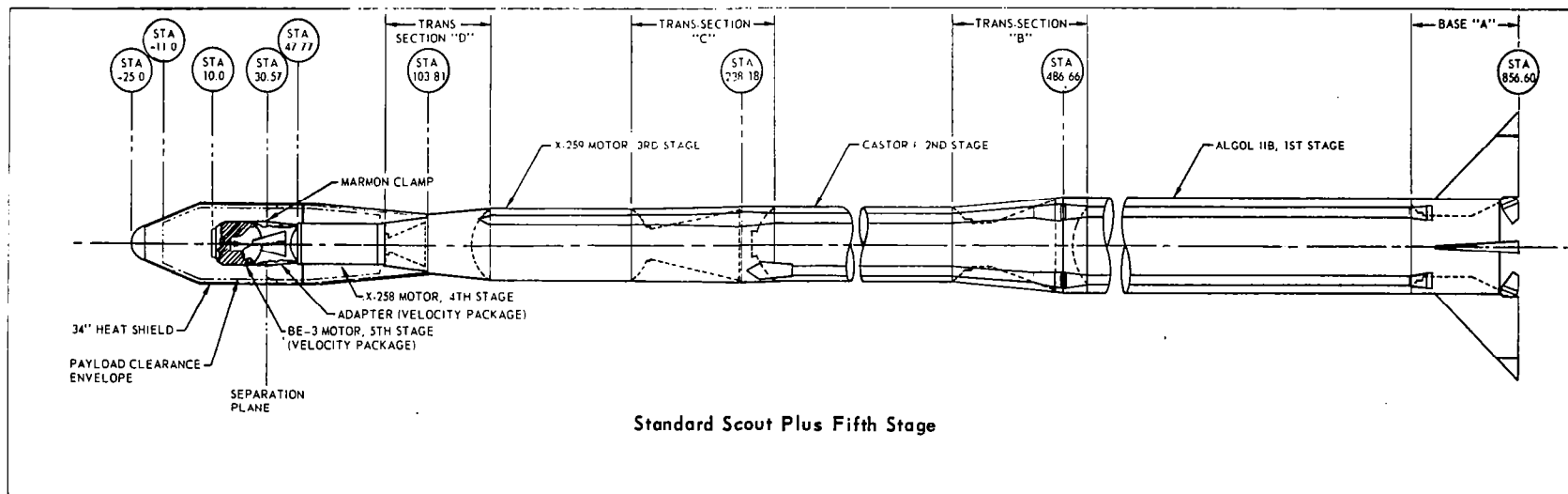


Figure 72. – Standard and Improved Five Stage Scout Vehicles External Profile

Standard and Improved Scout Payload Envelope

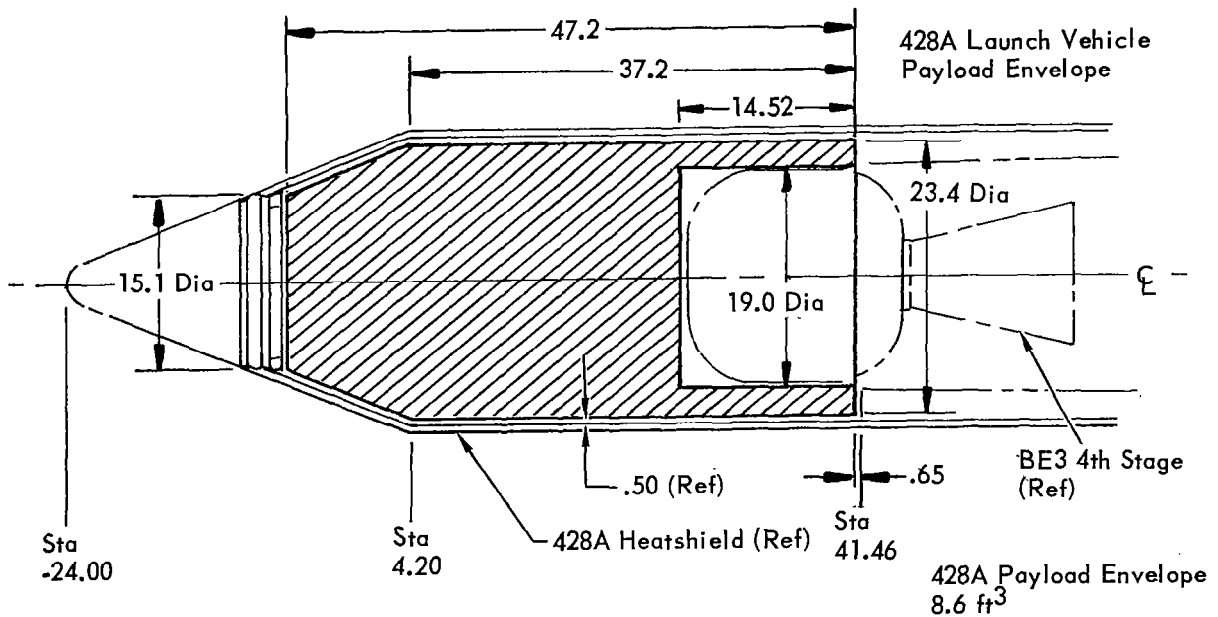
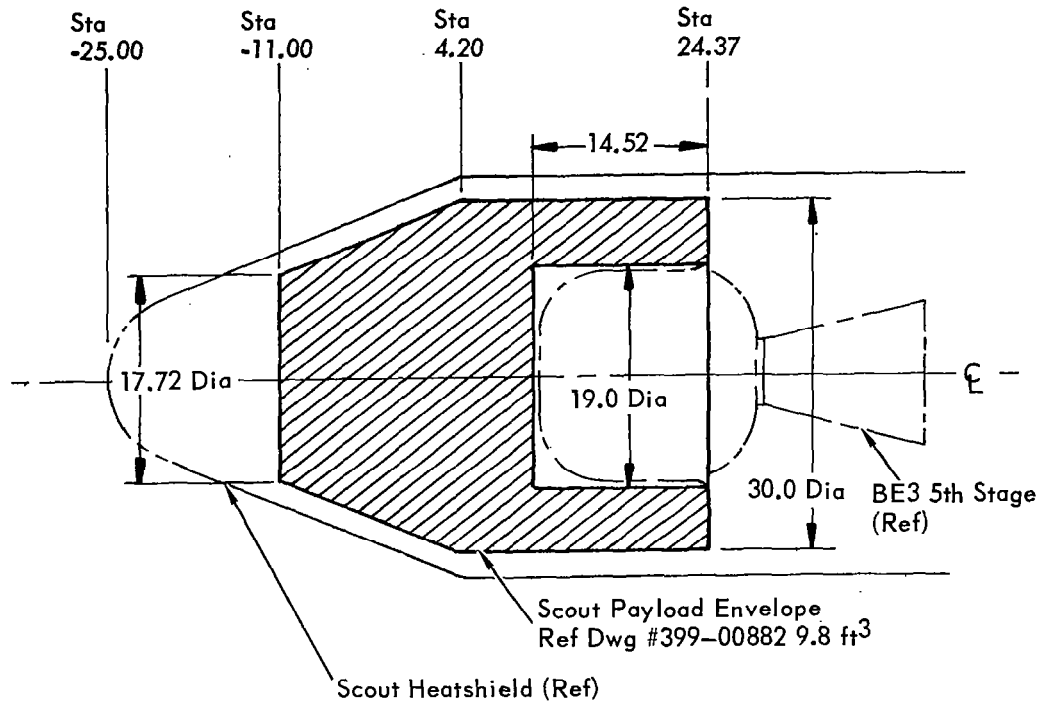


Figure 73. - Payload Volume Comparison - 428A Vehicle Versus Five Stage Scout Vehicle

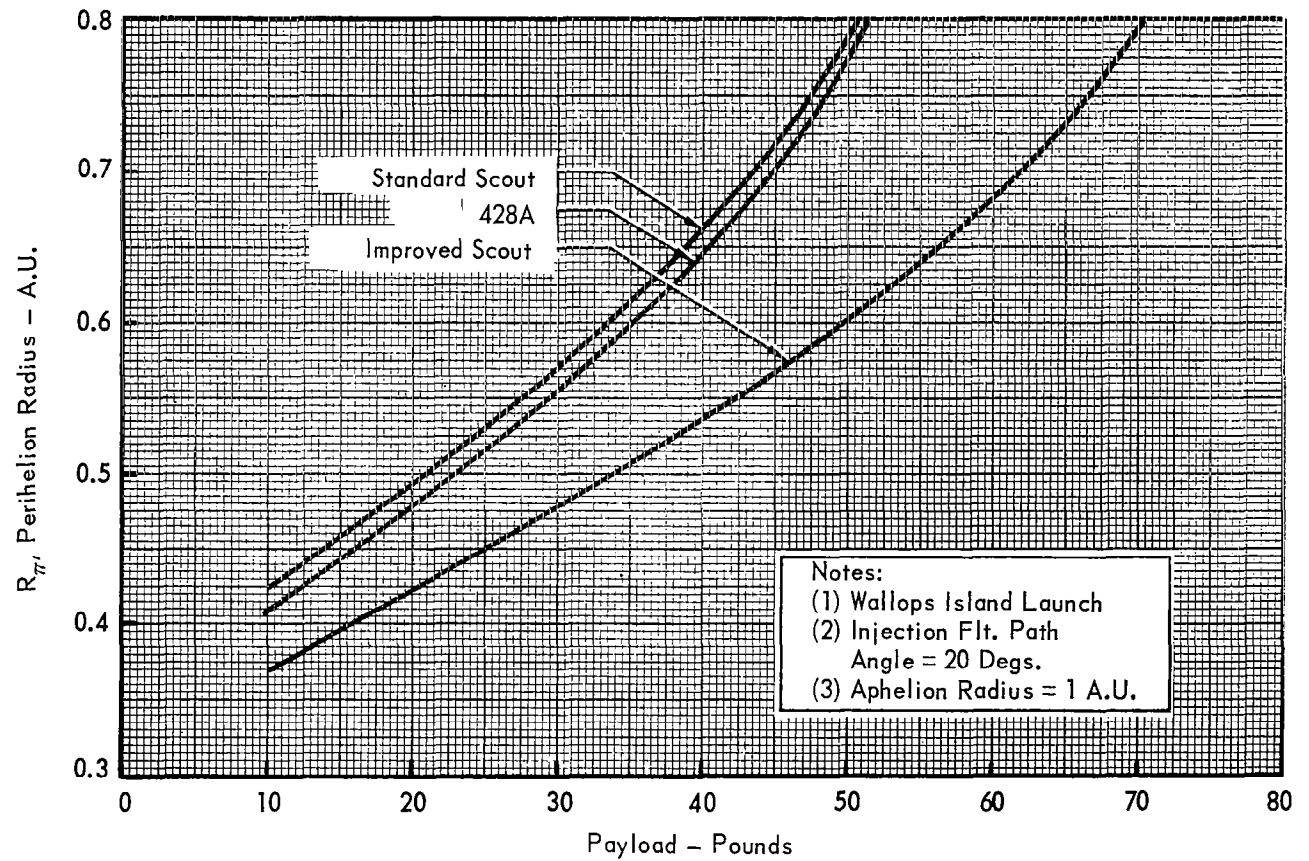


Figure 74. - Comparison of Solar Orbit Mission Capabilities

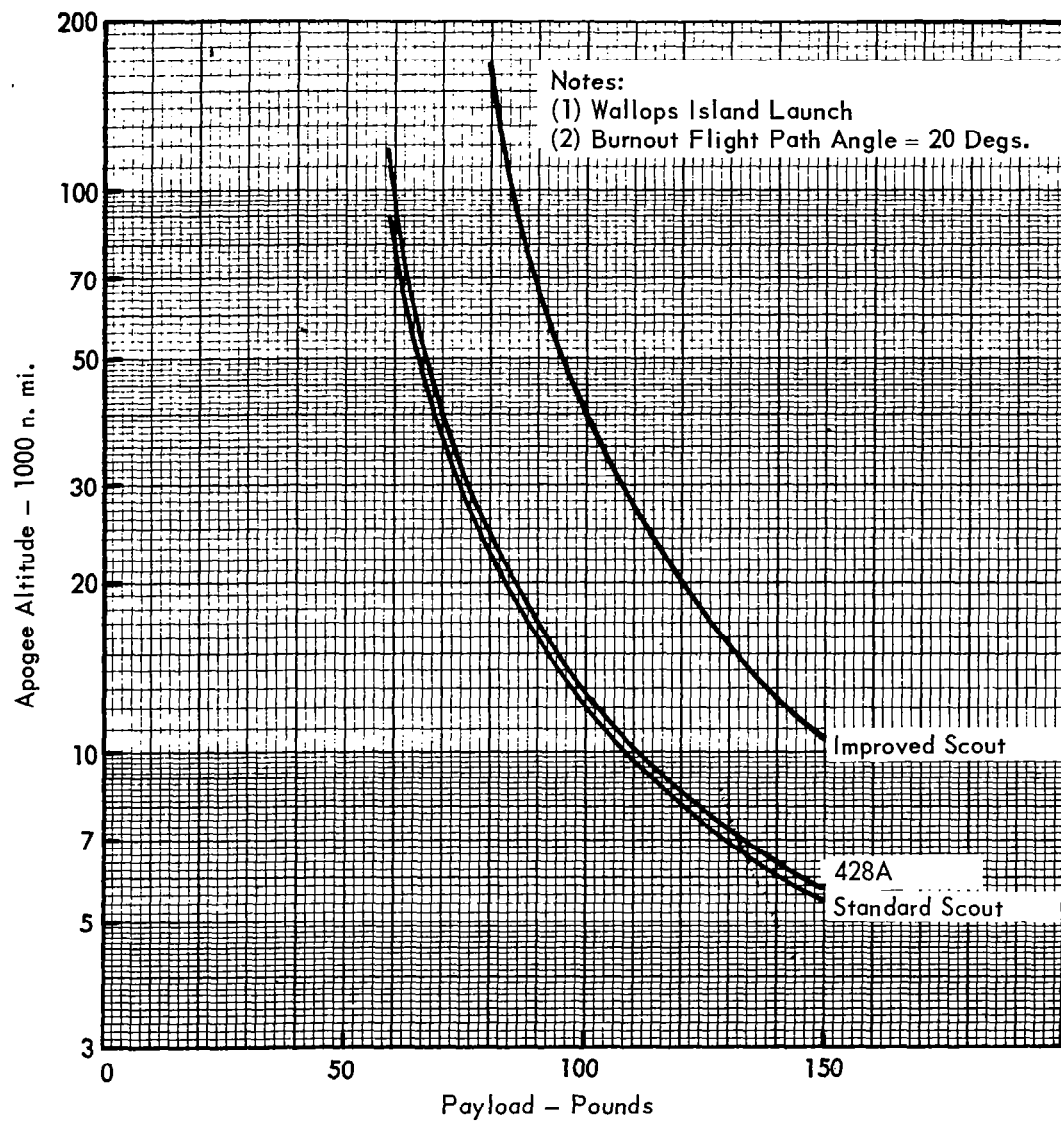


Figure 75. - Comparison of Earth Probe Mission Capabilities

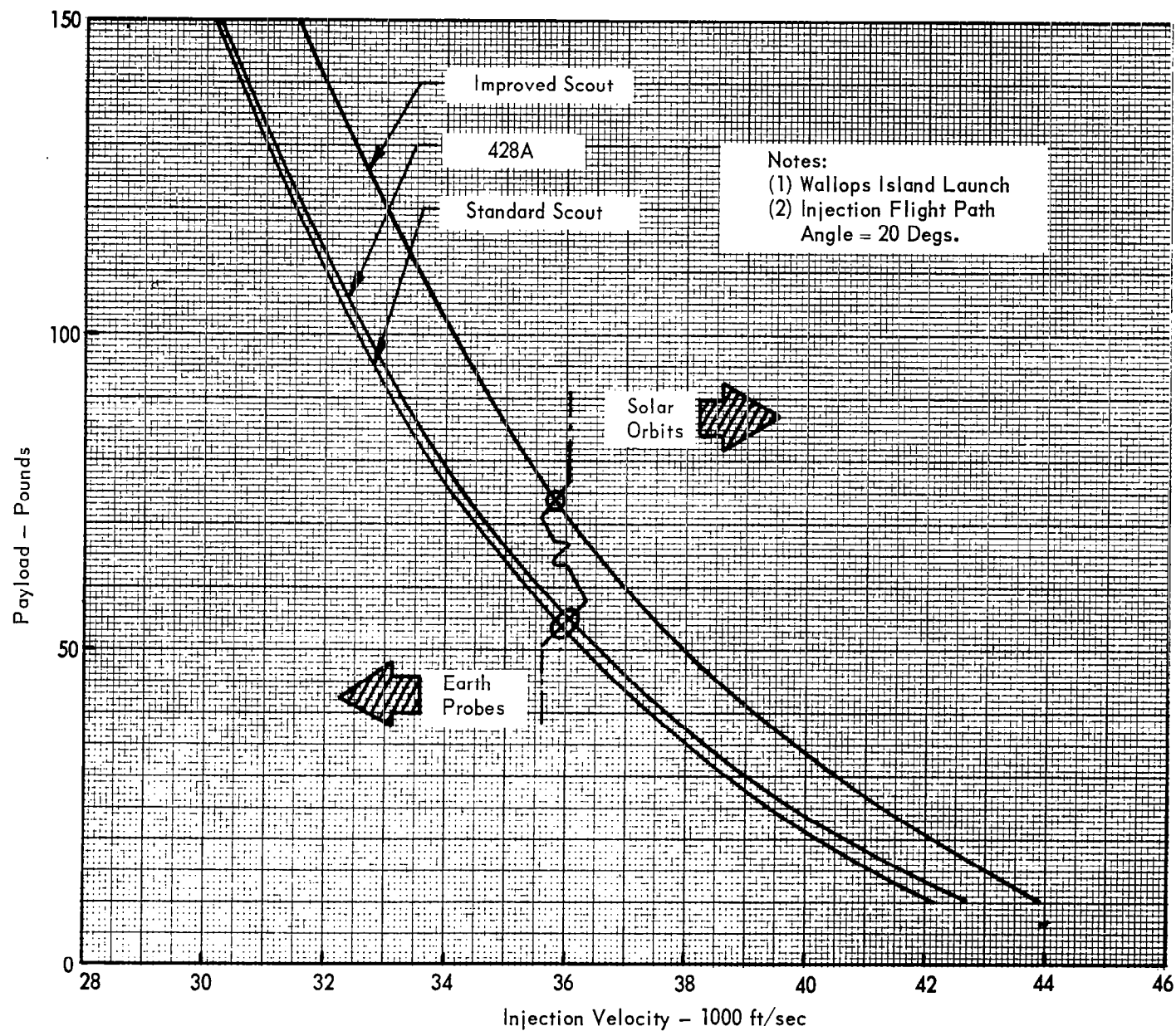


Figure 76. - Comparison of Injection Velocity for Probe and Solar Missions

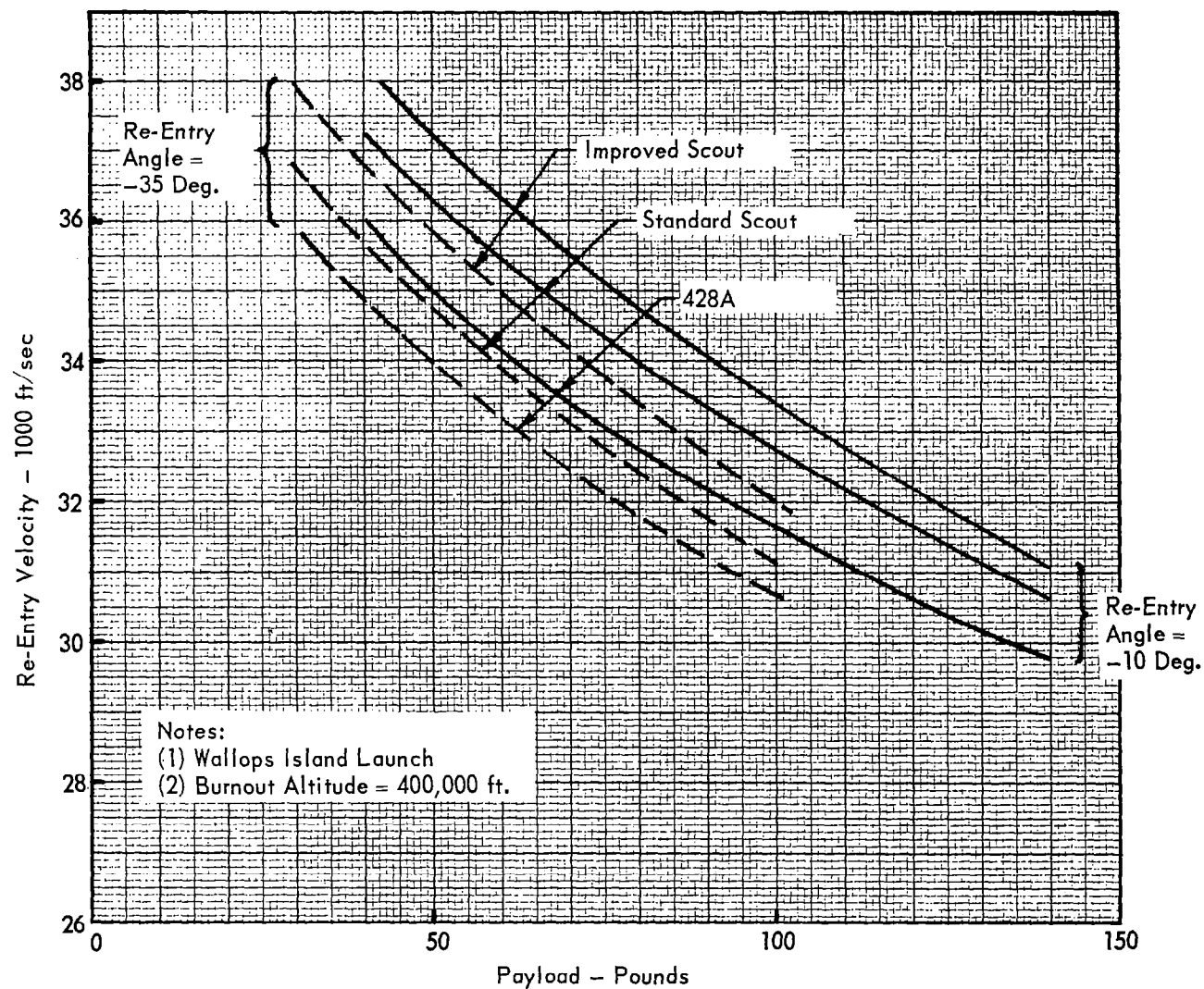


Figure 77. - Comparison of Re-Entry Mission Capabilities Without Range Restrictions

Notes:

- (1) Payload = 40 lbs.
- (2) Wallops Island Launch
- (3) Burnout Altitude = 400,000 ft.
- (4) Range at Burnout = 550 n. mi.

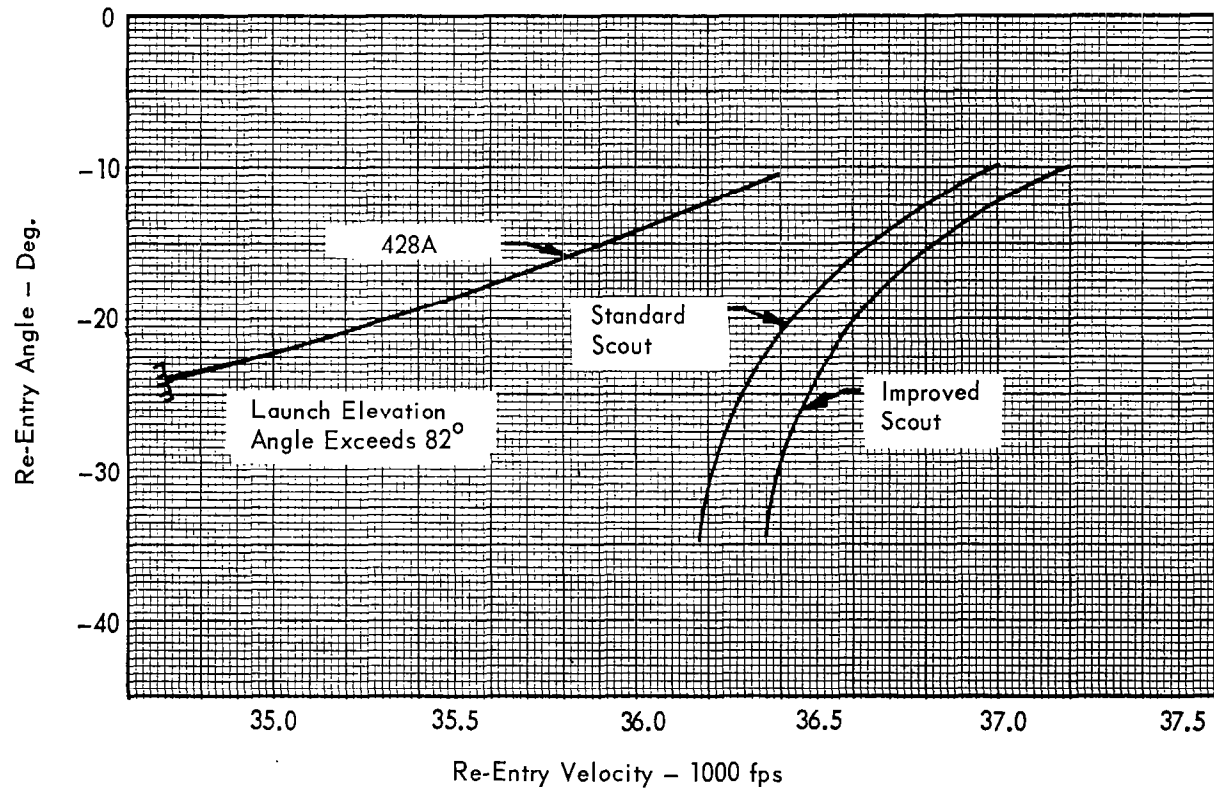


Figure 78. - Comparison of Re-Entry Mission Capabilities at Bermuda for a Constant Payload Weight

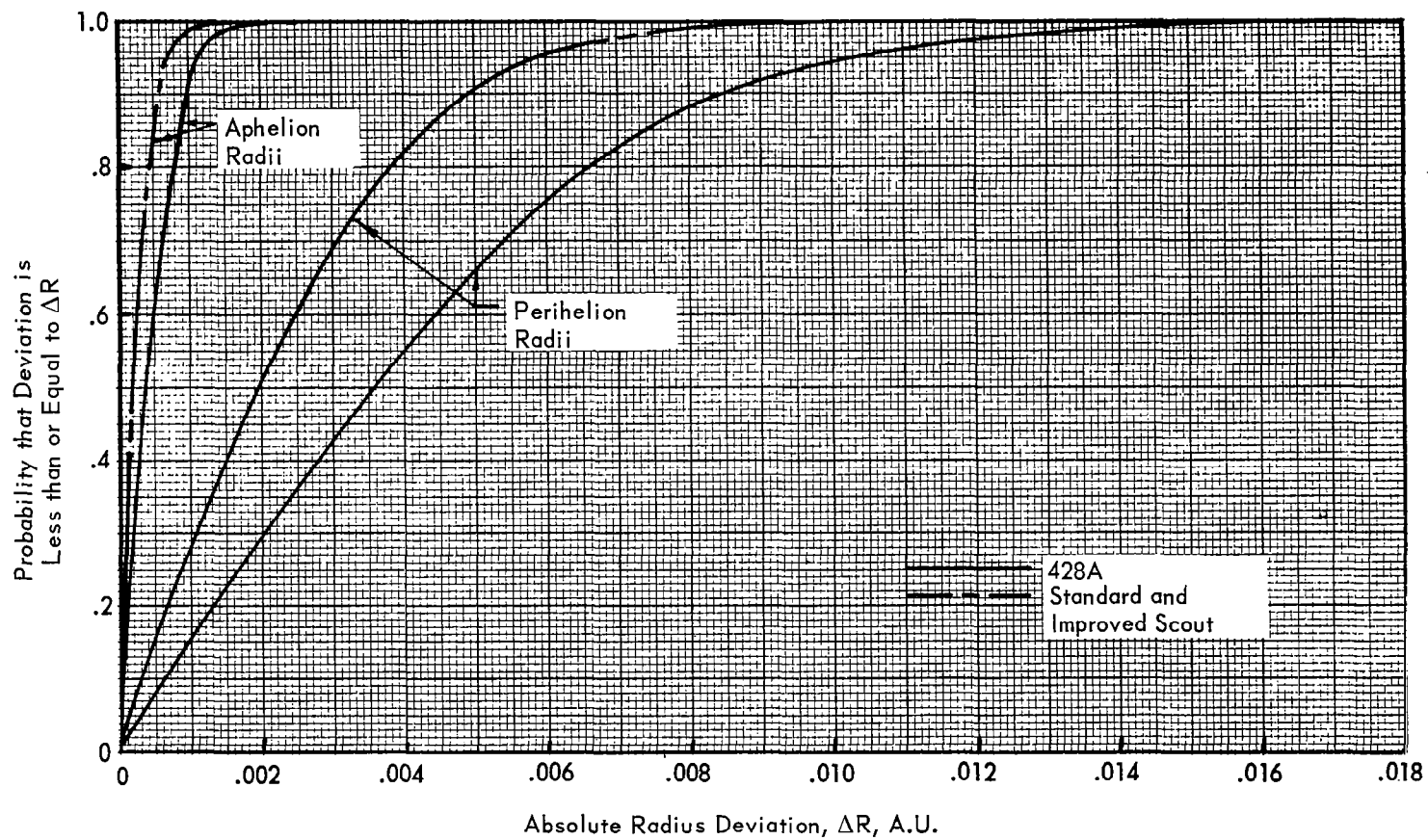


Figure 79. - Comparison of Perihelion and Aphelion Deviations

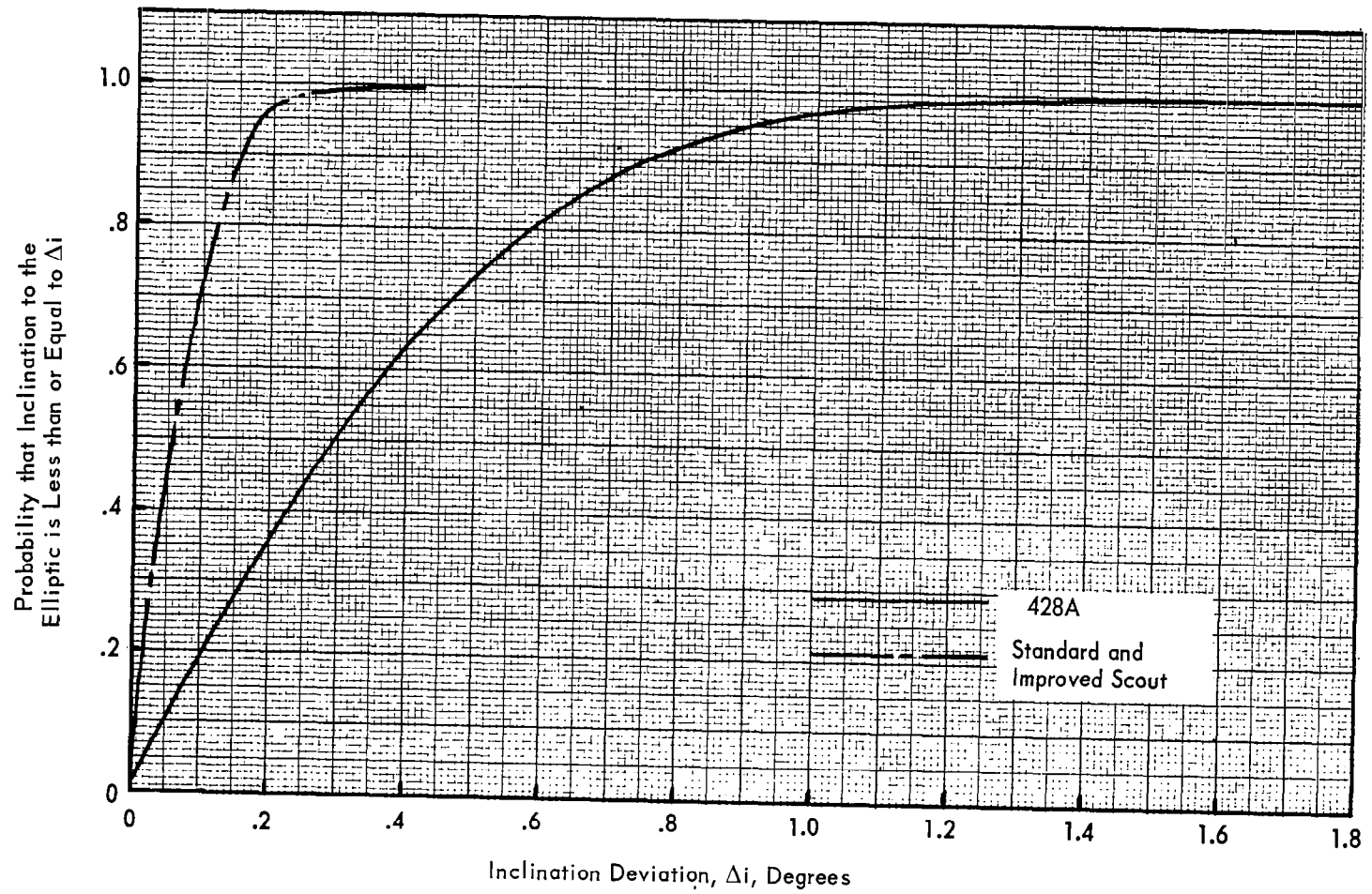


Figure 80. - Comparison of Inclination Deviations

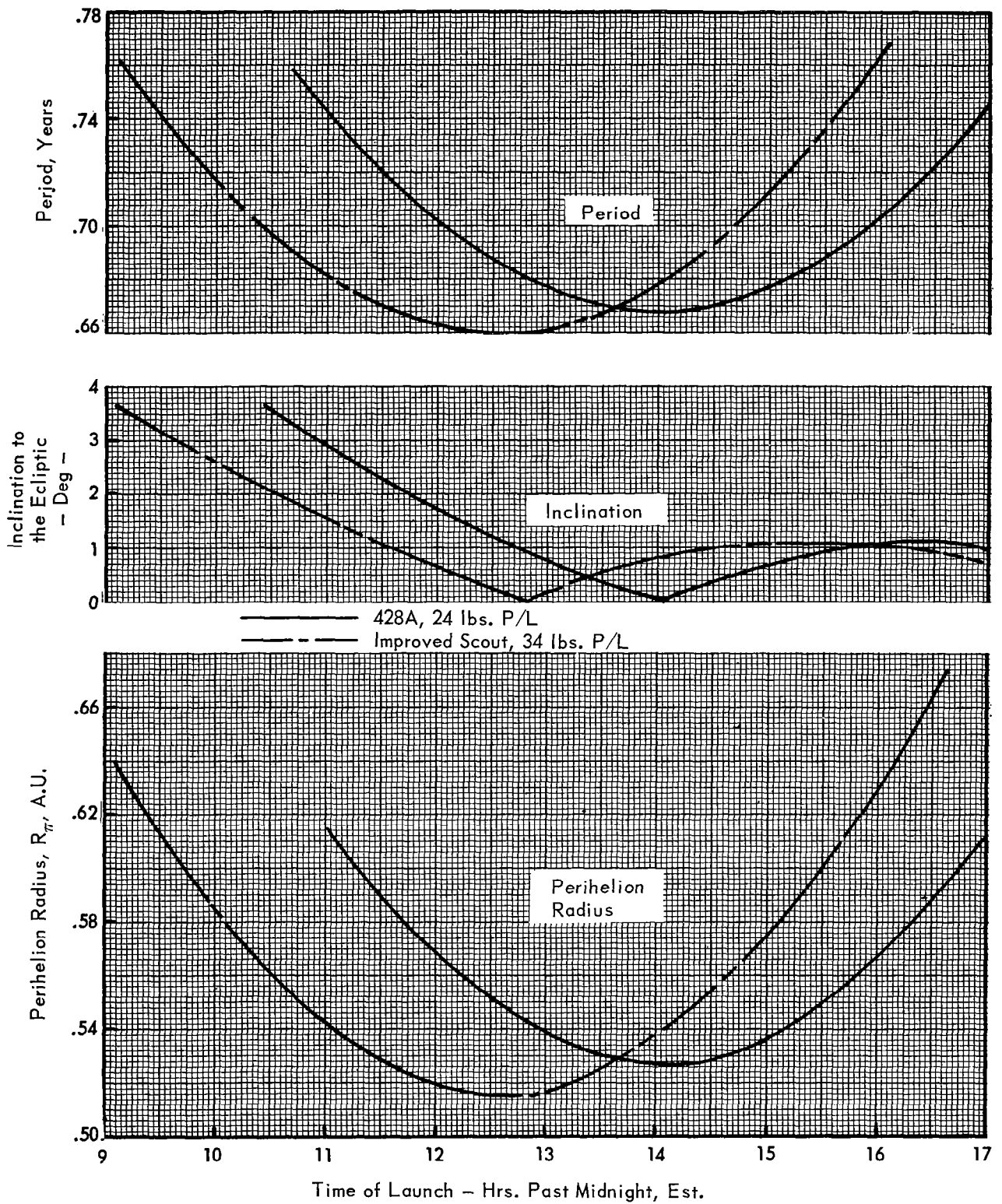


Figure 81. - 9 August 1966 Launch Window Comparison